Final Technical Report

CONTROLLING MECHANISMS OF PULSATING INCINERATION PROCESSES

ONR Grant No. N00014-93-1-1349

September 30, 1996

Prepared For:

Office of Naval Research

Scientific Officer:

Dr. Judah Goldwasser

Prepared By:

B. T. Zinn
J. I. Jagoda
L. M. Matta

School of Aerospace Engineering
Georgia Institute of Technology
Atlanta, GA 30332

Abstract

The purpose of this research program is to study the fundamental processes that control the performance of acoustically excited incineration systems. The information learned will be used in the development of a compact, high-efficiency waste incinerator for shipboard use. Tests performed during the course of this program have demonstrated that mixing and heat transport processes, both crucial to the incineration process, can be enhanced by imposing acoustic oscillations. Because the combustion efficiency and pollutant emission characteristics of incinerators are directly affected by the mixing of in-flowing air with fuel, acoustic control of turbulent jets is of interest to the development of compact incinerators. Studies of jets subjected to transverse mode oscillations have shown that, under the proper conditions, the jet will shed large, alternating, vortical structures that can cause the jet to bifurcate. This process results in a greater spatial mixing rate. Transverse mode acoustic forcing had the greatest effect in the range of St = 0.2 - 0.3. The effect of acoustic oscillations upon solid fuel pyrolysis was investigated by studying the effect of acoustic oscillations upon dry ice sublimation. This study showed that the presence of pulsations enhanced the sublimation process, which strongly suggests that they would also enhance the processes involved in incinerating solid wastes. Finally, the effects of acoustic oscillations on the combustion of simulated solid wastes in an incinerator were studied. Measurements of the burning rates and the emissions of NOx, CO, and CO_2 were performed for different fuels and conditions. In all cases, it was shown that pulsations dramatically increased combustion rates. The results indicate that the effects of pulsations on NOx emissions are relatively insignificant with respect to other factors, such as combustor temperature. The effect of acoustic oscillations on the emission of CO differs with the fuel type used and the conditions present.

I. Introduction

The goal of waste incineration is to completely burn the combustible portion of the waste material without emitting hazardous substances into the environment. The incineration of solid wastes generally proceeds through a number of individual processes, which, depending upon the phase of the waste, may include heating of the waste, evaporation of its water content, devolatilization, pyrolysis, mixing of gaseous fuel and oxidizer, ignition, and combustion. In order to obtain complete incineration within the limited volume of a compact incinerator, the rates of all the above-listed processes must be high. At present, high gas phase mixing rates are generally attained by providing the incinerator with an air flow rate that is considerably higher than that required for a stoichiometric combustion process. This reduces the global fuel/air ratio within the incinerator, resulting in lower reaction temperatures. Thus, while high air flow rates promote faster gas phase mixing and increase the rate of convective heat transfer between the gas phase and the solid waste, the effect is compensated by lower temperatures and the resulting reduction in waste heating rates and slower chemical kinetics.

The identification of processes and the development of techniques that can enhance the rates of various transport processes are crucial to the development of incinerators that are more compact, more efficient and emit less pollutants than state of the art incineration systems. Recent investigations have demonstrated that the presence of acoustic oscillations and flow pulsations can increase the rates of transport processes. Patera et. al.,[1,2] for example, have shown that mixing and heat transfer rates in laminar flow in a channel can be considerably increased by oscillating the flow rate into the channel at a frequency at which the flow's shear layer is unstable. While there is considerable evidence that mass[3] and heat[4,5,6] transfer rates are increased by acoustic oscillations, the precise mechanisms responsible for these increases are not entirely understood. Strong evidence[4,7] suggests that the increased transport rates are due to the excitation of turbulence and vortical structures by the acoustic oscillations. In a study by Vermeulen et al.,[8] flow oscillations were shown to reduce flow stratification and improve mixing. This was demonstrated by the elimination of localized pockets of high temperature gas, or "hot spots", at the exit plane of a gas turbine combustor, which can damage turbine blades downstream of the combustor. The capability to reduce or eliminate this type of local stratification is of practical importance in incinerators because non-uniform loading of waste materials leads to fuel rich regions in the incinerator, which can result in the emission of "puffs" consisting of soot, CO, and unburned hydrocarbons. Also, "hot spots" may be the cause of increased thermal nitrogen oxide production by the Zeldovich mechanism.

Results of several investigations of pulse combustors suggest that when combustion occurs in an oscillatory flow field, the combustion time is reduced and combustion efficiencies are increased with respect to combustion in a steady flow field. For example, Lyman[9] showed that

pulsations increased the burning rates of individual coal particles, and Zinn et al.[10] found that unpulverized coal nuggets can be burned in a Rijke type pulse combustor with high combustion efficiency while utilizing little excess air. Bai [11] showed that heavy fuel oils, which are generally difficult to burn, can be burned with high combustion efficiencies in a pulse combustor specifically designed for this purpose.

A recent study supported by the EPA investigated the effects of pulsations upon the incineration process.[12] In the study, a tunable pulse combustor was retrofitted to an existing EPA rotary kiln incinerator simulator and used to excite large amplitude acoustic oscillations within the incinerator. Toluene and polyethylene were burned as surrogates for hazardous and municipal wastes, respectively. Pulsations were shown to reduce the magnitude of "puffs" and soot emissions. Interestingly, reductions in soot emissions observed when burning toluene with pulsations were, in some cases, accompanied by increased levels of CO and hydrocarbon emissions. In contrast, when polyethylene was burned in the presence of pulsations, the emissions of soot, CO, and hydrocarbons were all reduced. In both cases, the pulsations reduced the O_2 concentrations in the exhaust to very low levels, indicating that the pulsations improved the utilization of available oxygen in the incineration process.

II Research Accomplishments

The objective of this study was to investigate the mechanisms through which pulsations affect the incineration process in order to obtain information that will aid the development of an efficient and compact incinerator for ship-board use. Specifically, the effects of acoustics on the mixing rates, flow characteristics, burning rates of solid and liquid wastes, and soot, NO_x, CO, and unburned hydrocarbon emissions were investigated in simulated incinerators.

Gas Phase Mixing Resulting By Resonant Acoustic Forcing:

In an effort to better understand the mechanisms of mixing rate enhancement due to acoustic oscillations isolated from the mixing effects of the mean flow into and out of the combustor, the characteristics of gas phase mixing in an environment of large amplitude, resonant, acoustic oscillations in a rectangular cavity with no mean flow was investigated. Previous research has shown[13] that under such conditions, acoustic streaming often plays a significant role in the mixing process. It is well known that periodic sound sources can generate non-periodic motions of the medium[14-16]. Eckart[14], in his paper on streaming and vorticity generated by sound waves, shows that circulation necessarily follows as part of the solution to the wave equation when one accounts for the viscosity and second order terms. While such motions could provide effective means for enhancing mixing processes, their effect upon mixing rates in cavities has not been investigated to date. In this section, the results of an experimental study of the effects of the mode and amplitude of resonant acoustic oscillations in a cavity upon the rate of gas phase mixing will be reported.

Acoustic Mixing Facility

A schematic of the experimental setup used in the mixing rate studies is shown in Fig. 1. It consists of a rectangular wooden box with one acrylic side. The cavity has dimensions of 68.6cm x 20.3cm x 12.7cm. These dimensions were chosen to prevent redundant natural frequencies over the range of interest. A removable partition can be inserted into the middle of the box to divide the cavity into two sections. Four University Sound, 75 watt, compression type, acoustic drivers were used to excite standing acoustic waves in the box. The drivers were mounted on the ends and bottom of the setup, which allowed longitudinal, transverse, and multidimensional acoustic modes to be excited. Sound pressure levels as high as 158 dB can be driven for certain modes.

In this report, the resonant acoustic modes are identified by the longitudinal mode number (in the direction of the long axis of the chamber) and the mode number in the direction perpendicular to that direction (ie., the 20.3cm direction), which is referred to as the transverse mode. Oscillations in the 12.7cm direction were not excited in this study, and so the mode numbers in this direction are assumed to be zero. For example, by this convention, the (1,0) mode

refers to the fundamental longitudinal mode and the (2,0) mode refers to the second longitudinal mode, the (1,1) mode and the (3,1) mode refer to the multi-dimensional modes which are combinations of the first longitudinal and the first transverse modes and the third longitudinal and the first transverse modes, respectively.

The acoustic driving in the facility can be achieved by either open or closed loop operation. In open loop operation, a signal to the drivers is provided by a function generator at a chosen frequency. In closed loop active control operation, the acoustic pressure signal in the chamber, measured using a piezoelectric pressure transducer, is amplified, phase-shifted, and fed back into the acoustic drivers. By adjusting the gain, phase-shift, position of the pressure probe and the combination of utilized drivers, the system can be tuned to resonate in various acoustic modes. While open loop operation is advantageous in its simplicity, closed loop active control provides the benefit of automatically finding and 'locking on' to various resonant modes.

The removable partition in the middle of the cavity, shown in Fig. 1, was used to establish an initial condition for the experiment. Before each test, the partition was inserted and half of the box was filled with smoke (i.e., one side of the partition). The smoke-filled air in this half of the box was well-mixed and allowed to become quiescent. The rate of mixing between smoke-filled air and smoke-free air in the cavity was measured under various modes of acoustic excitation. A high speed, intensified, digital imaging system was used to record and quantify the mixing process on a plane illuminated by a light sheet (see Fig. 1). The light sheet was created with an argon ion laser and the necessary optics, and a Kodak EctaPro intensified CCD camera was used to acquire images of the Mie scattering from the smoke particles. At the beginning of each test, the partition was then removed, the camera was triggered, and oscillations were excited in the box. The camera, which has a maximum resolution of 239 x 192 pixels and 3634 frame memory buffer, was configured to record 50 frames/second with a 20μs gate time that effectively froze the motion. This allowed a maximum run time of 72 seconds. The collected images were then downloaded to a Intel 486 based computer for storage and analysis.

Analysis Method

A sequence of frames from a typical test is shown in Fig. 2. The first frame shows the initially separate smoke and air in the box just after the partition has been removed and as the resonant acoustic driving is initiated. As time increases, mixing proceeds from large to small scale until, as seen in the final frame, mixing is complete to the scale of the resolution of the camera. Comparison of the relative degree of mixing between two frames can be obtained from the histograms of the images, which show the total number of pixels in an image at each of the possible discrete intensity levels. The black and white intensified camera used in this study has 8 bits of gray scale resolution, which results in 256 possible discrete intensity levels for each pixel.

Figure 3 shows the histograms of the frames as they evolve in time. At the beginning of a test, the histogram of the pixels with respect to light intensity is bimodal. A bimodal histogram represents a highly unmixed situation like that existing, for example, when half of the box is filled with smoke, which scatters light strongly and results in a high intensity region of the image, while the other half has no smoke, and, therefore, appears dark on the image and has a relatively low light intensity level. After the sound is initiated, the smoke and air begin to mix. Fewer of the pixels in the image have either a very high or very low value of intensity while increasingly more pixels have a medium intensity value. After 8 seconds, most of the pixels are at a uniform light intensity, indicating that the system has become well mixed. This is represented by the relatively sharp single peak in the histogram.

The analysis technique used to quantify the mixing observed in this study is based upon a method employed by Liscinsky et al.[17,18] In this technique, a parameter called the "spatial unmixedness" (*Us*) is used to provide a measure of the degree to which a population is mixed. In the present study, the definition of *Us* that is somewhat modified from that given by Liscinsky et al[17,18]. Here, *Us* is defined as

$$U_s = \frac{\mathrm{Var}(I)}{\mathrm{Var}_{t=0}(I)} \tag{1}$$

where

$$\mathrm{Var}(I) = \frac{1}{m}\sum_{n=1}^{m}\left(I_n - I_{ave}\right)^2$$

$=$ spatial variance of pixel intensity

$\mathrm{Var}_{t=0}(I) =$ spatial variance of the $t = 0$ frame

Stated simply, the "spatial unmixedness" *Us* is defined here as the variance of the intensity of the frame at time t normalized by the variance of the frame at $t = 0$ (immediately before the sound was initiated). Normalization allows comparisons between runs where the total amounts of smoke added to the box or the intensity of the light sheet may not be exactly the same. The value of *Us* at t = 0 is, from Eq. 1, defined as 1. As the image becomes increasingly mixed, *Us* approaches 0.

A typical example of the change of *Us* over time is shown in Fig. 4. In this test, the fundamental longitudinal mode (f = 250 Hz at 144 dB RMS.) was driven in the chamber by the two end mounted drivers operating 180° out of phase. Note that local increases (e.g. just after 20 seconds) in the value of *Us* do not violate the second law of thermodynamics, because the measured *Us* represents only a planar slice of the three dimensional volume. While the overall volume cannot " unmix ", measured increases in the value of *Us* represent a localized effect of the

three dimensional mixing process. As the mixing approaches completion, the length scale of the mixing decreases, and the maximum possible fluctuation in *Us* due to three dimensional effects decreases proportionally. The times at which *Us* has decreased to values of e^{-n} for n = 1,2,3 and 4 are shown in the figure. At $\tau(e^{-4})$, *Us* has decreased to 1.83% of its original value. In this study, this was considered to be the point at which the smoke-filled and smoke-free air were fully mixed. The results of a typical measurement of the change of *Us* over time for a test without sound is also shown in Fig. 4 for comparison. In this case, the mixing is driven mainly by convection due to the buoyancy of the smoke (which is slightly warmer than the air temperature) and, to a lesser extent, diffusion. Tests without acoustic driving show that while the air in the box "rolls around" in a slow large scale motion, mixing at smaller scales proceeds rather slowly. This large scale motion accounts for the large fluctuations in the value of *Us*, because these motions will carry the "cloud" of smoke filled air in such a way that more or less of it is in the plane of the laser sheet at any given time.

Mixing Study Results:

A series of experiments were performed to determine the effect of the amplitude of the oscillation upon the characteristic mixing rate (calculated by inverting the measured value of the mixing time) of the smoke and air in the chamber. Because of the chaotic nature of the mixing process, each test was repeated six times to provide better statistical accuracy. Figure 5 shows the measured dependence of the characteristic mixing rate upon the RMS. acoustic amplitude. In the tests, drivers mounted on opposite end walls were used to excite the fundamental longitudinal (1,0) mode, as noted by the inset sketch in Fig. 5.

The figure shows that the characteristic mixing rate increases as the amplitude of the acoustic oscillations increases. The curve in the figure is a least-squares fit through the average of the six data at each amplitude of the equation $r = c/p^{v}$, where r is the mixing rate, p is the amplitude of the pressure oscillations on a linear scale and c and v are determined by curve fitting.

The second series of tests were performed to determine the dependence of the average mixing rate upon the mode of the excited acoustic oscillations. The results of one such series of tests are shown in Fig. 6. In these tests, acoustic oscillations at different longitudinal modes but at a constant RMS. amplitude of 152dB were driven using 2 drivers mounted at opposite end of the cavity. The drivers were operated 180° out of phase for odd modes and in phase for even modes to provide efficient driving. The average mixing rates of the (4,0) and (6,0) modes could not be calculated, because *Us* did not decrease to a value of e^{-4} during the 72 seconds of storage time available with the camera, indicating that the average mixing rate in both cases is below 0.014 s^{-1}.

In this configuration, driving at frequencies corresponding to even acoustic modes appears to produce slower mixing than driving at frequencies corresponding to odd acoustic modes. This

can be attributed to the presence of an acoustic velocity antinode at the interface plane between the smoke-filled and smoke-free air for odd modes of oscillation, and an acoustic velocity node at this interface plane when even modes are excited. The presence of a large acoustic velocity and the analogous large amplitude acoustic displacement at the interface appears to promote more rapid mixing in the cavity. Inspection of the measured mixing rates for excitation of odd modes reveals that increasing the mode number while maintaining a constant acoustic pressure amplitude decreases the mixing rate. The same behavior is shown to occur in at least the first two even modes, and although the mixing rates for the (4,0) and (6,0) modes were too low to be measured at this amplitude, the trend was observed by eye to continue at least to the (6,0) mode.

In order to determine whether the mixing rate depends not only on the mode of acoustic oscillations but also on the geometric configuration of the acoustic drivers, further tests were conducted using non-symmetrical driver configurations. The driver placement was found to strongly influence the mixing behavior observed in the chamber. The results of two experiments using different non-symmetrical driver placements are shown in Fig. 7. In neither of these cases are the mixing rates for even acoustic modes noticeably less than for the odd modes. In fact, in both cases, the mixing provided by the (6,0) mode, which was the slowest mode observed in tests with two, symmetrical, end-mounted drivers, is quite fast with respect to other modes. The marked differences between the results of the three experiments shown in Figs. 6 and 7 demonstrate that the mixing rate of the smoke-filled and smoke-free air in the box depends not only upon the excited acoustic mode, but strongly depends on the placement of the acoustic drivers as well. This result suggests that the mixing is influenced by three dimensional acoustic processes in the "near field" of the drivers and/or acoustic streaming phenomena associated with the drivers. These two processes are discussed in the next section.

Purely longitudinal modes represent only a fraction of the resonant acoustic modes of the cavity. Therefore, experiments were also performed to investigate the effects of transverse and multi-dimensional mode excitation upon the mixing rates. Mixing rates measured for a number of transverse and two dimensional modes are plotted in Fig. 8. The tests were performed using the two bottom mounted acoustic drivers to excite oscillations of 148dB RMS. amplitude in the chamber. The figure shows that while the second pure transverse mode produces a slower mixing rate than the fundamental transverse mode oscillation, this trend is reversed for two dimensional modes where driving the (n,2) combined mode results in consistently faster mixing than the (n,1) mode.

While studying the relationship between the excited acoustic mode and the mixing rate in the experimental test facility, the orientation of the acoustic drivers was found to strongly influence the mixing behavior. In order to investigate the influence of the driver position upon the average mixing rate, disturbances in the acoustic mode velocity distribution in the vicinity of the

driver and acoustic streaming were investigated with laser Doppler velocimetry. The acoustic modes in the cavity were determined by assuming solid boundaries with an infinite acoustic impedance. The drivers mounted on the walls, however, present a finite acoustic impedance and acoustic energy enters the volume through the driver openings. This impedance mismatch between the walls and the drivers results in curvature of the standing wave pattern in the vicinity of the drivers. This effect produces variations in the acoustic mode shape due to the position of the drivers. The magnitude of this effect can be seen in acoustic velocity measurements. Also, velocity measurements as well as observation of the LDV seeding material (aluminum oxide particles) showed that the oscillating driver induces a mean flow radially inward along the wall and outward along the axis of the driver, as shown in Fig. 9. This "acoustic jetting" is similar to the streaming patterns observe by Ingard[16] in a study of the impedance of a circular orifice. Figure 10 shows the axial components of the mean and acoustic velocities along the centerline of the cavity for a test in which one end mounted driver was used to excite the (3,0) mode at 150 dB. The corresponding theoretical velocity amplitude for a standing wave in a solid walled cavity is shown for comparison. The distortion of the standing wave observed in the vicinity of the driver is due to the impedance mismatch between the acoustic driver and the end wall in which it is mounted. The induced mean jet is shown to extend about half a wave length from the driver. The flow appears to reverse over the second half wave length, but the accuracy of the measurements is questionable at such low velocities. The magnitude of the acoustic jetting suggests that it provides an important contribution to the process of mixing in this experimental setup.

Acoustic Control of a Free Jet Using Transverse Excitation:

The main objective of acoustic excitation of free jets is to gain control of the processes that govern the downstream evolution of the jet, generally with the goal of increasing the rate of mixing of the jet with the surrounding flow. Because the burning efficiency and pollutant emission characteristics of combustion processes are directly affected by the mixing of the reactants, acoustic control of turbulent jets is of interest to the development of compact waste incinerators.

The effects of acoustic and mechanical excitation on shear layers and jets has long been the subject of investigation. An overview of the available information on this subject can be found in reviews by Cantwell[19] and Ho and Huerre[20]. It has been shown that the formation and pairing of large, coherent vortices in jet flows can be affected by excitation (for example, Refs. 21-26). By modifying the size and character of the large scale structures, the spreading rate and entrainment of the jet can be influenced.

Transverse and three-dimensional mode oscillations are of interest because of the potential application to combustor cavities in which such modes are often more easily excited than purely longitudinal modes. Ogawa et al.[27] showed that, by using speakers perpendicular to the axis of a jet to provide excitation, the time-averaged cross section of the jet could be distorted to have an elliptical shape.

The goals of the study reported here were to determine whether such a phenomenon would be observed in a ducted jet, to investigate the role of large scale, coherent vortices in the elliptical jet, and to study the effect of this behavior on entrainment and mixing. The affects of transverse mode, standing, acoustic oscillations on the characteristics of a turbulent, circular jet of air were investigated in two different experimental configurations.

Jet mixing Facilities:

In this study, transverse, resonant oscillations were used to excite a subsonic, axisymmetric jet discharging into a chamber with a rectangular cross-section. Tests were performed in two similar experimental facilities. The first facility consisted of closed-ended rectangular duct with inside dimensions of 20.3cm (8in.) wide x 12.7cm (5in.) high x 68.6cm (27in.) long. A schematic diagram of this facility is shown in Fig. 11. The top, the downstream end, and one side of the facility are constructed of acrylic to enable visualization of the jet from various angles. The jet was introduced into the duct through a 0.43in. (1.09cm) ID stainless steel tube. While this facility offers a fairly good model of air flow into a combustor, the recirculation region downstream of the jet dump plane causes difficulty in measurement of the mixing rate and results in generally poor conditions for visualization of the vortical processes involved. Therefore, the second facility, shown in Fig. 12, was developed to minimize recirculation and improve conditions for studying the effect of resonant, transverse, acoustic oscillations on the mixing of a jet with the surrounding

fluid. The important differences between the first facility and the second are the end conditions and the dimensions. The second setup is open at both ends, and the duct has a square cross-section with 12 in. (30.5 cm) sides. In this configuration, the jet induces a mean flow of air through the duct by entrainment. A major limitation of the open-ended duct is that, due to increased losses, high amplitude oscillations are much more difficult to excite.

In both facilities, transverse mode, standing, acoustic oscillations were excited using two Atlas 100W, compression-type, siren drivers mounted on opposing walls near the downstream end of the duct, as shown in Figs. 11 an 12. While the position of the drivers near the downstream end of the duct reduces their efficiency in forcing purely transverse mode oscillations near the jet inlet, it was necessary to place them as far as possible downstream of the inlet to minimize the effects of mean flow disturbances which arise in the vicinity of the acoustic drivers. The maximum acoustic pressure amplitudes that can be achieved in the closed and open-ended facilities are 158dB and 137dB, respectively. Acoustic pressures were measured using Kistler piezoelectric pressure transducers, and mean velocities were measured using a Pitot probe and a Datametrics Barocel pressure sensor.

Excitation of oscillations in the fundamental transverse, resonant, acoustic mode was chosen so that the exit plane of the jet would be subjected to the greatest possible transverse velocity oscillation. This corresponded to frequencies of 850Hz in the closed-ended duct and 585Hz in the open-ended facility. The excited acoustic fields were characterized by mapping the pressure distribution in cross-sections perpendicular to the flow axis. The pressure amplitude for each test was measured at a corner of the duct to assure measurement at a pressure maximum, and at the exit plane of the jet to avoid influence from axial pressure variations in the duct.

Flow Visualization:

For visualization studies, cooled tobacco smoke was introduced into the flow, and Mie scattered light from a laser sheet was observed. In the closed-ended facility, the smoke was injected through a 2.5mm (0.1in.) annulus around the jet to produce a visible mixing layer. In the open-ended setup, smoke was mixed directly into the stream of air injected through the jet. Light sheets could be introduced into the duct either from the downstream end, which allowed a planar slice of the jet to be observed, or through the side of the duct, which provided cross-sectional views of the jet at various downstream locations.

Two lasers with different advantages were used in this study. With a Metalaser Technologies 20W copper vapor laser and a combination of spherical and cylindrical lenses, a light sheet was produced that was approximately 1.9mm (0.075in.) thick at the investigated region. The pulse rate of the laser is optimized for 6kHz operation, and the pulse width is nominally 30ns FWHM. The short pulse width and relatively high pulse energy of the Cu vapor

laser make it especially well suited to stop-motion photography in high speed flows. To avoid focusing problems due to chromatic aberration, the two components of the laser light were separated using an optic that reflects the yellow light and transmits the green component. Only the green light (510.6nm) was used for visualization.

Flow visualization images were recorded using a Kodak EktaPro EM1012 intensified motion analyzer. This CCD based system allows a maximum full-frame collection rate of 1000 frames/sec. Acquiring images at a constant phase of the acoustic cycle and averaging a number of these phase-locked images provides a means to determine the observed periodic phenomena from turbulent processes. In order to collect phase-locked images, the laser was triggered by a pulse train synchronized with the acoustic signal. The camera provides 8 bit gray scale response and has a full-frame resolution of 239 x 192 pixels.. The imaging system is equipped with enough memory to store 3600 full size frames, which can then be downloaded to a PC for analysis and storage using an IEEE 488 interface.. The effective gate time was determined by the pulse width of approximately 30ns.

Visualization of the coaxial jet in the closed-ended facility indicates the presence of three distinct regions in the flow: 1) unmixed smoke in the shear layer that scatters much of the incident laser light, indicated by dark regions in negative images, 2) the core region of the jet where no smoke has penetrated, which appears bright, and 3) regions where the smoke and air are mixed, indicated by medium intensity in the images. Recirculation of mixed smoke and air causes poor contrast on the outside of the shear layer. Figure 13 shows a sequence of images (shown in negative for clarity) in which the jet exit velocity is 31m/s (101.4ft/s) and the amplitude of the oscillation was varied from no sound to 948Pa RMS (154dB), which corresponds to a velocity amplitude at the jet exit of approximately 3.3m/s 0 to peak. When oscillations were excited, the jet was observed to 'flap' back and forth in the plane of the oscillations as large scale, coherent, vortical structures were alternately shed from opposite sides of the jet inlet. By dividing the jet exit velocity by the measured distance between vortices it was determined that each side of the jet sheds one vortex per acoustic cycle, and that the opposing vortices are shed 180° out of phase. These structures are then convected downstream by the mean flow. No visible vortex shedding was observed in the plane perpendicular to the oscillations. This behavior causes the excited jet to have, in a time-averaged sense, an elliptical cross section, as was observed by Ogawa et al.[27] The phase of oscillation at which these images were obtained was not fixed; therefore, the stage of vortex shedding in each image varies. It was observed that the size of the vortex structures shed from the jet mouth depended upon the amplitude of the oscillation.

Time averages of images (random phase images, not phase-locked) in which the jet exit velocity was 31m/s (101.4ft/s) for various amplitudes of oscillation were used to measure the effect of the sound amplitude on the effective spreading angle of the jet and on the jet core length,

which provide measures of the scale of the induced vortical structures. The averaging was performed on sequences of 200 images, which corresponds to 0.2 seconds and 117 acoustic cycles. The data in Fig. 14 show that as the amplitude increases, the length of the jet core decreases. The rate of shortening decreases as the amplitude increases, which is to be expected, since the core length can never reach zero. The angle between the outer edge of the mixing layer and the jet axis is also graphed in the figure as a function of the oscillation amplitude, and is shown to increase with oscillation amplitude.

Tests were conducted in which the jet velocity was varied and the amplitude of the acoustic oscillation was held fixed at 632Pa RMS (150 dB). The jet velocity was varied from 10.3m/s (33.8ft/s) to 41.2m/s (135.2ft/s), and the frequency was a constant 855Hz, resulting in a variation of Strouhal number from 0.91 to 0.23. Instantaneous images from these tests are shown in Fig. 15. The data suggest that, over the investigated range, the size of the structures shed from the jet exit plane increase with the jet velocity, while the time over which these structures remain coherent decreases. The vortex structures observed in the image of the 10.3m/s jet are small, distinctly formed and remain coherent for approximately three convective wavelengths (3.3 jet diameters). At a jet velocity of 41.2m/s, the alternating nature of the vortex shedding causes the jet to flap back and forth. The structures of the vortices are less clear at this velocity, and the vortices appear to lose coherency after only one convective wavelength (4.4 jet diameters). While the length over which these structures remains coherent increases with the jet exit velocity, the time of coherence decreases from approximately 3.5ms at 10.3m/s to about 1.2ms at 41.2m/s.

The effect of the Strouhal number on the effective spreading angle of the jet and on the jet core length was measured from time-averaged images. Figure 16 shows the half angle of the outer edge of the jet in the plane of the acoustic oscillation as a function of the Strouhal number. For comparison, data showing the effect of the Strouhal number on the spread angle of the jet with no oscillations present is also shown, and as expected, is independent of the jet velocity. On the other hand, experiments with transverse acoustic oscillations present in the cavity show that the spread angle of the jet in the plane of the oscillations has a maximum of about 60° degrees that occurs near $St = 0.5$. Similarly, the jet core length is shown to be independent of the jet velocity when no oscillations are present. With oscillations present, the jet core length has a minimum value of about 1.3 jet diameters near $St = 0.5$.

Visualization of the jet in the open-ended setup provides a clearer view of the processes occurring at the outer edge of the shear layer and farther downstream of the jet than images in the closed duct. However, since the maximum oscillation amplitude is an order of magnitude smaller than that in the closed cavity, the size of the shed structures achievable in the open-ended facility is significantly smaller. Figure 17 shows a phase-locked average image of the jet in the open-ended setup with the light sheet in the direction of the oscillation. The flapping motion that had

been observed in the closed duct is apparent near the jet exit in Fig. 17. Downstream of this region, the periodic structures lose coherence, and the smoke appears to mix turbulently. This region could not be clearly observed in the closed-ended facility due to the recirculation of the mixed smoke and air.

Instantaneous cross-sectional images of the jet were obtained at a distance of 13.6cm (5.4in.) downstream of the jet exit, which is beyond the distance where the vortical structures appear to lose coherence. With no oscillations present, the images show roughly circular smoke distributions with dark, high concentration cores and light, low concentration fringes. A typical image is shown in Fig. 18a. Light and dark pockets at the fringe and core are distributed randomly. Instantaneous images of excited jets (a typical image is shown in Fig. 18b) show highly distorted distributions, in which the core is stretched or bifurcated into two distinct cores in the direction of the excitation. The angle of the tilt is consistent with pressure field measurements, which showed that the direction of the acoustic oscillations was at a slight angle to the horizontal centerline.

Comparison of the phase-locked averaged images of the unexcited and excited jet in Fig. 19 shows a distinct effect due to the acoustics. The transverse mode acoustic excitation has clearly caused bifurcation of the jet, because there are two jet cores visible at the same instant of the acoustic cycle. Such jet bifurcation phenomena was first observed by Brown, [28] who described and photographed the phenomenon. Jet bifurcation was also observed by Reynolds *et al.* [25, 26, 29] in several studies on jet excitation, but from these studies it was concluded that a combination of axial and transverse excitation was required to bifurcate the jet.

Measurements of the mean velocity profile in the open-ended facility, with and without oscillations present, were performed along the horizontal and vertical axes of the duct using a Pitot probe inserted from the downstream end of the duct. Each average velocity was calculated from 500 samples collected at 100Hz. Due to the non-linearity of Pitot-probe velocity measurements, the relative error increases as the measured velocity decreases. Therefore, the accuracy of measurements below about 2m/s (6.6ft/s) is questionable.

Comparisons of the velocity profiles in the horizontal axis (in the direction of the acoustic oscillations) are shown in Fig. 20. At each of the three axial locations measured, the presence of oscillations resulted in a wider velocity profile. The profile at 13.6cm (5.4in.) downstream of the jet exit plane is obviously bimodal, which confirms that the jet has bifurcated. Comparisons between the unexcited and excited mean velocity profiles perpendicular to the direction of the oscillations are shown in Fig. 21. While the centerline velocities are lower when oscillations are excited, no broadening of the jet is evident in this direction.

Mixing Rate Measurements:

In order to quantify the effect of the bifurcation on the spatial mixing rate, a computer code was developed that used pixel intensities to compute a quantity that represents the entropy of mixing from instantaneous cross-sectional images. This procedure was based on a similar technique by Everson *et. al.* [30] A quantity that represents the total 'mixing entropy' of an image is determined by calculating the sum of the mixing entropy, based on pixel intensities, at each point. The equation used to calculate the entropy of mixing of two gases is:

$$S_m = -\sum_x \left[C(x) \ln(C(x)) + (1 - C(x)) \ln(1 - C(x)) \right] \quad (2)$$

where *C(x)* is the local concentration of one component and (1-C(x)) is the local concentration of the second component. The first term on the right side of the equation represents the entropy of mixing of the first component into the second, and the remaining term is the entropy of mixing of the second component into the first. The state at the exit of the jet, where virtually no mixing has taken place between the jet and the surrounding air, is considered to have zero entropy. The state far downstream, where the smoke and the entrained air are uniformly distributed, was considered to be the maximum entropy state, and was used to normalize the measured entropy values. This procedure minimizes the influence of the rate of smoke seeding, the laser brightness, and the gain of the intensifier on the results. Due to the turbulent nature of the mixing process, the entropy varies over time. Therefore, the entropies were calculated for 100 instantaneous frames and then averaged. The process is not commutative; calculating the entropy of an averaged image produces a much different result.

Figure 22 shows a plot of the change in normalized entropy of mixing with the jet exit velocity. The entropy of mixing for the acoustically excited jet is consistently higher than that of the unexcited jet. The peak effect of the acoustic excitation occurs when the Strouhal number is between 0.2 and 0.3. This does not agree, however, with the preferred range of Strouhal number measured in the closed-ended setup, which was observed to peak near $St = 0.5$.

In other studies of acoustically excited jets, the preferred Strouhal numbers observed vary somewhat. The peak Strouhal number reported by Vlasov and Ginevskii [31] is 0.5, Crow and Champagne [32] report 0.3, and Lepicovsky *et al.* [33] suggest a range between 0.4 and 0.5. These agree with the results obtained in the closed-ended facility, even though the current study uses asymmetric rather than symmetric excitation. The preferred Strouhal number range measured in the open-ended facility is somewhat lower than those of previous jet excitation studies. In dual-mode excitation tests, however, Parekh *et. al.* [25] determined the preferred value of *St* to be 0.3 when calculated with the transverse mode frequency, which corresponds well with the results of the open-ended facility.

The fact that both the open and closed-ended results are reasonable, however, does not explain the difference. One possible explanation for this discrepancy is that one of the two mixing quantification techniques may be producing erroneous results. In order to determine whether this is the case, the average spreading angles in the open-ended facility of excited and unexcited jets at various jet velocities with a constant acoustic pressure level and frequency were measured, and the results were compared to those of the mixing entropy measurements. The results of the two methods are shown in Fig. 23. It should be noted that the units of these measurements are completely different, so the comparison can be qualitative only. While the angle measurements are noisier, due to difficulties inherent to the technique, both techniques show that the fastest mixing occurs when *St* is between 0.2 and 0.3. This leads to the conclusion that the difference in the results in the open and closed-ended boxes is not due to the analysis techniques used.

If the difference in results from the two facilities is not due to the analysis techniques used, then it is due to some physical cause. The difference is most likely due to the presence of the recirculation region in the closed-ended experiment, which may affect the vortex shedding and interacting processes.

The data plotted in Fig. 24 show the effect of the amplitude of oscillation on the entropy of mixing. The three curves shown represent different jet exit velocities, and therefore, different Strouhal numbers. While the error at the lowest sound pressure level is estimated to be 5%, the curves all show increased mixing with increased amplitude. It is also clear that while the jets with velocities of 22.13m/s (72.6ft/s) and 25.22m/s (82.75ft/s), which correspond to Strouhal numbers of 0.29 and 0.25, respectively, are affected very similarly by the amplitude of the oscillation, the jet at 12.35m/s (40.5ft/s), St = 0.52, is much less sensitive to the amplitude. Note that the curves appear roughly linear with amplitude in decibels, which suggests an exponential dependence of the mixing rate upon the pressure.

Sublimation Rate and Heat Transfer Studies:

The rate at which solid fuel pyrolyzes is important to the solid waste incineration process. Previous research suggests that the increased heat and mass transfer associated with oscillatory combustion systems will increase the rate of pyrolysis. In a study of the velocity coupling phenomena by Van Moorhem *et. al.*[34], in which dry ice (solid phase carbon dioxide) was used to simulate the fluid dynamic aspects of flow above a burning solid propellant, it was clearly shown that acoustic velocity oscillations affect sublimation process of the dry ice. Results suggested that turbulent forced convection was responsible for the increase in sublimation rate.

In previous studies that used dry ice to simulate solid fuel combustion by Van Moorhem *et al.*[34, 35], the mean flow through the cavity consisted solely of the sublimated gas from the surface of the dry ice. This technique, while similar to a solid rocket motor, in which all the flow is released from the burning propellant, does not allow for independent evaluation of the effects of mean velocity. In the study reported here, the effect of acoustic mode velocity oscillations on the pyrolysis rate of solid fuel, simulated by the sublimation of dry ice, under a variety of acoustic and flow conditions was investigated.

The use of dry ice sublimation to simulate the pyrolysis of solid fuel in an acoustically excited incinerator allows the fluid mechanics of the problem, i.e., the heat and mass transfer processes, to be separated from the combustion process. The experimental setup also simulates the pyrolysis of wood or coal in a pulsed combustor or acoustically excited combustion chamber. The results may be extrapolated, with some caution, to provide insight into the combustion of propellant in a rocket motor or fuel in a hybrid rocket or solid fuel ramjet.

There are a number of reasons why dry ice makes an attractive model for solid fuel pyrolysis. First, the sublimation of dry ice provides a reasonable model of the pyrolysis process; the rate of sublimation depends upon the heat transfer rate to the dry ice and the sublimated mass is transferred away in gas phase. Second, due to ambient water vapor convected to the surface of the dry ice and the presence of a small amount of water trapped in the dry ice during the manufacturing process, dry ice produces a visible "fog" as it sublimes, which provides an excellent visualization opportunity. And third, it has been shown that dry ice sublimation provides a reasonable degree of dynamic similarity to a burning solid propellant.[34]

Experimental Facilities:

Figure 25 is a schematic diagram of the utilized experimental setup. The facility consists of a rectangular wood and acrylic box with a 3.8cm (1.5in.) diameter air inlet on one end and a 5.1cm (2.0in.) diameter exhaust port on the opposite end. The inside of the cavity is 69.9cm (27.5in.) long, 20.3cm (8.0in.) wide, and 12.7cm (5.0in.) high.

Two Atlas 100W, compression-type, siren drivers are mounted in the centers of the opposing 12.7cm (5.0in.) walls near the downstream end of the chamber. While it has been the authors' experience that positioning the drivers near the downstream end of the duct reduces the maximum amplitude obtained when driving the fundamental transverse resonant mode (i.e., with velocity oscillations perpendicular to the flow axis) with constant input power, it was necessary to place them as far as possible downstream of the inlet to minimize the effects of secondary mean flows generated by the acoustic drivers[36]. This positioning of the drivers was reasonably effective for driving the longitudinal, transverse, and combined, two-dimensional resonant modes of the cavity. The acoustic amplitude was determined using Kistler piezoelectric pressure transducers mounted on the walls and a Brëul and Kaër 0.25in. microphone on a movable probe.

Dry ice for this experiment was produced using an Insta-Ice, 454g (1lb.) capacity, dry ice form and standard 23kg (50lbs.) cylinders of commercial grade CO_2. This produces rectangular blocks of dry ice, 17.2 cm (6 3/4in.) x 7.3cm (2 7/8in.) x 4.8 cm. (1 7/8in.). The center of a block of dry ice was placed at 0.25L (where L is the chamber length) downstream of the air inlet and centered between the sides. The blocks were placed on a 1cm (3/8in.) thick layer of quartz felt insulation to minimize heat losses to the bottom wall. Tests were performed in two different configurations; with the long axis (17.2 cm) of the blocks aligned with the long axis (69.9cm) of the cavity, referred to as longitudinal orientation, and with the long axis of the dry ice block perpendicular to the long axis of the cavity, referred to as transverse orientation. The smallest dimension of the dry ice block, 4.8 cm, was always in the vertical direction.

The exhaust flow from the chamber was sampled with a Beckman model 864 infrared CO_2 analyzer to measure the percentage of carbon dioxide present. The CO_2 concentration was recorded using a Pentium based computer using a LabVIEW data acquisition program and an IOTech 488/8SA A/D converter. From the measured exhaust CO_2 concentration data and the known flow rate of incoming air, the amount of excess CO_2 sublimated from the block of dry ice was calculated using the following formula:

$$\dot{m}_{CO_2} = \left(f_m - f_{air}\right)\left(\frac{\dot{m}_{air}}{1 - f_m}\right)\left(\frac{W_{CO_2}}{W_{air}}\right) \tag{3}$$

where $\dot{m}_{CO_2}$ is the sublimation rate of the dry ice, f_m is the measured volume fraction of CO_2, f_{air} is the volume fraction of CO_2 present in the incoming air, $\dot{m}_{air}$ is the measured mass flow rate of air into the chamber, and W_{CO_2} and W_{air} are the molecular weights of CO_2 and air. A digital balance was used to measure the mass of the dry ice block at the start and conclusion of each test. The difference of these masses equals the mass of CO_2 lost by the dry ice block. Comparison of this

value and the sublimated mass calculated from the exhaust gas analysis technique described above was used to check the results of the experiments.

The presence of a cold dry ice block in the cavity results in temperature and density gradients in the facility. These gradients affect the speed of sound, and, therefore, the wavelength of the standing acoustic oscillation in the cavity. In order to confirm that the acoustic velocity maximum was indeed located above the block of dry ice, pressure measurements were taken at a number of positions along the axis of the cavity with an inlet flow velocity of 1.0m/s and a 145dB acoustic oscillation amplitude. Figure 26 shows the measured acoustic pressure along the axis of the cavity for the second longitudinal (2,0) mode with the dry ice block in both the longitudinal and transverse orientations. The frequencies that corresponded to these modes were 490Hz and 470Hz, respectively. To provide uniform scaling, the measured pressure amplitudes were normalized by the maximum pressure amplitude measured at those conditions. It is clear that while the temperature effects and the geometrical disturbance imposed by the dry ice affect the standing wave shape, the location of the acoustic pressure minimum (and the acoustic velocity maximum) occurred near the center of the ice block. Also shown in Fig. 26 is the pressure distribution when the cavity was excited in its fourth longitudinal (4,0) mode with the block oriented longitudinally, which corresponds to a driving frequency of approximately 1000Hz. In this mode, an acoustic pressure maximum occurred at the center of the dry ice block.

A time sequence of events was established to maintain as much repeatability of conditions between runs as possible. This sequence included making a dry ice block, weighing the block, placing the block in the facility, triggering the data acquisition system, and initiating the acoustic driving. Because the temperature of the gas in the cavity was dependent upon the heat transfer to the ice block, the frequencies corresponding to the various resonant modes varied slowly with time. To compensate for this, the driving frequency and power input to the speakers were periodically adjusted to maintain a constant amplitude of the driven acoustic mode. The amplitude of the oscillation was never allowed to vary more than 5% during a run. At the end of a specified time period, the block was weighed again.

In order to establish the repeatability of the procedure, a series of tests was performed in which the start-up procedure was followed but no acoustic driving was used. The results of this series of tests is shown in Fig. 27. The data show that about one minute was required for the cavity to reach operating conditions and for the exhaust gas to pass through the sampling system. After this period had passed, the maximum difference in measured CO_2 flow rates observed between runs was about 0.3L/m (0.01cf/m).

Flow Visualization:

Flow visualization images were recorded using a Kodak EktaPro EM1012 intensified motion analyzer, described previously in this report. A Metalaser Technologies 20W copper vapor laser and optics necessary to produce a light sheet, also described previously, were used to illuminate the condensed fog layer near the dry ice.

The images in Fig. 28 show close-up views of the fog layer at the downstream corner of the dry ice block. The images have been printed in negative for clarity. Figure 28a shows the thin, uniform layer present in the absence of mean flow and acoustic oscillations. Figure 28b shows the same block positioned with its center at a velocity maximum of a 145dB acoustic oscillation that is directed left and right across the page. This amplitude corresponds to a velocity fluctuation amplitude of approximately 1.3m/s (4.3ft/s) above the ice block. The frequency of the acoustic driving was 490Hz. A vortical structure is visible near the corner of the block. When a mean flow of air is injected into the chamber (from left to right) at 0.5m/s (1.6ft/s) without acoustics, as shown in Fig. 28c, small, irregular structures are present in the boundary layer, and convected downstream by the flow. Figure 28d is an image in which the same mean flow is present and a 145dB oscillation is excited. In this case, the combined effects of the mean convective flow and the acoustically forced velocity oscillations increase the size of the cloud and the chaotic behavior of the flow above the dry ice.

Figure 29 presents images of the illuminated fog layer with higher amplitude acoustic oscillations present in the chamber. The perspective has been slightly altered, providing a more complete view of the flow around the block The light sheet enters from the downstream end of the facility, thus placing the upstream face of the block in a shadow. In Fig. 29a, where no oscillations and no mean flow are present, the condensation layer above the dry ice block is very thin, as in Fig. 28a, and the cold, sublimated gas simply spills over the edges of the block. Figure 29b illustrates the mixing effect of the acoustic oscillations. The fog layer, under these conditions, extends above the dry ice to a height greater than the thickness of the block. At this amplitude, laminar coherent structures like those visible in Fig. 28b no longer occur, and the boundary layer appears turbulent. In Figs. 29c and 29e, the fog layer above the block is again thin, but in these images some fog can be seen to collect in the wake of the dry ice block. The images in Figs. 29d and 29f show that the thick cloud generated above the block by the acoustic excitation is sheared downstream by the mean flow.

Experimental Results

In the first series of tests performed, the cavity was forced to resonate in the fundamental transverse acoustic mode (0,1). The frequency corresponding to this mode is approximately 835Hz. when the box is filled with air at room temperature, and roughly 10% lower when dry ice

is positioned in the cavity. For these tests, the block of dry ice was placed in the transverse orientation (described previously), where it was subjected to the maximum amplitude of acoustic velocity oscillations. The mean air velocity at the inlet for this sequence of tests was 1.25m/s. Tests were performed at six amplitudes of acoustic oscillation, ranging from no excitation to 150dB. Each curve in Fig. 30 shows the averaged results from three tests. The sublimation rates are observed to reach a peak when newly formed blocks are place in the box and then slowly decrease, due to the reduction in surface area of the dry ice blocks as mass sublimes over time. The acoustic driving is initiated at 2min. into the run, which accounts for the discontinuity apparent in some of the curves at that time. It is clear from the data that the sublimation rate increases in the presence of acoustic excitation. The magnitude of the increase depends upon the amplitude of the oscillations. Figure 30 indicates that for the investigated test conditions, an amplitude of 145dB is needed before the effects of the oscillations become evident, and an amplitude at or above 150dB is necessary before these effects become significant. It is interesting to note that 145dB corresponds to a velocity amplitude of roughly 1.25m/s, which is the air inlet velocity.

Comparison between the measured mass of CO_2 lost by the dry ice block and the integral of the flow rate of CO_2 in the exhaust determined by gas sampling is shown in Fig. 31. The measured weight losses are shown to be in good agreement with the values calculated from the exhaust sampling procedure, which provides validation of the gas sampling results.

A sequence of tests was performed in which the effect of the acoustic amplitude upon the average sublimation rate was investigated at various mean flow velocities. In these tests, the second longitudinal resonant mode of oscillation (the 2,0 mode) was excited. In this mode of excitation, the center of the dry ice blocks were subjected to an acoustic velocity maximum. Tests were performed with the dry ice blocks positioned in both the longitudinal and transverse orientations. The frequency corresponding to this mode is approximately 490Hz with longitudinal orientation of the dry ice block and roughly 470Hz with transverse orientation.

Results of this series of tests, plotted in Fig. 32, present the total mass change of a block of dry ice at the given acoustic amplitude for several mean flow rates. The results show that, for both longitudinal and transverse orientations of the block, the sublimation rate increases with the amplitude of the acoustic oscillation. It is also clear that, as expected, increasing the mean flow rate of air into the cavity increases the sublimation rate.

Figure 33 shows the relative importance of the acoustic velocity effects at different mean flow velocities. It is difficult to directly compare results measured with different mean flow rates, because the sublimation rate depends on both the mean flow rate and the acoustic velocity amplitude. In order to allow comparison of data acquired with different mean flow rates, the data was normalized by dividing the total mass change at any given air flow rate and amplitude by the

total mass change at the same air flow rate but without acoustic excitation, then subtracting unity so that the results show only the increase in sublimation rate. This is expressed as:

$$E = \frac{\Delta m_{v,p'} - \Delta m_{v,0}}{\Delta m_{v,0}} \tag{4}$$

where E is the normalized sublimation increase, $\Delta m_{v,p'}$ is the change in mass at with mean flow and acoustic oscillations, and $\Delta m_{v,0}$ is the change in mass with the same oscillation amplitude but without acoustics. The results show, quite interestingly, that when the acoustic velocity amplitude was held constant and the mean air flow rate was increased, the relative effect of the acoustic velocity on the sublimation rate increased. An explanation for this unexpected behavior is suggested by the images shown in Fig. 28. When acoustic oscillations are present, the mass transport rate in the vicinity of the dry ice is apparently much greater than when no oscillations are present. At low mean velocities, the mass that is released from the dry ice is recirculated in the vicinity of the block. As the convective velocity increases, however, this sublimated mass is sheared away from the dry ice block and is replaced by the flow of warm incoming air. Therefore, in this configuration, the combined effect of the acoustic "scouring" action and the forced convection provides an effective means of transporting warm air to the surface of the dry ice block and cold sublimated gas away from the surface.

Tests were also performed to compare the sublimation rates measured with the dry ice block located at an acoustic velocity maximum to the rates measured with the block located at an acoustic pressure maximum. Maintaining the mean velocity distribution was considered more important to the results of the test than the frequency of the excitation. Therefore, the position of the transversely oriented dry ice block in these tests was the same in each run. An acoustic velocity maximum could be excited above the dry ice block by driving the system in its second longitudinal (2,0) mode. Alternately, by forcing the cavity to resonate in its fourth longitudinal (4,0) mode (approximately 1000Hz), a pressure maximum was positioned above the center of the block instead of a velocity maximum, as shown in Fig. 26. For both acoustic modes, the acoustic amplitude was fixed at 150dB. The results of this test, normalized using Eq. 4, are shown in Fig. 34. The results indicate that the acoustic velocity oscillations have a much more pronounced effect upon the sublimation rate than pressure oscillations for this experimental configuration and test conditions.

Effects of Pulsations on Incineration:

A model incinerator capable of burning liquid and solid waste surrogates in the presence of transverse and multi-dimensional mode acoustic oscillations was developed. This facility was used to measure the effects of acoustic oscillations on combustion rates as well as NOx, CO, and CO_2 levels present in the incinerator exhaust. This study was performed in three parts: liquid fuel, smoldering solid char, and burning solid fuel. Each of these parts is discussed below.

Facilities:

A schematic of the pulsed incineration facility, configured for liquid fuel combustion, is shown in Fig. 35. The majority of the combustor is made of carbon steel, with the exceptions of an access panel in the top, which is aluminum, and the fused quartz windows. The bottom surface of the combustor is fitted with blow-out panels that are designed to protect the operator and the equipment in the event of an explosion. The side panels are constructed to be modular, so that the windows, the acoustic drivers, and all wall-mounted instrumentation can be repositioned wherever desired. The acoustic drivers are 100W Atlas siren drivers, and air cooling is provided to prevent burning of the diaphragms. The amplitude of the pressure oscillation is measured with a water cooled, Kistler piezoelectric pressure transducer, and a number of transducers mounted to moveable probes allows for characterization of the pressure away from the walls and are used as a signal source for the active control system discussed below. Temperatures are measured using Omega type K thermocouples. Exhaust gases were sampled and analyzed using Beckman carbon dioxide, carbon monoxide, nitrogen oxide, and oxygen analyzers. The outputs of the gas analyzers were measured with an Iomega data acquisition system on a Pentium based computer with LabView software.

The acoustic driving in the incinerator is achieved through one of two methods. First, for open loop operation, a sine wave at a chosen frequency from a function generator is amplified and fed into the acoustic drivers. In closed loop active control operation, the acoustic pressure signal in the chamber, measured using piezoelectric pressure transducers, is amplified, phase-shifted, and fed back into the acoustic drivers. By adjusting the gains, phase-shifts, and the positions of the pressure probes, the system can be tuned to resonate in various acoustic modes. While open loop operation is advantageous in its simplicity and constant frequency, closed loop active control provides the benefit of finding and 'locking on' to various resonant modes.

The ability of the active control system to lock on to a resonant acoustic mode is quite useful in the incinerator, because temperature distribution in the combustion chamber not constant, which causes the resonance characteristics to behave unpredictably. It has been observed, however, that when the losses associated with a certain resonant mode become excessive, usually due to the temperature distribution in the chamber, that the active control

system can 'jump modes', i.e., suddenly change from one frequency to another. Pure transverse modes appear to be especially difficult to maintain in the presence of large axial temperature gradients. Therefore, many of the hot flow tests were performed using multidimensional modes that were combinations of the first transverse mode with a longitudinal mode. The (4,1) mode, for example, could be maintained during the varying thermal conditions of combustion tests. Also, simply maintaining the correct mode does not provide a constant amplitude of oscillation. Large variations in the acoustic amplitude are observed in some tests, especially when the temperatures vary widely over the test period when using the active control system. These variations are, however, much less that those observed with constant frequency driving.

Liquid Fuel Study:

A problem with studying the burning of solid wastes is that when solids burn, their surface regresses, which results in a time dependence of the combustion rate and characteristics. The goal of modeling solid waste incineration with liquid fuel pool combustion was to create a steady state model of a burning material with constant size and burning surface area. Liquid fuel was fed into the burner using a system described in Fig. 36. The aluminum liquid fuel burner was 5cm (2in.) square and 1.9cm (3/4in.) high. The fuel level in the burner was maintained by pumping fuel to both the burner and the leveling vessel at a rate faster than the burning rate. Excess fuel overflowed into the standpipe of the leveling vessel and flowed back to the pump reservoir. The leveling vessel was mounted to a micrometer that controlled its height, and therefore, the fuel level in the burner. The burning rate was determined by measuring the rate of decrease of fuel in the reservoir. The flame was extinguished by dumping the fuel from the burner by opening the control valve.

Initial results, shown in Tables 1 and 2, suggest that acoustic oscillations increase the rate of liquid fuel incineration for both methanol and a mix of methanol and gasoline. The results also suggest that the emissions of CO are increased by the presence of oscillations, while the NOx emissions are reduced by oscillations. These results, however, are rather untrustworthy due to a myriad of problems associated with the liquid combustion studies.

One major difficulty encountered with this study is that the combustion was not steady even when oscillations were not present. On a time scale of minutes, a methanol flame would switch from burning with a blue flame at a certain combustion rate to a yellow flame with a significantly higher combustion rate, then switch back again. Also, the temperature in the combustor, and therefore the evaporation rate of the fuel, varied considerably during runs. These effects made determining a base line burning rate impossible. Also of significance is that flames could not stay attached to the liquid fuel burner at high amplitudes of acoustic oscillation, and would blow off.

Table 1. Exhaust gas analysis of liquid fuel burning

Fuel : Methanol

Run No.	p' max [dB]	NOx [ppm]	CO2 [%]	CO [%]	O2 [%]	Fuel Flow Rate [mL/min]
1	(no sound)	5.4	3.10	0.003	16.97	2.81
2	(no sound)	5.1	3.17	0.003	16.88	2.81
3	123	4.7	3.36	0.003	16.64	3.20
4	130	4.6	3.62	0.004	16.29	3.20

Table 2. Exhaust gas analysis of liquid fuel burning

Fuel : 80% Methanol, 20% Gasoline

Run No.	p' max [dB]	NOx [ppm]	CO2 [%]	CO [%]	O2 [%]	Fuel Flow Rate [mL/min]
1	(no sound)	5.5	4.00	0.005	15.59	2.40
2	(no sound)	6.1	4.21	0.007	15.32	2.40
3	142	5.3	4.40	0.027	15.00	2.73
4	143	4.7	4.47	0.034	14.91	2.73

Another interesting problem associated with the liquid fuel system is that when the acoustic velocity amplitude reached a certain level, the fuel began to spray out of the burner. The sequence of images in Fig. 37 shows a methanol spray generated by the high amplitude acoustic oscillations. Figure. 37a shows the burner, with no flame, illuminated from the side by a light sheet. The image is shown in negative for clarity. In Fig. 37b, a transverse mode, 850Hz, 158dB, acoustic oscillation has been initiated, and the fuel has begun to spray from the edges of the burner. A short time later, the spray appears to come from the center of the burner and fills the chamber with droplets, as shown in Fig. 37c. Preliminary testing shows that the acoustic amplitude necessary to generate a spray is greater for water than for methanol, which suggests a surface tension and/or specific gravity dependence. While this effect is very interesting, for obvious reasons, it makes the use of the liquid fuel burner unacceptable for modeling solid waste incineration at high acoustic amplitudes.

Due to the difficulties encountered with the liquid fuel burner, combined with our lack of confidence in the ability of the liquid pool fire to adequately model the incineration of a solid fuel, it was decided to use solid fuels as waste surrogates in the remainder of the study.

Char Smoldering Study:

The combustion of a solid material typical of waste produced on board a ship can generally be divided into two phases. In the first phase, the majority of the reaction takes place in a luminous flame region, in which volatiles pyrolized from the waste oxidize in a diffusion type flame structure. In the second phase, after a large portion of the volatiles have been burned, most of the reaction takes place near the surface of hot char, which consists mainly of carbon and non-combustible ash. Of course, there is usually no clear division between one phase and the next, and overlap of the two processes occurs. The reaction rate of the smoldering stage is expected to depend strongly upon the rate of oxygen transport into the surface of the solid. In this phase of the study, charcoal was burned in the pulsed incineration facility to study the effects of acoustic oscillations on the combustion rate and the emissions from a smoldering solid, representing the final stage of solid waste incineration.

Tests were performed in which a single piece of commercial charcoal was burned and with 5 briquettes burning together. The schematic of the experimental setup in Fig. 38 shows how charcoal briquettes were arranged in the combustor for 5 briquette tests. The charcoal was placed on a 0.125in. thick piece of quartz felt insulation to reduce heat transfer to the bottom wall of the combustion chamber. The charcoal are aligned along the centerline of the combustor so that they are exposed to a maximum velocity oscillation in the transverse direction. Because the temperature distribution in the chamber is unsteady, the exact relationship between the acoustic pressure and the acoustic velocity amplitudes is unknown. The pressure amplitude, however, which is measured at the wall adjacent to the center of the charcoal arrangement, does provide an approximate measure of the velocity amplitude to which the charcoal is exposed.

At the start of each test, a small quantity of mineral spirits was added to the charcoal to aid ignition. Combustion was assumed to be complete when the CO_2 concentration in the exhaust gas returned to its original, pre-combustion value. Typical time traces of the NO_x, CO_2, and CO present in the exhaust for combustion of 5 charcoal briquettes are plotted in Figs. 39 and 40 for steady combustion and oscillating combustion, respectively. The most obvious difference between combustion with and without pulsations is that the total burning time is significantly shorter when oscillations are present. The rates of CO and NO_x emissions are much higher, but occur over a shorter duration due to the increased burning rate.

Figure 41 shows the total burning times of the charcoal and the sound pressure level present in the chamber for a number of tests. Tests were conducted for the 5 charcoal block arrangement with both pure transverse mode oscillations and higher frequency but lower amplitude combined mode oscillations. When no sound is present, the burning time for a 5 briquette arrangement is shown to be 1.5 times greater than the burning time for a single block of charcoal. This is reasonable, because the presence of multiple blocks reduces the oxygen available and the rate at

which oxygen can reach the surface of any one briquette by physically blocking the surface. The same factors, reduced oxygen availability and surface interference, are exactly the reasons that we would expect the 5 briquette arrangement to be more affected by acoustic mixing enhancement than a single charcoal block, and the results show (neglecting, for the moment the difference, in amplitude) that this is the case. There is simply more room for improvement in the case of 5 briquettes. The data shows that, for each configuration, the burning rate tends to increase with the acoustic amplitude. Note that the amplitudes shown for the tests without acoustics represent the lower sensitivity limit of the pressure transducers (~20Pa as configured), and the actual sound levels without acoustic excitation are believed to be much lower than 120dB. The results for one charcoal briquette show that, with an average SPL of 145dB, the total combustion time was reduced to less than 50% of the unexcited burning time on average. For the 5 briquette tests, with an average SPL of 153dB, the total combustion time was reduced, on average, to 24% of the burning time without oscillations.

Figures 42 and 43 show the total CO and NO_x emissions for a number of tests in arbitrary units and normalized by the number of charcoal briquettes burned. When no oscillations are present, the total emission of CO per briquette is observed to be greater when 5 blocks are burned simultaneously. This is believed to be due to the fact that, since the heat loss from a pile of charcoal blocks is expected to be lower than that from a single block, the temperature in the vicinity of the charcoal is higher when burning 5 blocks than when burning a single block. A number of studies suggest that the ratio CO/ CO_2 exhausted when chars are burned is greater when combustion occurs at higher temperatures. [37-39] This temperature difference also explains the difference between emissions from 1 and 5 briquettes without oscillations. The data shows that the total emissions of CO and NO_x are greater when acoustic oscillations are present. It is not clear why the relative increase in emissions is greater when 5 charcoal briquettes are burned.

It must be noted, however, that the total amount of carbon converted by combustion is less when oscillations are present. By summing the total amount of CO and CO_2 released by the combustion with and without oscillations present, we can get a measure of the combustion efficiency. The measured change in the total amount of carbon in the exhaust with and without oscillations is less than 1% when only one block is burned. This is less than the variation in mass from one block to another, and therefore, meaningless. When 5 blocks are burned, however, the total carbon in the exhaust is 15% lower than when the combustion takes place without oscillations. This is believed to be due to the fact that the velocity oscillations break up the charcoal blocks as the end of the combustion period is reached, and the greater heat losses from these small bits is too great for combustion to continue. The reason this is not observed with the single block is most likely not the result of the number of blocks, but because the amplitudes were greater when 5 blocks were burned. Normalizing the total emissions of CO and NO_x by the total

carbon conversion, represented by the amount of CO_2 and CO released, provides more appropriate values for comparing the emissions with and without acoustic oscillations. When only one charcoal briquette was burned per test, the normalized results show that, when oscillations were present, the total emissions of CO increased by 80% and the total NO_x emissions increased by 28% above the values measured without pulsations. Tests performed in which 5 charcoal blocks were burned simultaneously showed that the presence of oscillations increased the total emissions of CO by 33% and the total NO_x emissions increased by 23% above the values measured without pulsations, which show the same trends as the single block results. These tests demonstrate that when a smoldering solid fuel is subjected to acoustic forcing, the burning rate is significantly enhanced, but the total CO and NO_x emissions are increased.

Solid Waste Burning Study:

In this phase of the study, investigation of the effects of acoustic pulsations on the combustion of a fuel that burns both a luminous flame phase and a smoldering phase was performed. Corrugated cardboard blocks were used as a solid waste simulant. The cardboard block samples were constructed by assembling 0.75in. x 2.0in. pieces of corrugated cardboard box into 2.0in. x 2.0in. x 0.75in. blocks, held together by a strip of masking tape. The samples were then placed in a cage, made from 0.25in. mesh, steel hardware cloth, with dimensions slightly larger than the sample. Because the combustion time of the cardboard blocks is on the order of minutes, as opposed to the hours necessary for the charcoal combustion tests, it became necessary to have a fast and highly repeatable method for igniting the fuel. Therefore, a methane/air burner was installed on the bottom of the incinerator that could be remotely ignited and shut off on demand. A schematic of the incinerator facility, configured for cardboard combustion tests, is shown in Fig. 44. Also shown in the figure is a methane/air burner upstream of the air inlet. This burner was used to heat the incoming air in some tests, so that the effect of temperature could be investigated. This burner is referred to as the pre-heater. Note that the air in the pre-heated tests is vitiated. When the pre-heater was used, enough oxygen was added to the flow to bring it back to 20% oxygen. This was done so that the net oxygen flow into the combustor could be fixed for both pre-heated and not heated tests.

At the beginning of each test, a cardboard block sample was placed in the incinerator, centered over the igniter, and the igniter was turned on for a measured duration. This duration was 25s for tests in which room temperature air was introduced into the incinerator (henceforth referred to as 'cold air tests'), which was the minimum time required to assure ignition of the cardboard sample on every run. When pre-heated air used for incineration (henceforth referred to as 'heated air tests'), the average temperature near the sample was approximately 250°C, which is close to the flash temperature for paper, and therefore ignition was much easier. In these tests, the

igniter was turned on for only 5s. The exhaust gas concentrations of O_2, NOx, CO, and CO_2 were sampled beyond the time at which all visible signs of combustion had ceased.

In Figs. 45 and 46, time traces of the measured CO, CO_2, NOx and acoustic pressure measurements are shown for typical runs with cold air with and without acoustic oscillations present, respectively. Notice the step in the pressure curve at the beginning of the run in Fig. 45. This jump is caused by radio frequency noise from the spark plug in the igniter. The amplitude of this noise is small with respect to the pressure signal measured when acoustics are present, and does not significantly affect the data. This noise is useful, however, in that it provides an indication of the time delays associated with the exhaust gas analyzer. Combustion products released from the burning sample must be convected through the incinerator and the sampling lines before the analyzers indicate their presence. From the figure, it can be determined that, while each analyzer has a slightly different lag time, it takes approximately 25s for the ignition to be registered by the sampling system.

Examining the data if Fig. 45, the first event that occurs during a test is ignition of the cardboard sample with a methane/air flame. This results in the produces the initial peak in the CO, CO_2, and NOx plots. Interestingly, the CO spike is not present if the igniter is burned without cardboard in the incinerator. When the cardboard is lit and the igniter turned off, the CO concentration drops to nearly 0, while the CO_2 and NOx concentrations peak a second time. This indicates the presence of gas phase burning indicative of the first stage of solid combustion. Then, as the volatiles are burned off, the CO_2 and NOx concentrations begin to fall, and more CO is again produce as smoldering becomes the dominant combustion process. Finally, the CO concentration falls again as the smoldering phase comes to completion. This same process is observed in tests in which oscillations are present, as in Fig. 46, but the distinction between phases is not as clear, because the phases overlap more. The combustion time with oscillations is significantly shorter.

Figure 47 shows the total burning times of the cardboard samples and the sound pressure level present in the chamber for a number of tests with cold and heated air. The pressure level in the incinerator when no driving is occurring is higher when the pre-heater is running, due to the noise of the combustor. The data shows that the combustion time with oscillations is much shorter in both cases, completing in approximately 33% of the time required with no pulsations present in both cold air and heated air tests. There is no apparent effect of the temperature of the inlet air on the combustion time of the cardboard, with or without oscillations present.

Figure 48 shows the total CO released from the burning cardboard blocks during a number of tests with and without oscillations using cold and heated air. The results shown for tests using pre-heated air have been corrected to remove the contribution by the pre-heater to the measured CO. The total amount of CO emitted when oscillations are not present appears to be independent

of the temperature of the air coming in to the combustor. Other than the increase in scatter, there is also no difference between the total amounts of CO emitted with and without oscillations present when the inlet air is at room temperature. However, when the combustion takes place using pre-heated air, a significant reduction in the total CO produced is observed. Also, the total amount of CO_2 produced, indicative of the degree of completion of the burning, is greater when oscillations are present: 5% in cold air tests and 20% in heated air tests. If the total amount of CO produced in these tests is normalized by the amount of CO_2 produced (to correct for the carbon conversion efficiency), in tests using pre-heated air, the normalized amount of CO produced when oscillations are present is 53% of the amount produced when oscillations are not present. The amount of CO produced when cold air is used is unchanged, to the accuracy of the measurements, by the presence of oscillations.

NO_x emissions for a number of tests of cardboard samples burned in cold air and in heated air are plotted in Fig. 49. As with the CO measurements above, the results shown for tests using pre-heated air have been corrected to remove the contribution by the pre-heater to the measured NO_x. The first notable detail of this plot is that the NOx is significantly higher when pre-heated air is supplied to the incinerator. The use of the pre-heated air increases the temperature at the sample location to approximately 250°C prior to ignition of the cardboard from approximately 25°C measured when cold air is used. The data shows that the presence of pulsations has little effect on the generation of NO_x when cold air is used, and increases the total emission of NO_x slightly when pre-heated air is used. If these data are normalized by the total CO_2 produced, as was done with the CO results, then, because the total carbon converted is greater when acoustic oscillations are present, the normalized amount of NO_x is reduce by 20% when oscillations are used in cold air tests, and unchanged when pre-heated air is used. With or without normalization, however, the effect of the acoustic oscillations are small compared to the effect of the environment temperature.

Comparison of the Charcoal and Cardboard Results:

A comparison of the results observed when charcoal was burned in the pulsed incineration facility and the results obtained from cardboard combustion can aid in understanding how acoustic oscillations effect the incineration process. Cardboard, which, along with paper, is expected to constitute a large portion of wastes produced aboard ships, burns with both a gaseous flame phase and a smoldering phase (these phases can overlap significantly). Charcoal combustion takes place primarily in the smoldering phase.

The rates of combustion increased significantly in both the charcoal (2 times faster when a single briquette was burned, 4 times faster for 5 briquettes) and cardboard tests (3 times faster for both pre-heated and cold air) when oscillations were present. The fact that the cardboard results

fall within the range of the charcoal results shows similarity of the processes. The emissions of CO and NO_x from charcoal and cardboard were, however, affected differently by acoustic oscillations. The amount of CO produced when charcoal was burned increased when acoustic oscillations were present. An 80% increase when 1 charcoal briquette was burned, and a 33% increase was observed when 5 briquettes were burned. When cardboard was burned, however, the CO emissions were unchanged when room temperature air was used, and pulsations reduced the CO emissions by 46% from the unexcited results when pre-heated air was used. The charcoal results indicate higher temperature combustion, which would be expected because of the shortened combustion time, which has been shown to increase the ratio of CO to CO_2 produced when chars are burned. The reduced CO emissions from the cardboard combustion can be explained by several arguments. First, the mixing rate of pyrolized gaseous fuel with combustion air may be increased, which would improve the combustion efficiency. Second, the additional CO produced by the enhanced smoldering may be burned off in the gas phase flame, because the gaseous flame phase and the smoldering phases have been shown to have a greater amount of temporal overlap. Whether either or both of these explanations is correct remains to be proven. The emissions of NO_x were also found to increase due to pulsations in the pure smoldering case and remain unchanged or decrease slightly in cardboard burning tests when oscillations were present. The reason for this difference is, at present, unexplained. The affect of oscillations in the case of cardboard combustion, however, suggest that the presence of oscillations is much less important than the temperature of the combustion system.

III Summary and Conclusions

Gas Phase Mixing Resulting By Resonant Acoustic Forcing:

The goal of this study was to investigate the effect of driving high amplitude, resonant, acoustic oscillations upon the gas phase mixing in a closed cavity. A closed cavity was used so that the effects of the acoustic driving could be isolated from the mixing due to mean flow into and out of the chamber. Experiments were performed in which the mixing rate of smoke-filled and smoke-free air due to excited, resonant, acoustic oscillations were measured in a rectangular cavity with no mean flow. Experimental results show significant enhancement of mixing rate due to the presence of acoustics inside the mixing chamber in comparison to rates measured in the absence of acoustic driving. The rate of gas phase mixing is mainly determined by acoustic pressure amplitude, acoustic mode, and the position of the acoustic drivers relative to the experimental setup. While the quantitative results obtained in this study are dependent upon the experimental facility, it is believed that the results apply qualitatively to any resonant chamber forced by compact drivers.

The acoustic pressure amplitude has a strong influence on the mixing rate. Increased acoustic pressure amplitudes in the chamber were shown to decrease the mixing time and, thus, increase the mixing rate. The behavior can be approximated by a simple power relationship between mixing rate and acoustic pressure amplitude, given by. $r = c/p^{\nu}$, where r is the mixing rate, p is the amplitude of the pressure oscillations and c and ν are dependent upon the experimental configuration. While the significance of the mixing induced by resonant acoustic driving in an actual combustor, where mean flow is present, will depend on many factors, it appears that as the amplitude of the oscillations increase this mechanism will be increasingly important to the total mixing.

The mixing rate was shown to have a complex dependence on the mode of acoustic excitation. When the experimental setup was configured with two acoustic drivers mounted symmetrically at opposite ends of the cavity, the behavior of the mixing appeared to be influenced by the acoustic displacement amplitude at the interface between the smoke-filled and smoke-free air. Acoustic modes with a velocity antinode at the center of the cavity, where the removable partition was located, mixed faster than those that had an acoustic velocity node at the center. Also, in tests with constant acoustic pressure amplitude, the mixing rate was observed to decrease as the frequency of the oscillations increased, which corresponds to a decrease in acoustic displacement amplitude.

The mixing behavior in the chamber was found to depend strongly upon the placement of the acoustic drivers. This is believed to be due to distortions of the acoustic wave patterns in the

vicinity of the drivers that results from the impedance mismatch between the drivers and the walls in which they are mounted and acoustic streaming phenomena associated with the drivers. Velocity measurements in the cavity have shown that the velocity of the mean flow jetting induced by the drivers is on the order of the acoustic velocity. This acoustic jetting appears to be responsible the largest scale motion inside the chamber.

Acoustic Control of a Free Jet Using Transverse Excitation:

In this study, the effects of transverse acoustic excitation on a subsonic, round jet were investigated. Transverse, resonant oscillations were used to excite a subsonic, axisymmetric jet discharging into a rectangular duct. Tests were performed with the duct both closed at the ends, where recirculation patterns occur behind the dump plane, and open at both ends, where flow through the box is naturally induced by entrainment. It was observed that the presence of oscillations caused the jet to flap in the plane of the oscillations. This flapping motion resulted from the shedding of vortices from alternating edges of the jet mouth, which were subsequently convected downstream. The vortex generation was confined to the plane of the oscillation, which caused the jet to have an elliptical cross section on average. Mean velocity measurements and flow visualization studies revealed that as the vortical structures convect downstream and interact with each other, bifurcation of the jet occurs. Measurements show that the presence of transverse acoustic oscillations could significantly enhance the spreading rate of the jet in the plane of the acoustic velocity fluctuations.

A developed technique to measure the entropy of mixing from a cross-sectional image of the jet was used to quantify the increased spatial mixing rate of the bifurcated jet in the open-ended facility. It was determined that transverse acoustic forcing had the greatest effect on mixing over a Strouhal number range of 0.2 to 0.3. The enhancement in mixing was shown to increase with the amplitude of oscillation.

Sublimation Rate and Heat Transfer Studies:

In this phase of the study, dry ice sublimation was used to simulate the pyrolysis of a solid fuel in the presence of acoustic oscillations. The use of dry ice as a pyrolysis model allows investigation of the effects of the acoustic oscillations on the heat and mass transfer decoupled from the chemical combustion process.

Visualization revealed that oscillations greatly disturb the boundary layer above the dry ice. The mass transport rate in the vicinity of the dry ice appears much greater when acoustic oscillations are present, because the thickness of the fog layer around the dry ice is greatly increased. In the range of conditions tested, the combined effects of the mean convective flow and

the acoustic oscillations generated a more chaotic flow behavior than either acoustic driving or mean flow alone.

The presence of resonant acoustic oscillations generally increased the sublimation rate of dry ice used to simulate the pyrolysis of a solid waste. An oscillation amplitude of 150dB was shown to increase the average sublimation rate nearly 60% above the unexcited sublimation rate at the same conditions. Results of tests at different mean flow velocities and acoustic amplitudes were normalized by the sublimation rates without oscillations so that the effect of the mean flow rates on the sublimation rate could be compared at different amplitudes of oscillation. This revealed that, for the range of conditions studied, the effects of acoustic velocity oscillations at a given amplitude became more important as the mean velocity increased. This is believed to be due to the combined effects of the velocity oscillations, which cause increased heat and mass transfer at the surface of the dry ice, and mean velocity, which convects sublimated mass away from the dry ice region.

The facility used and the tests performed in this study investigated the pyrolysis of a simulated solid fuel under a variety of acoustic and flow conditions. The utilized dry ice was intended to represents a chunk of solid waste material in an incinerator or wood or coal in a pulsed combustor or acoustically excited furnace. The results of this study indicate that solid fuel will pyrolyze faster in an environment in which high amplitude acoustic oscillations are present. The fact that the sublimation rates did not change significantly with the orientation of the blocks suggests that the corner effects are not a critical factor in the acoustic interaction with the sublimation rate. However, in geometries where corners and edges are not prevalent, the results may differ from those measured here. Also, in the investigated configurations, the sublimated gas can be convected downstream where it no longer affects the sublimation process.

Effects of Pulsations on Incineration:

A model incinerator capable of burning waste surrogates in the presence of transverse and multi-dimensional mode acoustic oscillations was used to study the effects of acoustic oscillations on combustion rates as well as the NOx, CO, and CO_2 emissions from the simulated waste. This study was performed in three parts: liquid fuel, smoldering solid char, and burning solid fuel.

Operation with liquid fuel proved to be problematic, and the results of these tests are questionable. The most interesting result from this study is that when the acoustic velocity amplitude reached a certain level, the fuel was sprayed from the burner. Preliminary testing shows that the acoustic amplitude necessary to generate a spray is greater for water than for methanol, which suggests a surface tension and/or specific gravity dependence, but more research into the mechanism of this acoustic spraying is necessary.

Tests were performed using commercial charcoal as a solid waste simulant. By design, charcoal has had most of the volatiles removed, and therefore, it reacts primarily by smoldering. Results for one charcoal briquette show that, with an average SPL of 145dB, the total combustion time was reduced to less than 50% of the unexcited burning time on average. For the 5 briquette tests, with an average SPL of 153dB, the total combustion time was reduced, on average, to 24% of the burning time without oscillations. Tests show that the total emissions of CO and NO_x were somewhat increased when acoustic oscillations were present during charcoal combustion.

Corrugated cardboard blocks were used as a solid waste simulant to determine the effects of acoustic pulsations on the combustion of a fuel that burns both a luminous flame phase and a smoldering phase. The results show that the combustion time with oscillations was approximately 33% of the time required with no pulsations present The normalized amount of CO produced using pre-heated air and oscillations was 53% of the amount produced when oscillations were not present. The amount of CO produced when cold air was used was unchanged by the presence of oscillations.. The effect of the acoustic oscillations on the generation of NO_x appear to be small compared to the effect of the environment temperature.

III References

1) Patera, A. T. and Mikic, B. B., "Exploiting Hydrodynamic Instabilities: Resonant Heat Transfer Enhancement", Int. J. Heat Mass Transfer, Vol. 29, No. 8, pp. 1127-1138, 1986.

2) Ghaddar, N. K., Magen, M., Mikic, B. B., and Patera, A. T., "Numerical Investigations of Incompressible Flow in Grooved Channels, Part 2: Resonance and Oscillatory Heat-Transfer Enhancement", J. Fluid Mech., Vol. 168, pp. 541-567, 1986.

3) Hodgins, J. W., Hoffman, T. W., and Pei, D. C., "The Effect of Sonic Energy on Mass Transfer in Solid-Gas Contacting Operations", Canadian J. of Chem. Eng., pp. 18-24, June 1957.

4) Deck, J. E., Arpaci, V. S., and Keller, J. O., "Heat Transfer in the Oscillating Turbulent Flow of Pulse Combustor Tail Pipes", Final Report, Sandia Combustion Laboratories, GRI Contract No. 5084-260-1092, July 1989.

5) Hanby, V. I., "Convective Heat Transfer in a Gas-Fired Pulsating Combustor", Trans. ASME J. of Eng. for Power, No. 1, pp. 48-51, January 1969.

6) Arpaci, V. S., Dec, J. E., and Keller, J. O., "Heat Transfer in Pulse Combustor Tailpipes", Proceed. of Int. Symposium on Pulsating Combustion, Sponsored by Sandia National Laboratories and the Gas Research Institute, Monterey, CA, August 1991.

7) Merkli, P. and Thomann, H., "Transition to Turbulence in Oscillating Pipe Flow", J. Fluid Mech., Vol. 68, Part 3, pp. 567-575, 1975.

8) Vermeulen, P. J., Odgers, J., and Ramesh, V., "Acoustic Control of Dilution-Air Mixing in a Gas Turbine Combustor", ASME J. of Eng. for Power, Vol. 104, No. 4, pp. 844-852, October 1982.

9) Lyman, F. A., and Sabnis, J. S., "Combustion of Captive Coal Particles in Pulsating Flow", Proceed. Symposium on Pulse Combustion Tech. for Heating Applications, ANL/EES-TM-87, pp. 95-104, Argonne National Laboratory, Argonne, IL, 1979.

10) Zinn, B. T., et al, "Development of a Coal Burning Pulsating Combustor for Industrial Power", DOE/ER/10068-T2, Pittsburgh Energy Tech. Center, Pittsburgh, PA, 1983.

11) Bai, T., "Combustion of Liquid Fuels in a Rijke Type Pulse Combustor", PhD. Thesis, Georgia Institute of Technology, Atlanta, GA 1992.

12) Stewart, C. R., Lemieux, P. M., and Zinn, B. T., "Application of Pulse Combustion to Solid and Hazardous Waste Incineration", Proceed. of Intl. Symposium on Pulsating Combustion, Sponsored by Sandia National Laboratories and the Gas Research Institute, Monterey, CA 1991.

13) Rooney, J. A., *Ultrasound: It's Chemical, Physical and Biological Effects*, Ed. Suslick, K. S., VCH Publishers, Inc., New York, N.Y., 1988.

14) Eckert, C., "Vortices and Streams Caused By Sound Waves", *Physical Review*, Vol. 73, January 1948, pp. 68-76.

15) Nyborg, W. L., "Acoustic Streaming Due To Attenuated Plane Waves", *Journal of the Acoustical Society of America*, Vol. 25, No. 1, January 1953.

16) Ingard, K. U. and Labate, S., "Acoustic Circulation Effects and the Nonlinear Impedance of Orifices", ", *Journal of the Acoustical Society of America*, Vol. 22, No. 2, March 1950.

17) Liscinsky, D. S., True, B., and Holdeman, J. D., "Experimental Investigation of Crossflow Jet Mixing in a Rectangular Duct", AIAA 93-2037, Monterey, CA, June 1993.

18) Licinsky, D. S., True, B., and Holdeman, J. D., "Mixing Characteristics of Directly Opposed Rows of Jets Injected Normal to a Crossflow in a Rectangular Duct", AIAA 94-0217, Reno, NV, January 1994.

19) Cantwell, B. J., "Organized Motion in Turbulent Flow," *Ann. Rev. Fluid Mech.*, No. 13, pp. 457-515, 1981.

20) Ho, C. M. and Huerre, P., "Perturbed Free Shear Layers," *Ann. Rev. Fluid Mech.*, No. 16, pp. 365-424, 1984.

21) Zaman, K. B. M. Q. and Hussain, A. K. M. F., "Vortex Pairing in a Circular Jet Under Controlled Excitation, General Jet Response" *J. Fluid Mechanics*, Vol. 101, pp. 449-491, 1980.

22) Zaman, K. B. M. Q. and Hussain, A. K. M. F., "Turbulence Suppression in Free Shear Flows by Controlled Excitation," *J. Fluid Mechanics*, Vol. 103, pp. 133-159, 1981.

23) Ahuja, K. K., Lepicovsky, J., Tam, C. K. W., Morris, P. J., and Burrin, R. H., "Tone-Excited Jet, Theory and Experiments," NASA Contract Report 3538, 1982.

24) Ho, C. M. and Huang, L. S., "Subharmonics and Vortex Merging in Mixing Layers," *J. Fluid Mech.*, No. 119, pp. 443-473, 1982.

25) Parekh, D. E., Reynolds, W. C., and Mungal, M. G., "Bifurcation of Round Air Jets by Dual-Mode Acoustic Excitation," AIAA Paper No. 87-0164, 25th Aerospace Sciences Meeting, 1987, Reno, NV.

26) Juvet, P. J. and Reynolds, W. C., "Entrainment Control in an Acoustically Controlled Shrouded Jet," AIAA Paper No. 89-0969, 2nd Shear Flow Conference, 1989, Tempe, AZ.

27) Ogawa, N., Maki, H., and Kuroda, K., "Studies on Tone-Excited Jet", *Transactions of the Japan Society of Mechanical Engineers, Part B*, Vol. 59, No. 566, pp. 2975-2981, 1993.

28) Brown, G. B., "On Vortex Motion in Gaseous Jets and the Origin of their Sensitivity to Sound," *Proceedings of the Physical Society*, Vol. 47, pp. 702-732, 1935.

29) Lee, M. and Reynolds, W. C., "Bifurcating and Blooming Jets," AFOSR Final Technical Report, Grant No. AF-F49620-84-K-0005, August 1985.

30) Everson, R., Manin, D., Sirovich, L., and Winter, M., "Quantification of Mixing and Mixing Rate from Experimental Observations," AIAA Paper No. 95-0169.

31) Vlasov, E.V. and Ginevskii, A.S. "The Aeroacoustic Interaction Problem (review)," Sov. Phys. Acoust., Vol. 26, pp. 1-7, (1980).

32) Crow, S.C. and Champagne, F.H., "Orderly Structure in Jet Turbulence," Journal of Fluid Mechanics, Vol. 48, pp. 547-592 (1971).

33) Lepicovsky, J., Ahuja, K. K., Brown, W. H., and Morris, P. J., "Acoustic Control of Free Jet Mixing," AIAA-paper No. 85-0569.

34) Ma, Y., Van Moorhem, W. K., and Shorthill, R. W., "Experimental Investigation of Velocity Coupling in Combustion Instability," *Journal of Propulsion and Power*, Vol. 7, No. 5, Sept.-Oct. 1991.

35) Ma, Y., Huesser, E., Shorthill, R., and Van Moorhem, W., "A Simulation of the Flow Near a Burning Solid Rocket Propellant," AIAA-89-0301, AIAA 27th Aerospace Sciences Meeting, January, 1989.

36) L. M. Matta, C. Zhu, J. I. Jagoda, and B. T. Zinn, "Mixing By Resonant Acoustic Driving in a Closed Chamber", *Journal of Propulsion and Power*, Vol. 12, No. 2, March-April 1996, pp. 366-370.

37) Scala, S. M., *Jet Propulsion*, Vol. 28, pp340, 1958.

38) Spalding, D. B., *International Journal of Heat and Mass Transfer*, Vol. 2, pp. 283, 1961.

39) Denison, M. R. and Dooley, D. A., *Journal of Aeronautical Sciences*, Vol. 25, pp. 271, 1958.

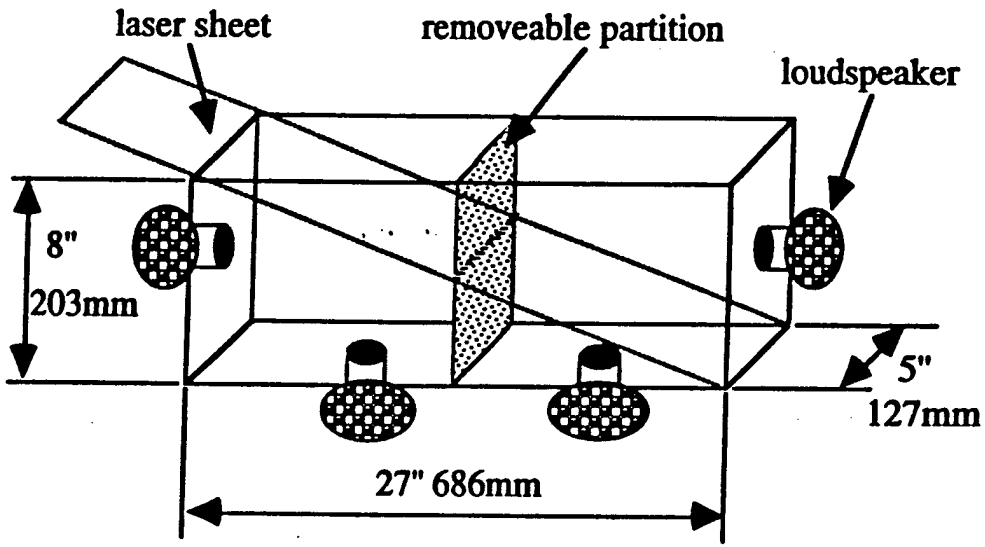

Figure 1. Schematic of the experimental setup

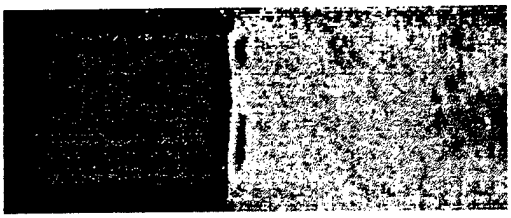

t = 0.00 sec.

t = 3.50 sec.

t = 1.00 sec.

t = 4.00 sec.

t = 1.80 sec.

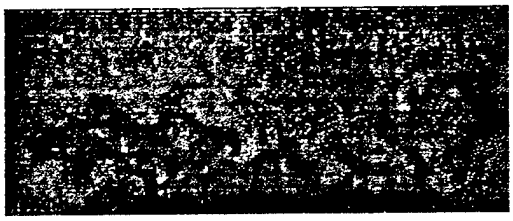

t = 5.00 sec.

t = 2.40 sec.

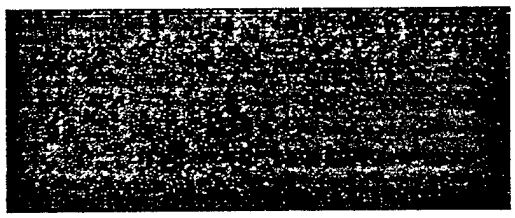

t = 8.00 sec.

Figure 2. Sequence of images from a typical test showing the mixing of smoke and air

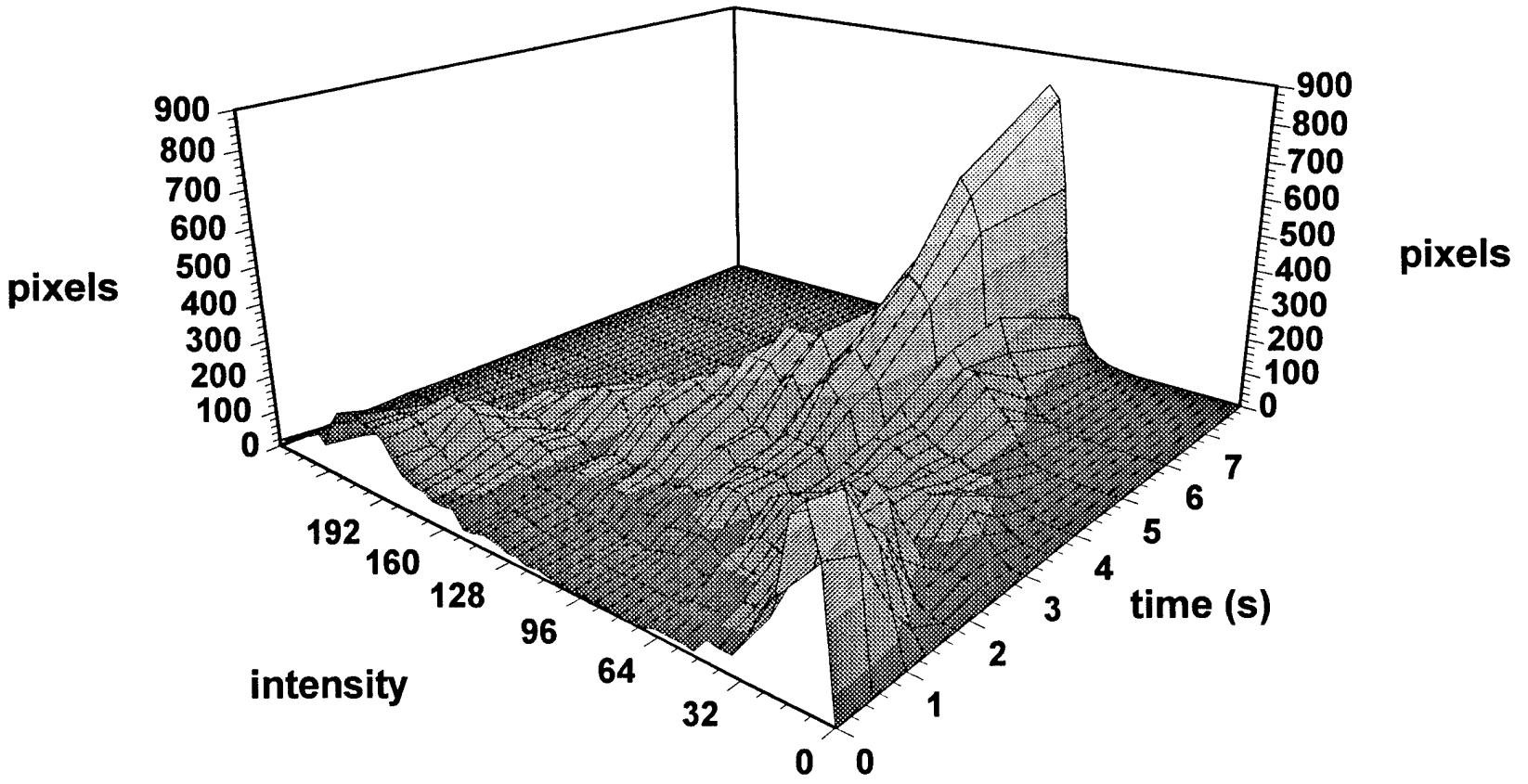

Figure 3. Temporal evolution of the image histograms during mixing

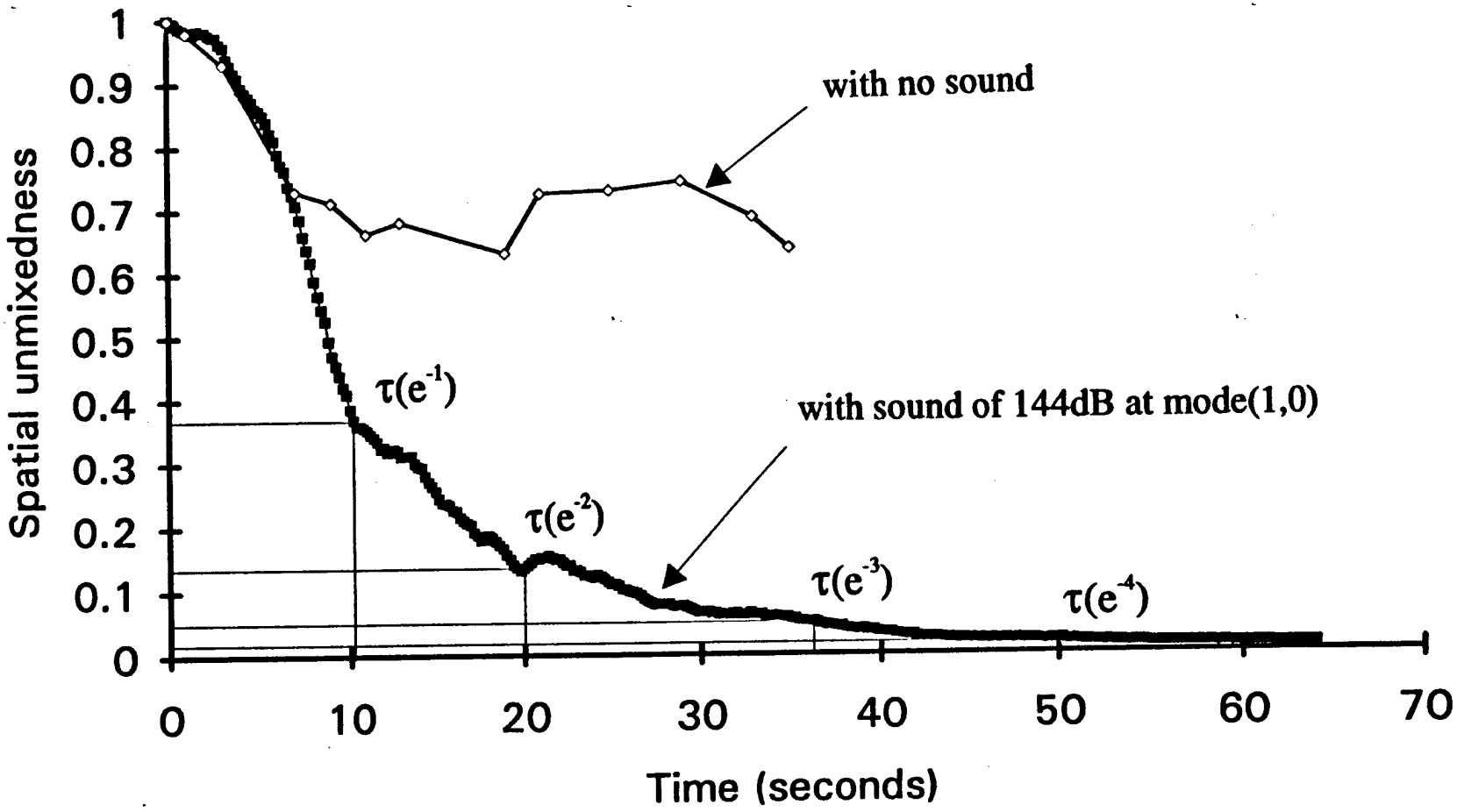

Figure 4. Spatial unmixedness vs. time for a 250Hz., 144dB oscillation and without sound

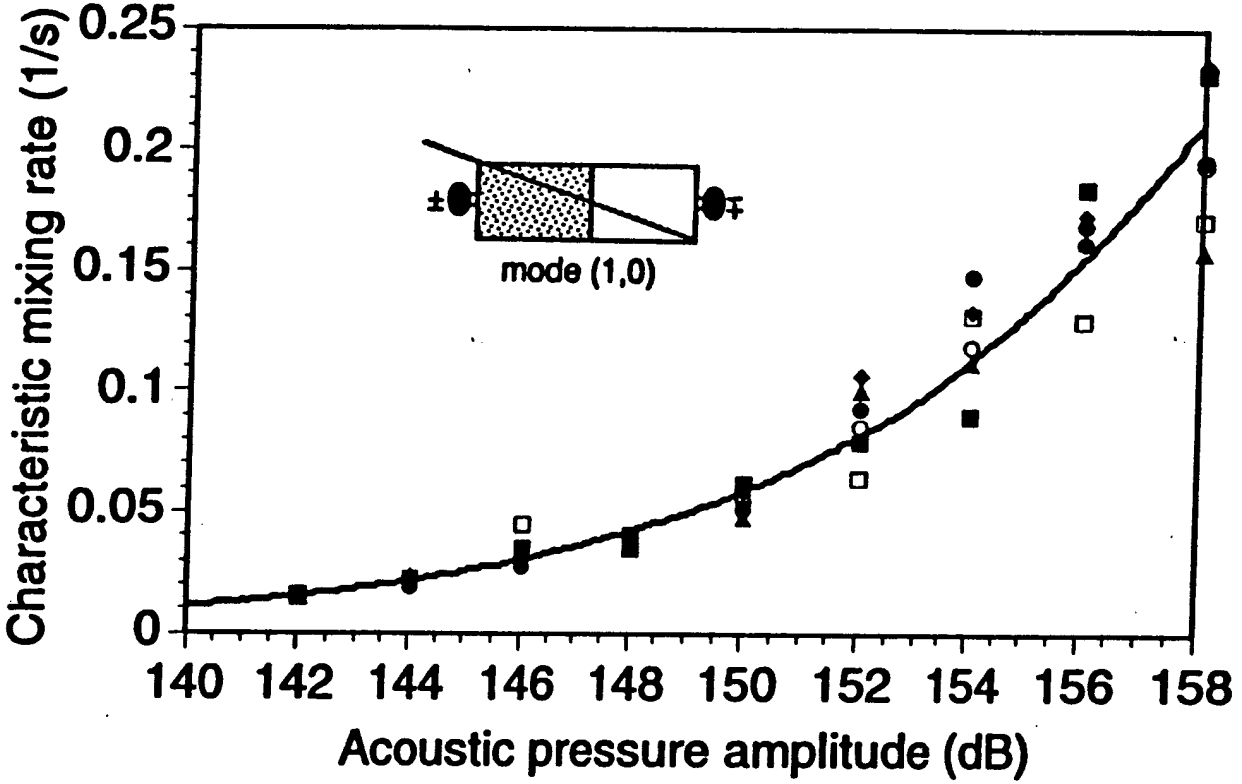

Figure 5. Characteristic mixing rate vs. acoustic pressure amplitude

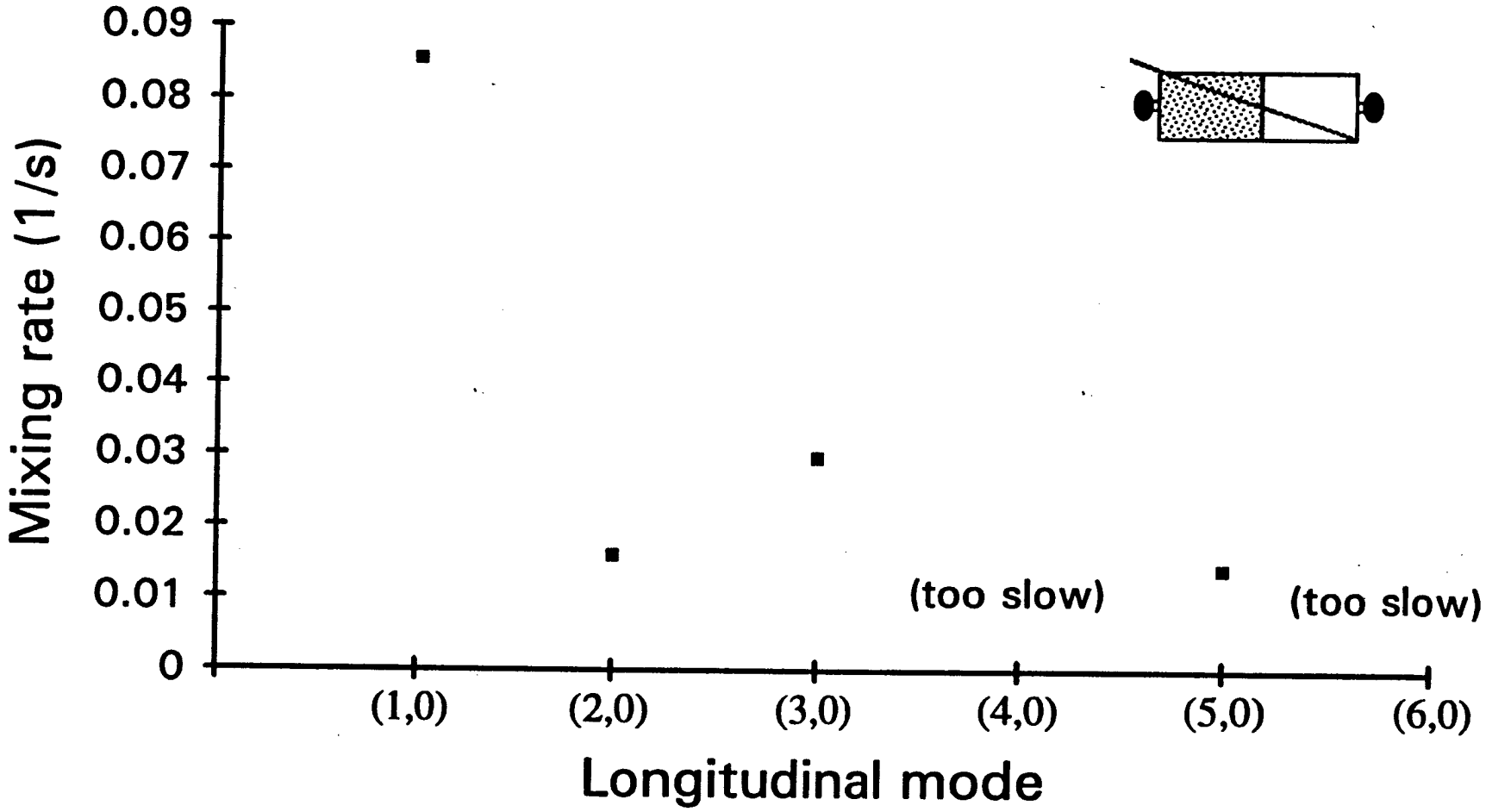

Figure 6. Dependence of mixing rate upon longitudinal mode at 152dB

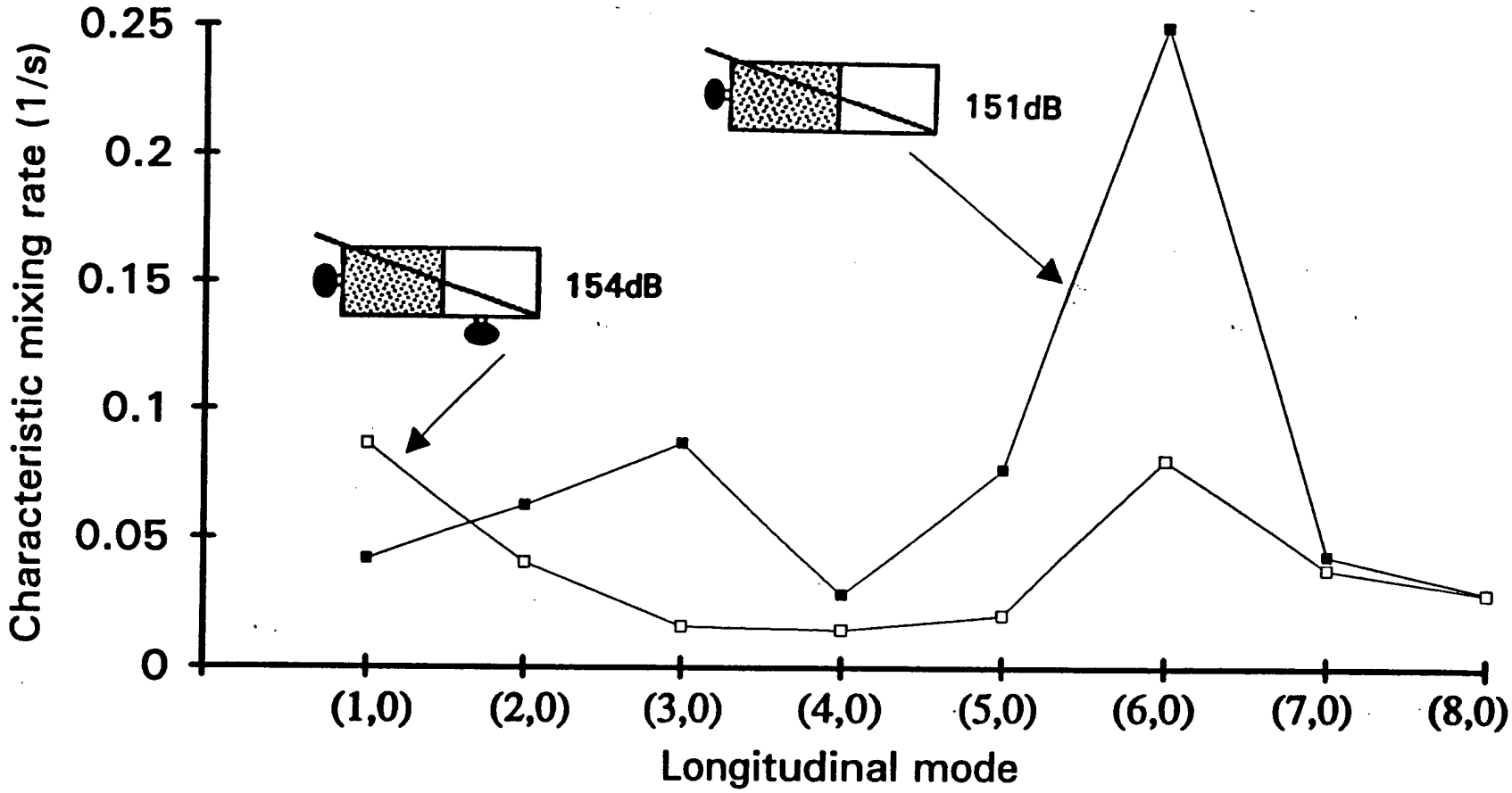

Figure 7. Comparison of mixing rate dependence upon longitudinal mode for different driving configurations

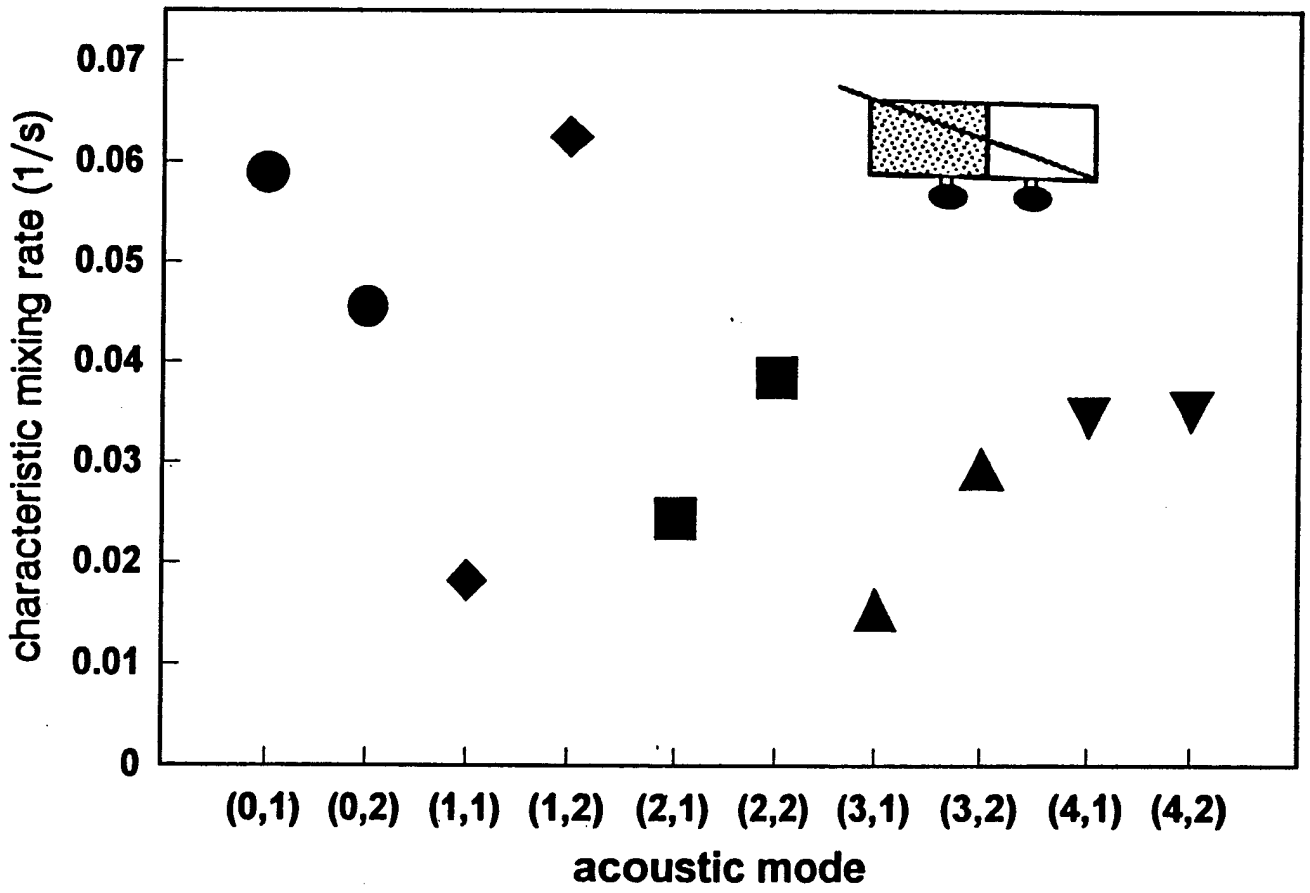

Figure 8. Dependence of characteristic mixing rate upon mode at 148dB

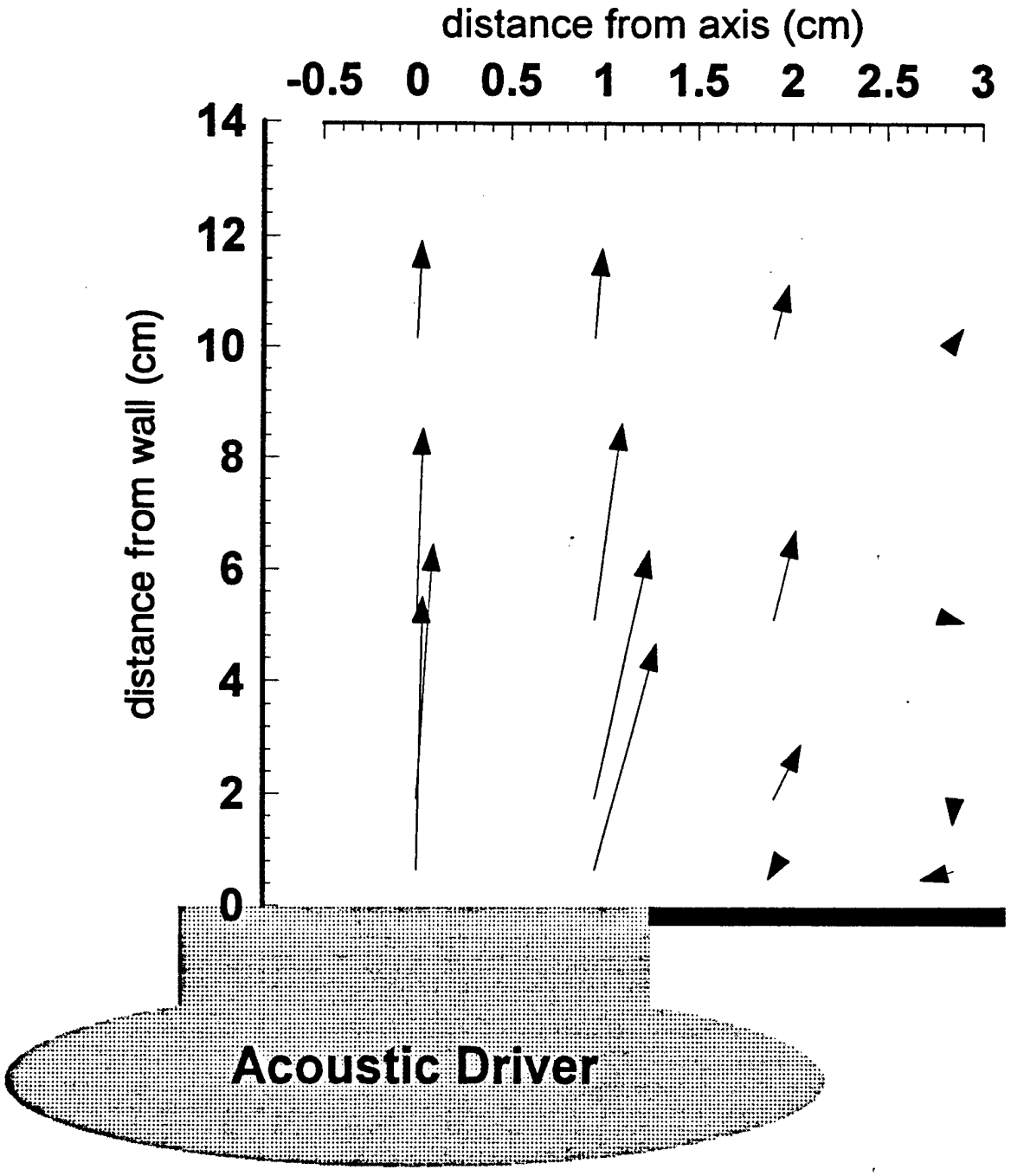

Figure 9. Acoustic streaming velocity profile in the vicinity of a driver

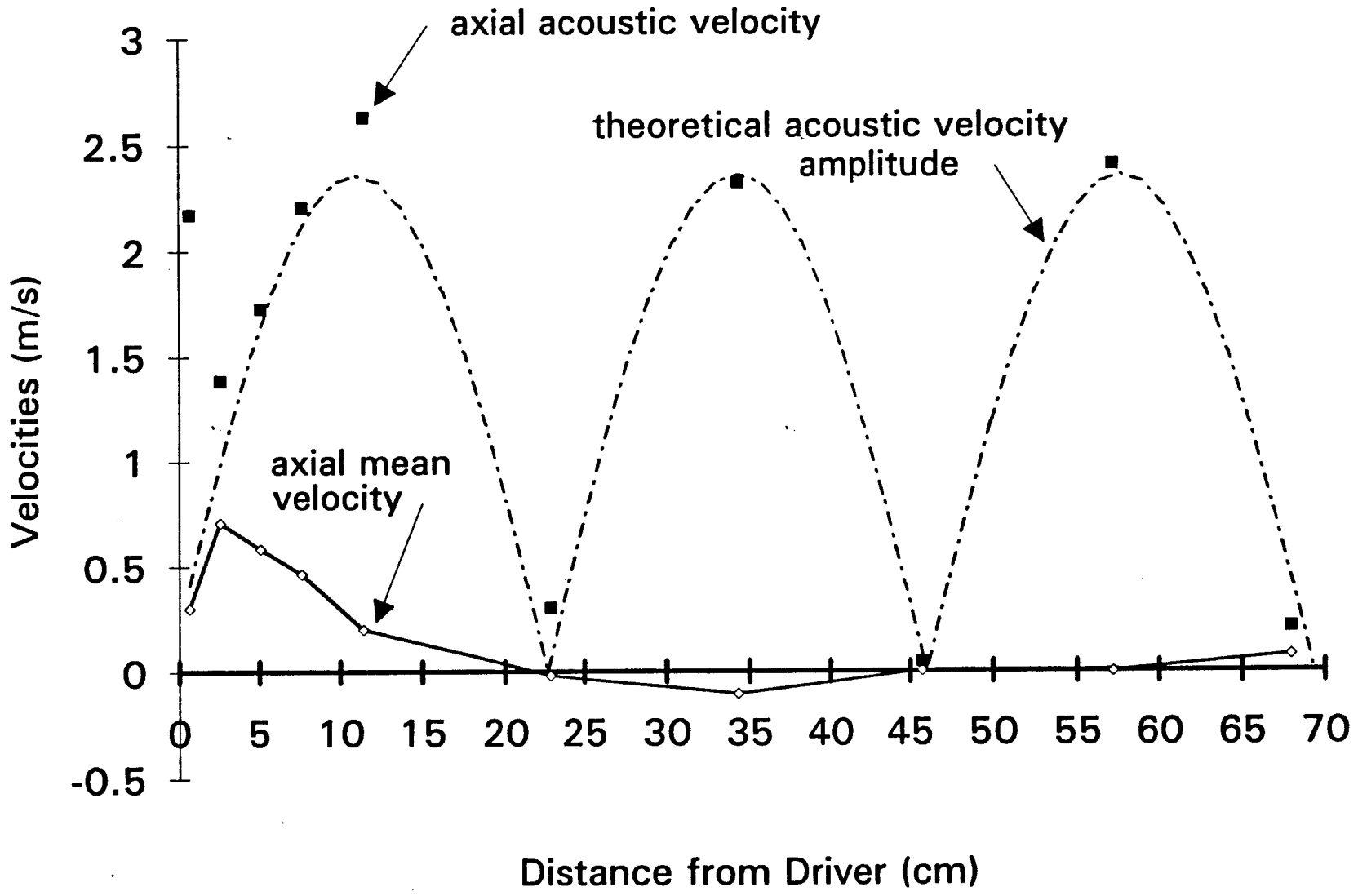

Figure 10. Dependence of the axial components of the mean and acoustic velocities upon distance from the driver at 150dB, mode(3,0)

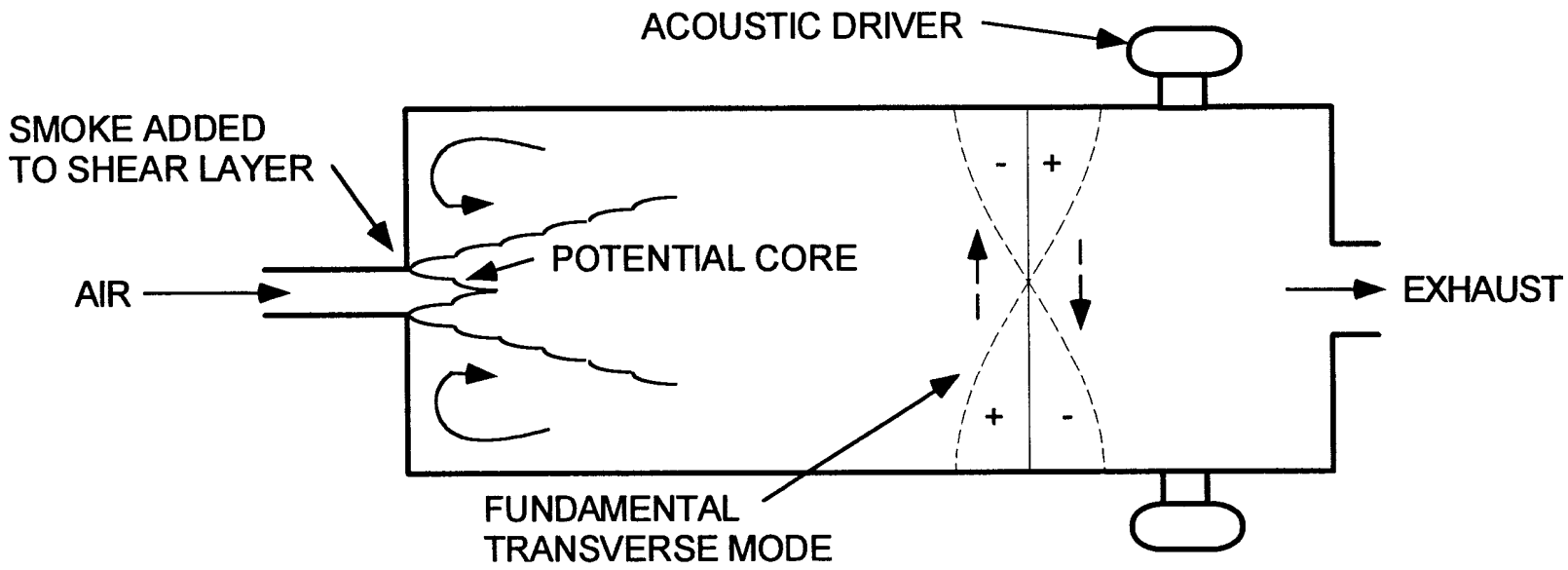

Figure 11. Schematic of the closed-ended jet excitation facility

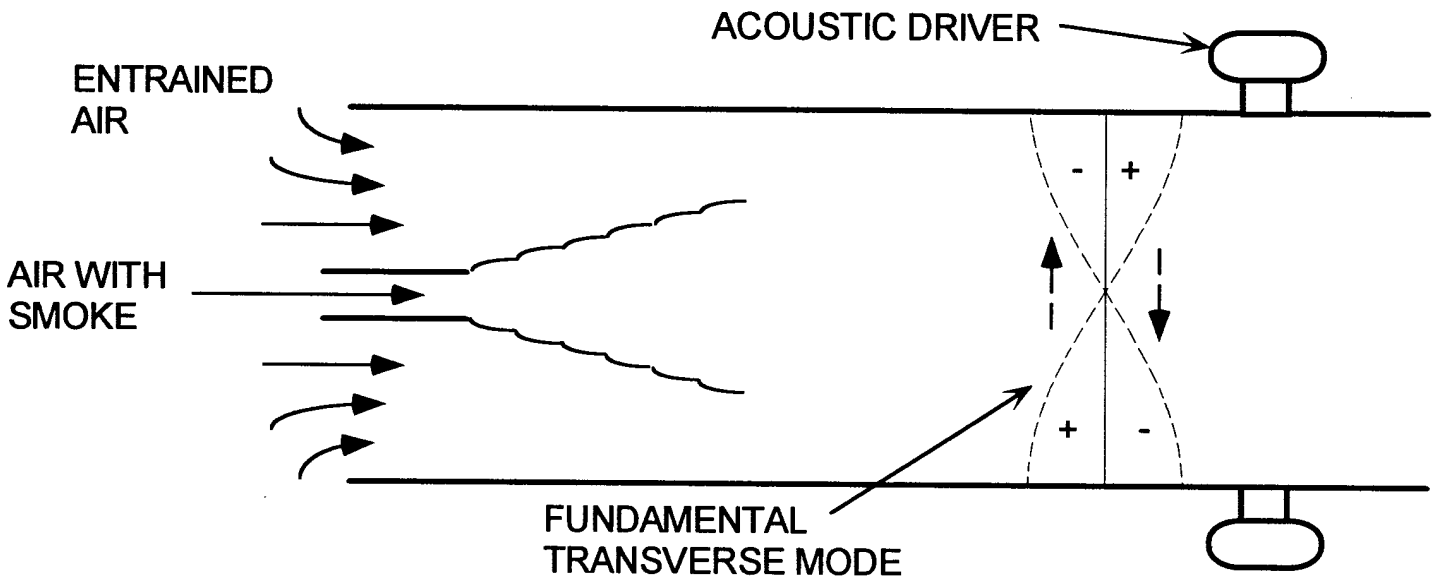

Figure 12. Schematic of the open-ended jet excitation facility

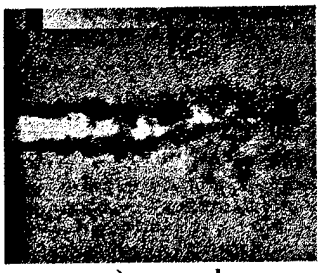

a) no sound

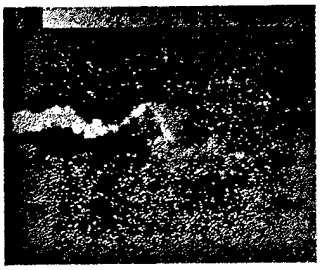

b) 138 dB

c) 144 dB

d) 150 dB

e) 154 dB

Figure 13. Instantaneous images of the excited jet with a velocity of 75ft/s at different amplitudes.

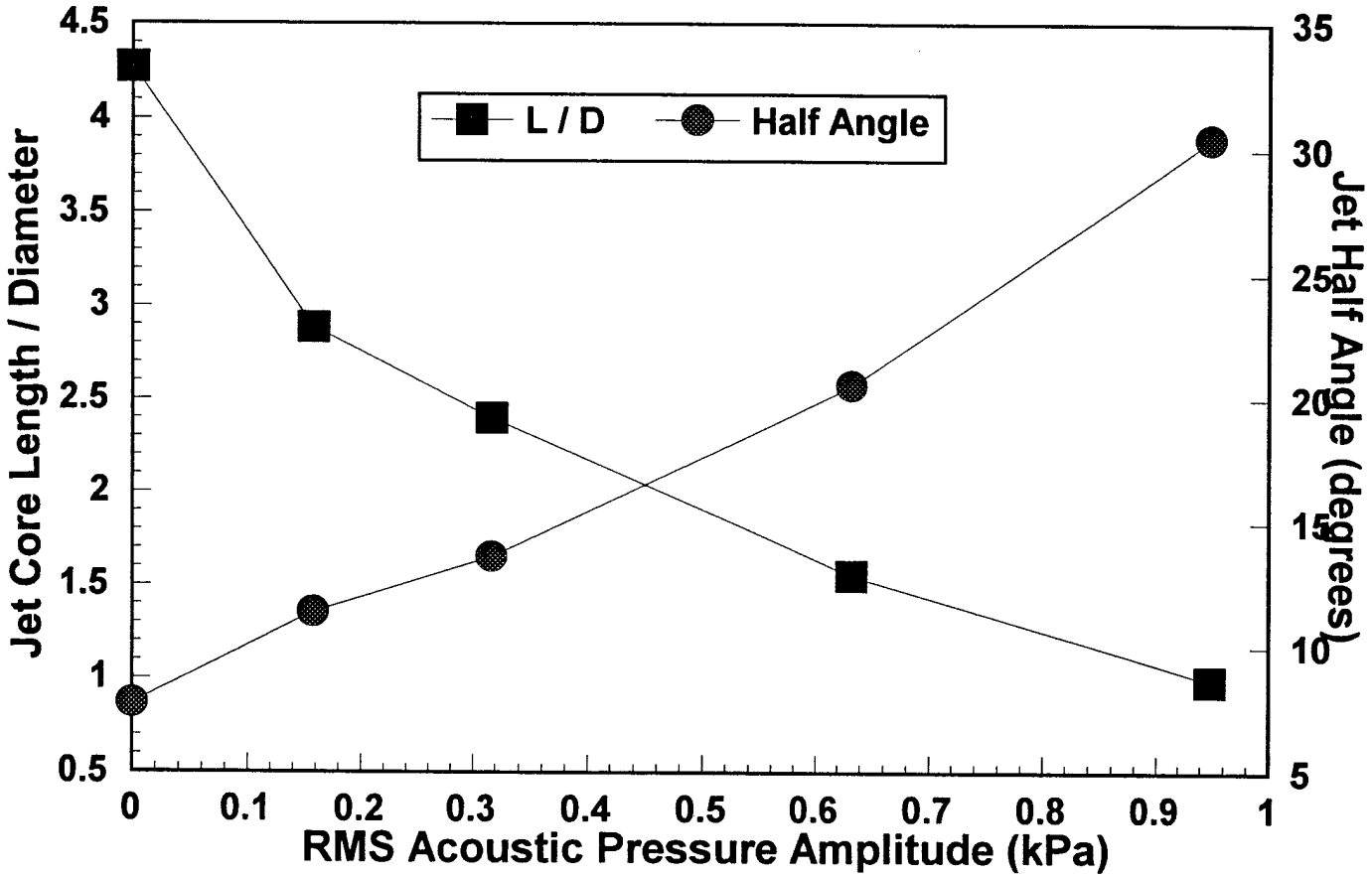

Figure 14. Effect of the oscillation amplitude on the characteristics of the jet

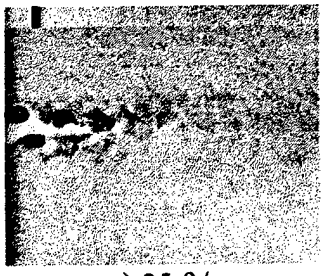

a) 25 ft/s

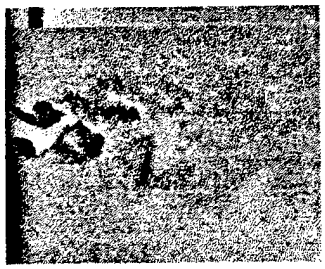

b) 50 ft/s

c) 75 ft/s

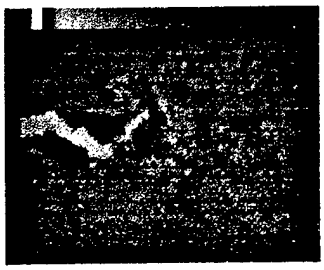

d) 100 ft/s

Figure 15. Instantaneous images of the jet at different speeds excited by a 150dB oscillation.

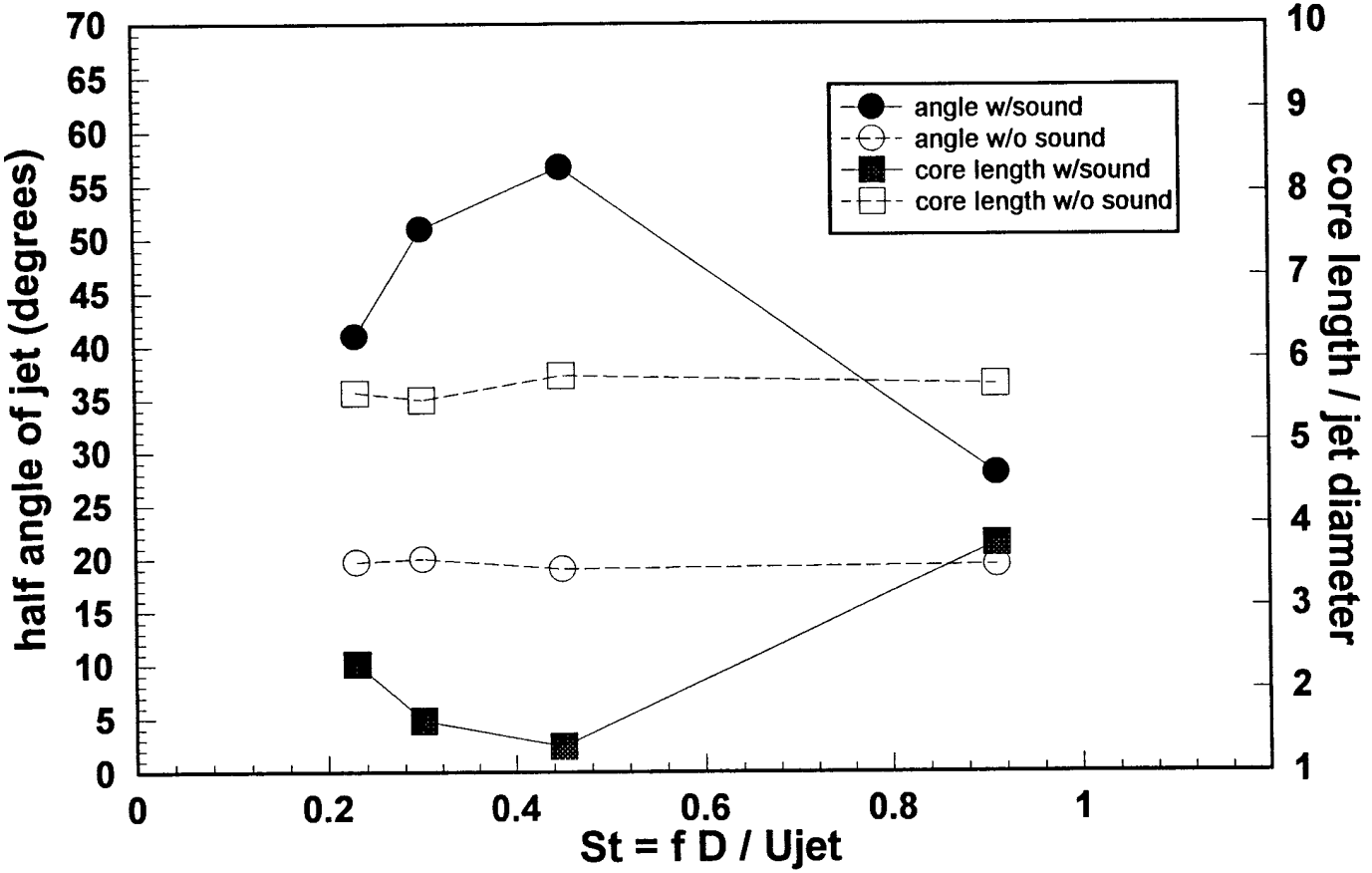

Figure 16. Effects of Strouhal number on jet characteristics

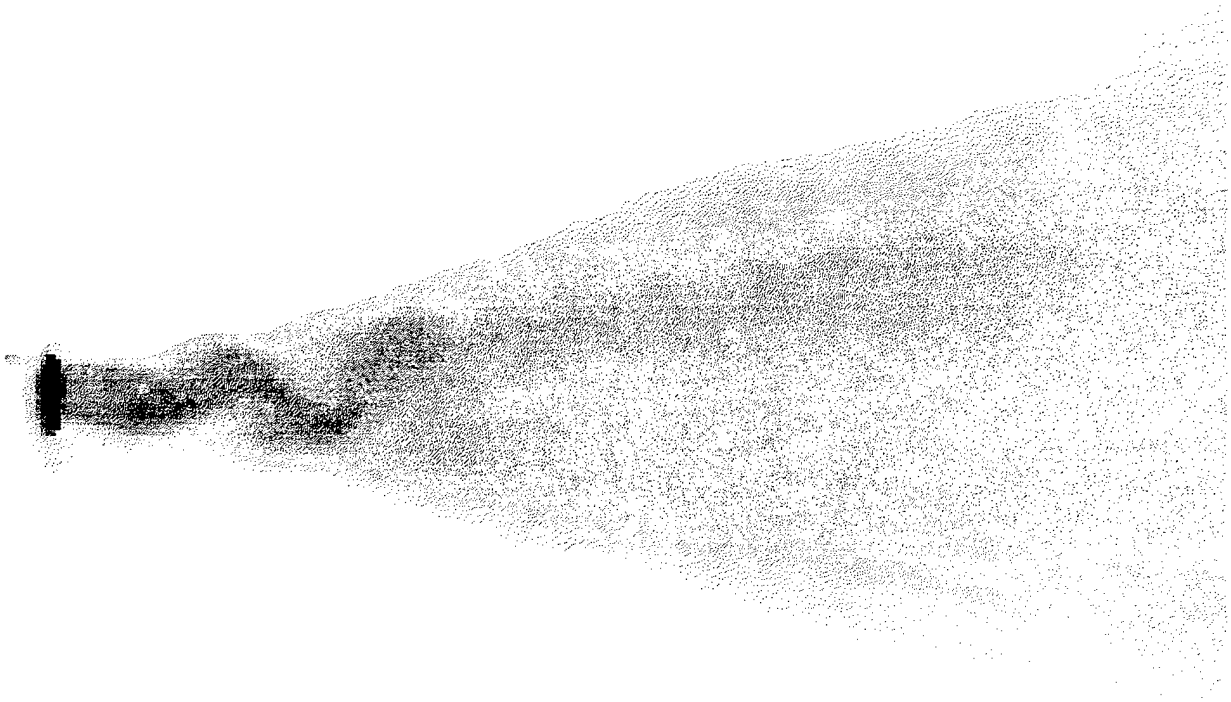

Figure 17. Phase-locked averaged image of the excited jet in the open-ended facility

a) no sound

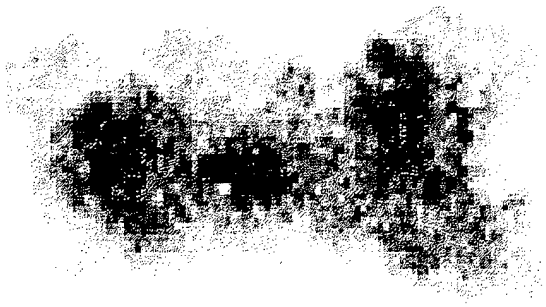

b) with sound

Figure 18. Instantaneous cross-section images

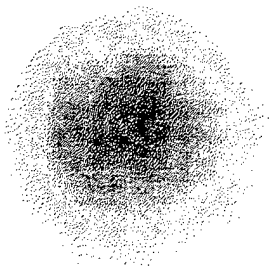

a) no sound

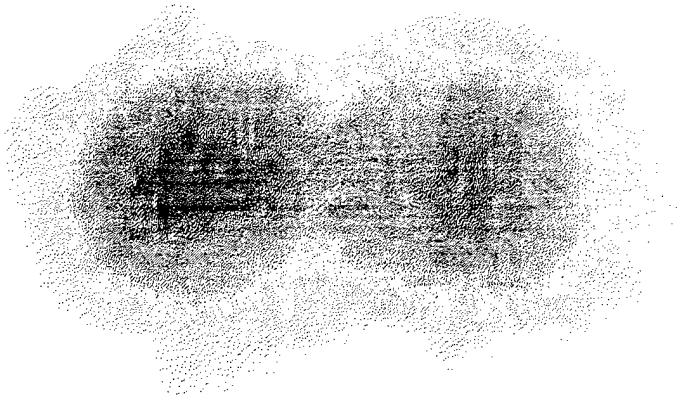

b) with sound

Figure 19. Phase-locked averaged cross-section images

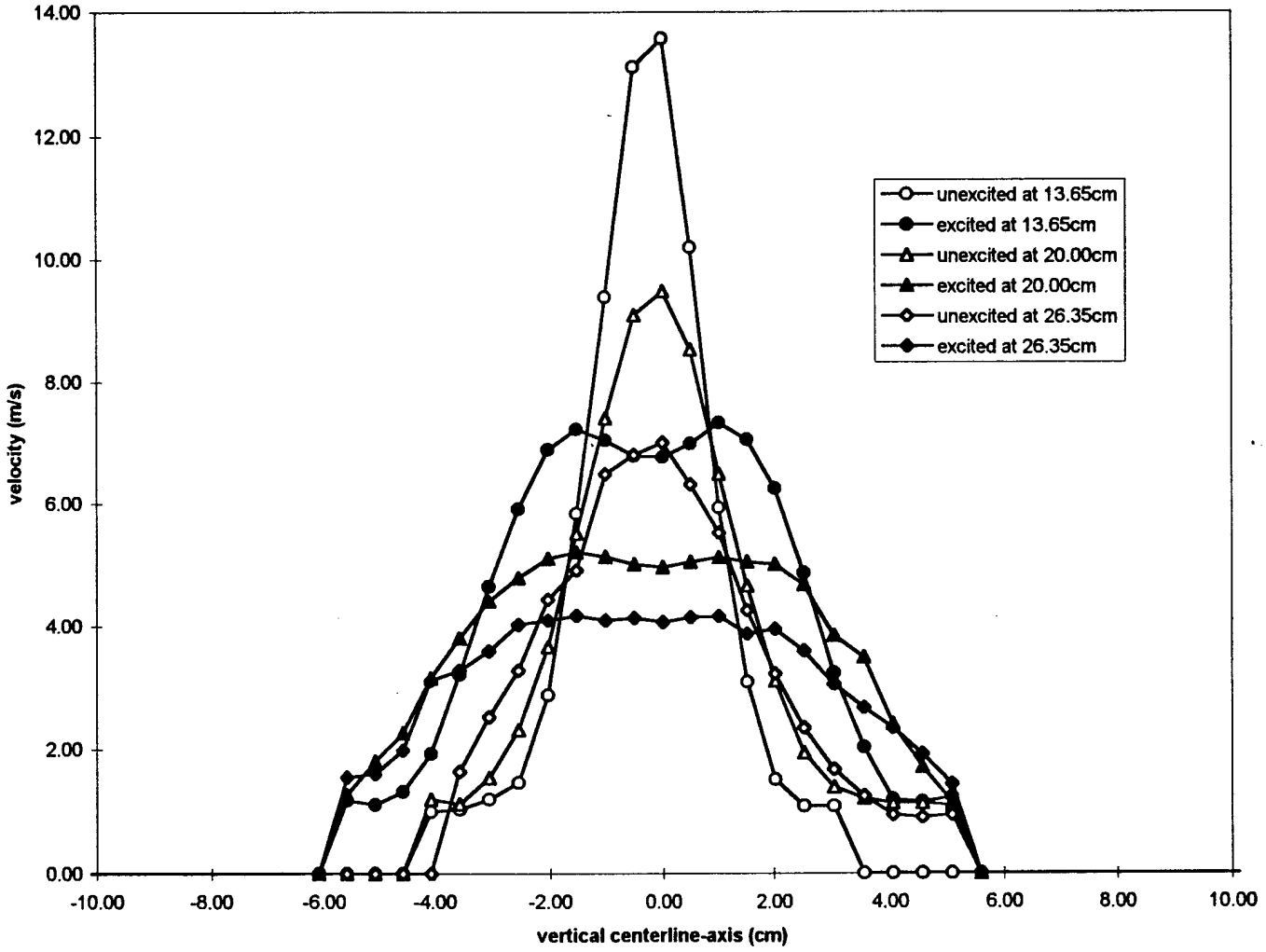

Figure 20. Mean velocity profiles in the direction of the acoustic oscillations

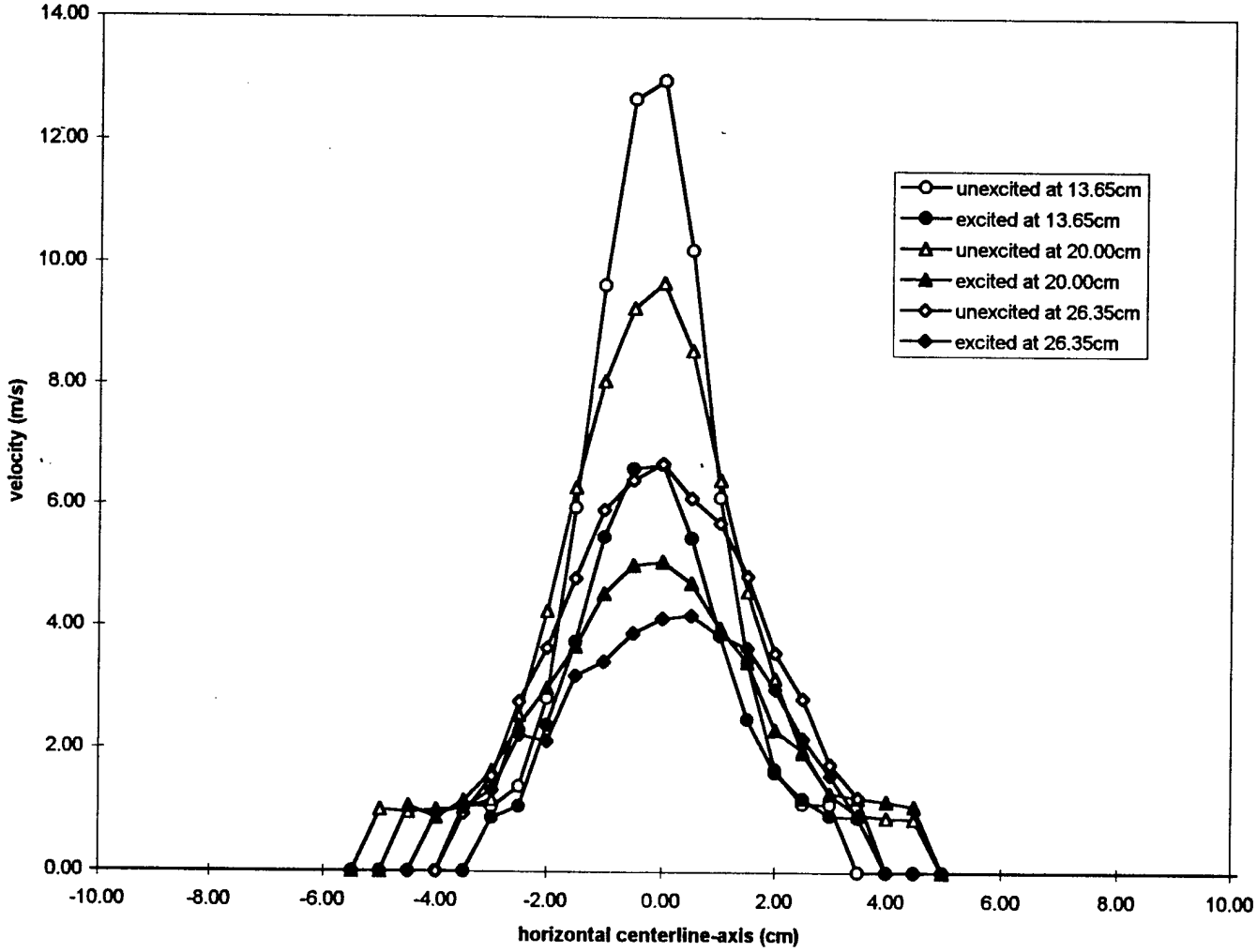

Figure 21. Mean velocity profiles perpendicular to the direction of the acoustic oscillations

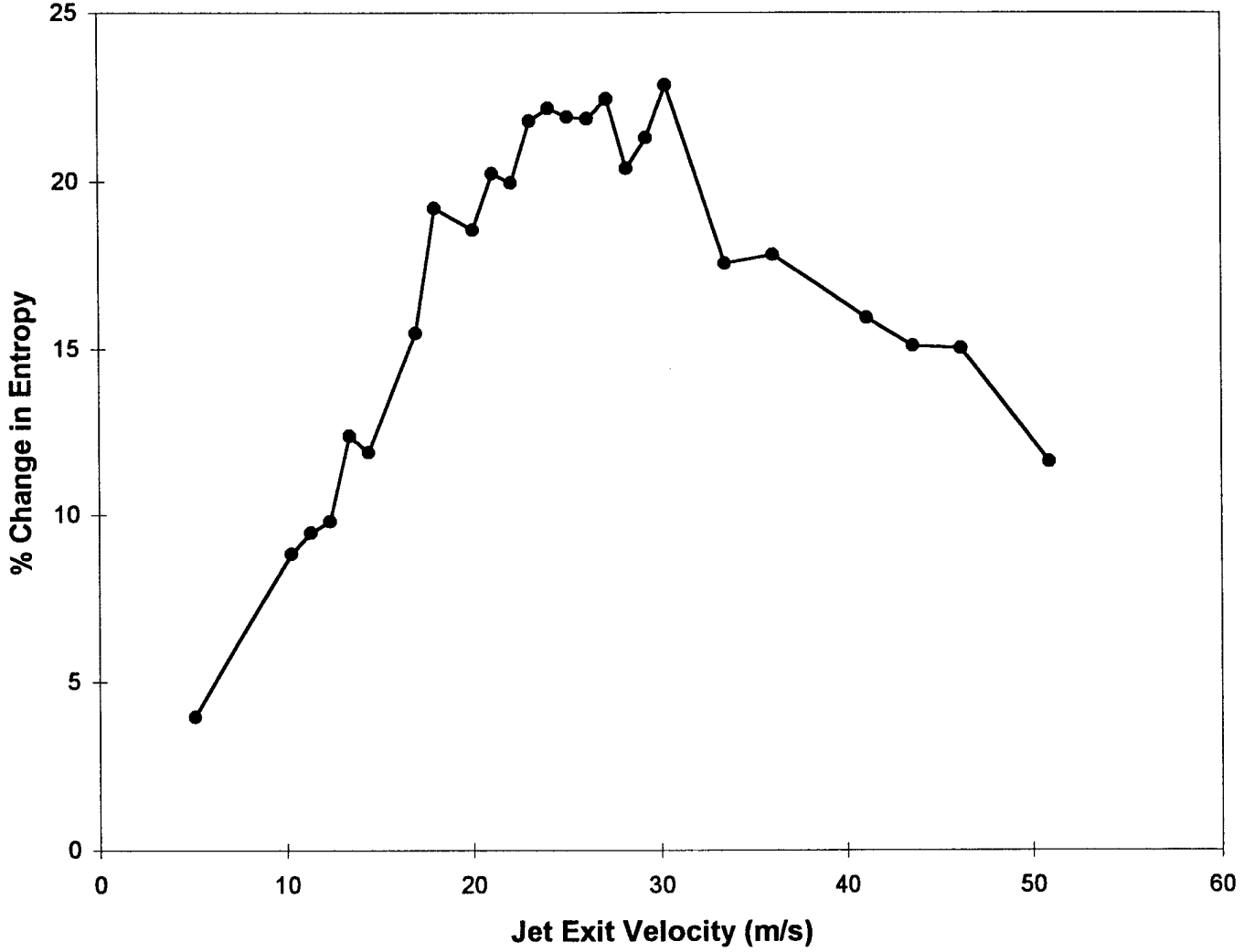

Figure 22. Difference between measured mixing entropy with a 134dB oscillation present and without sound

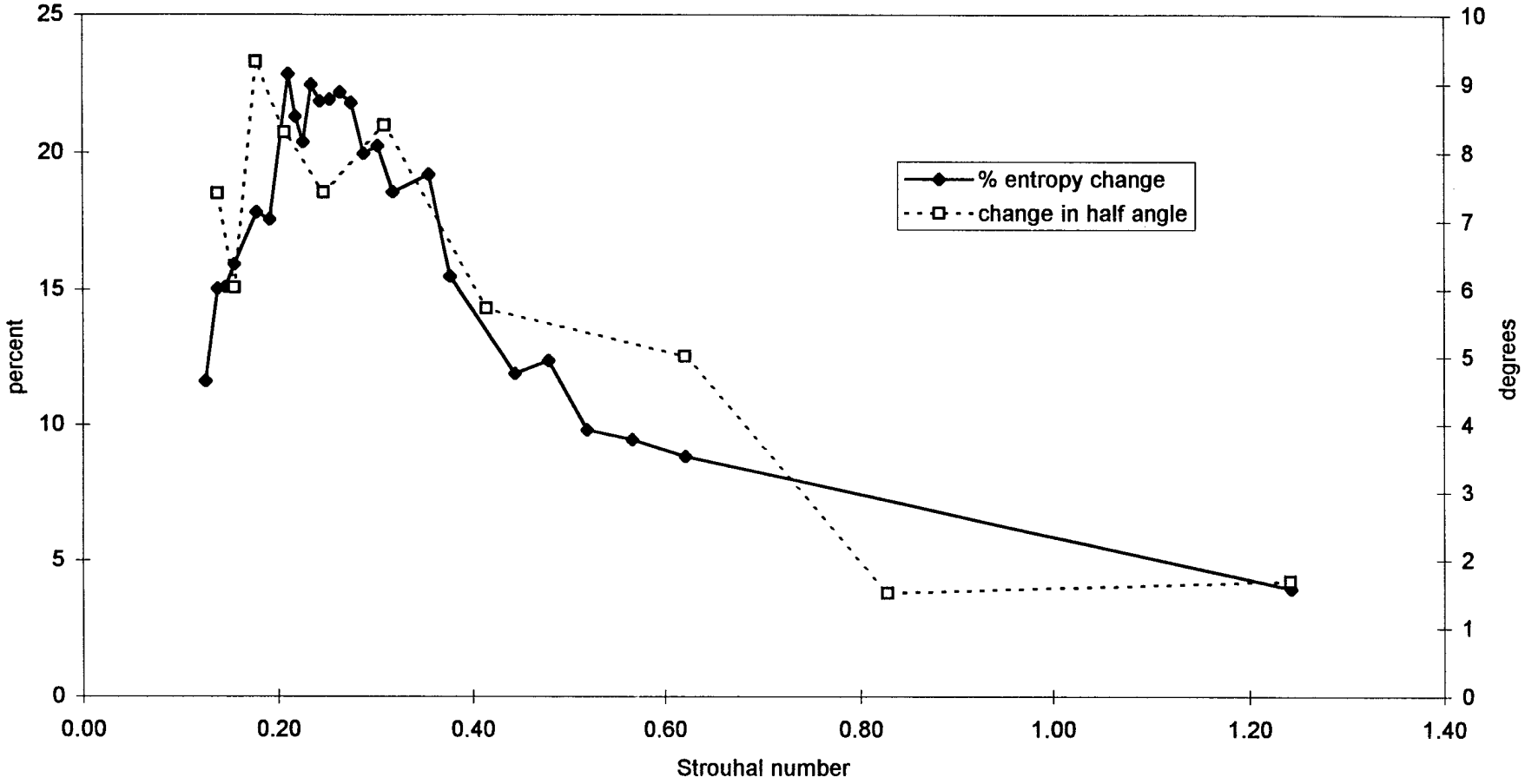

Figure 23. Comparison of the two techniques used to measure mixing as a function of St

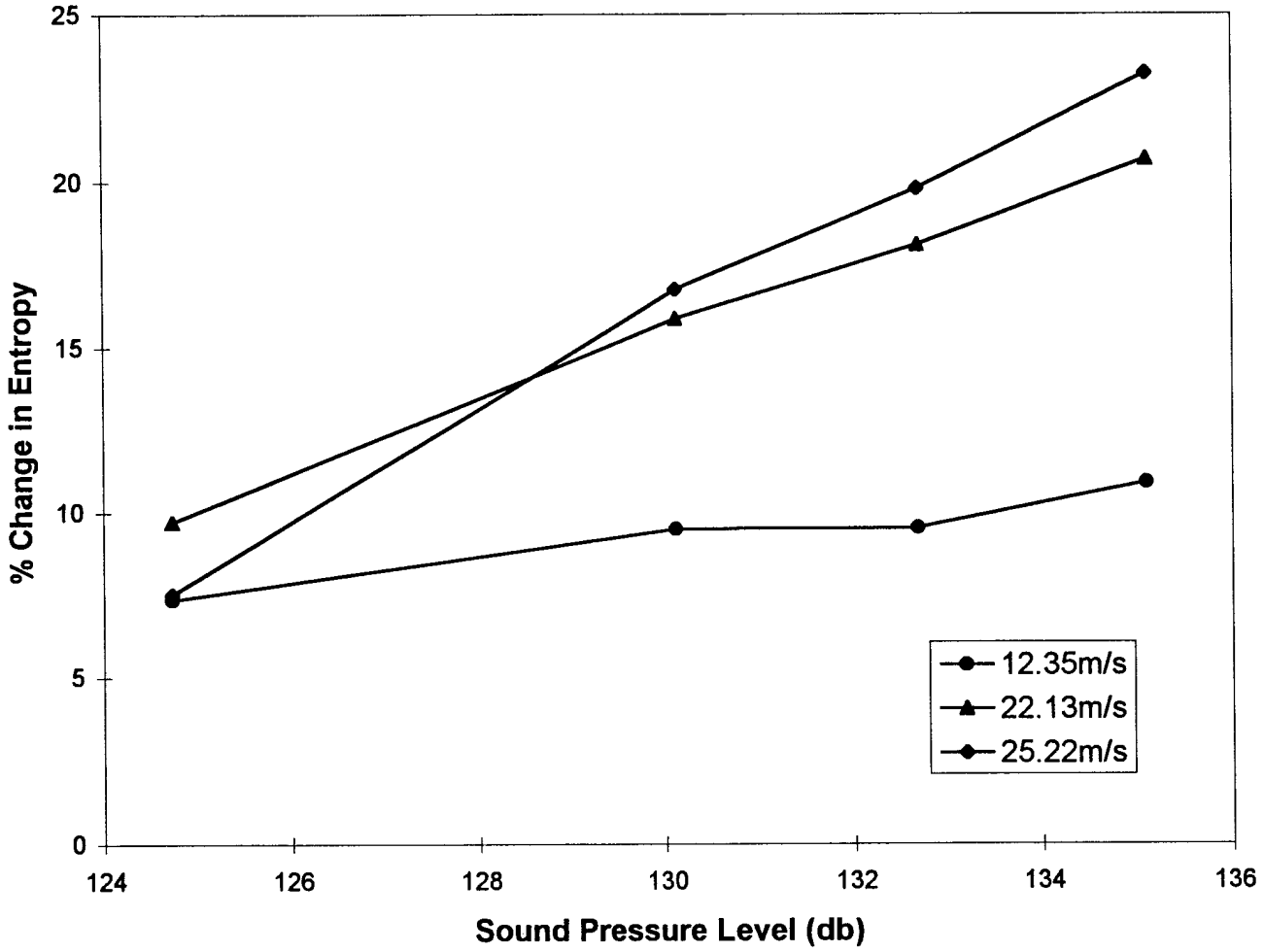

Figure 24. Effect of the oscillation amplitude on the change in mixing entropy

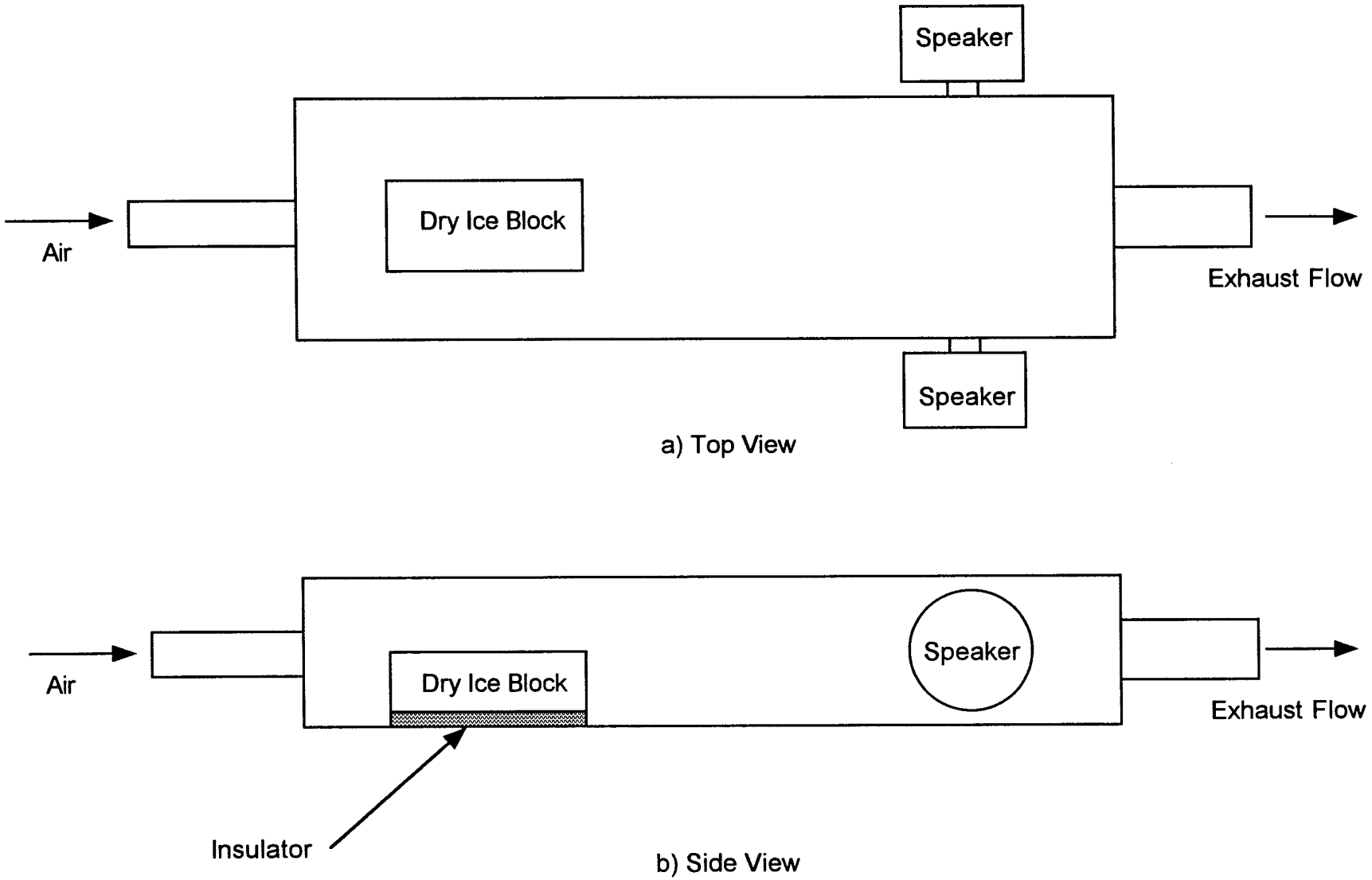

Fig. 25. Schematic of the dry ice sublimation facility

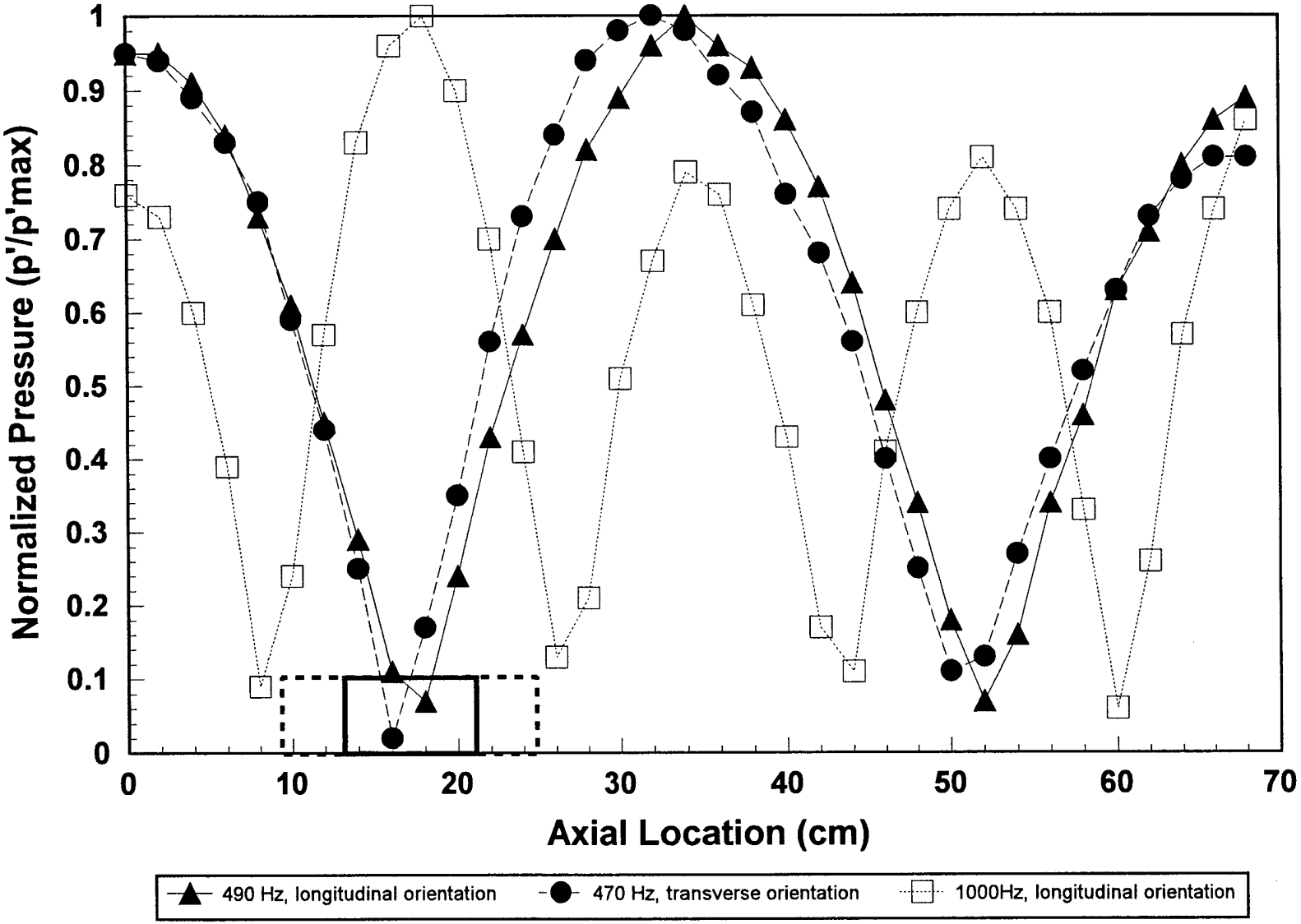

Figure 26. Measured axial dependence of the pressure amplitude of several resonant modes excited in the chamber

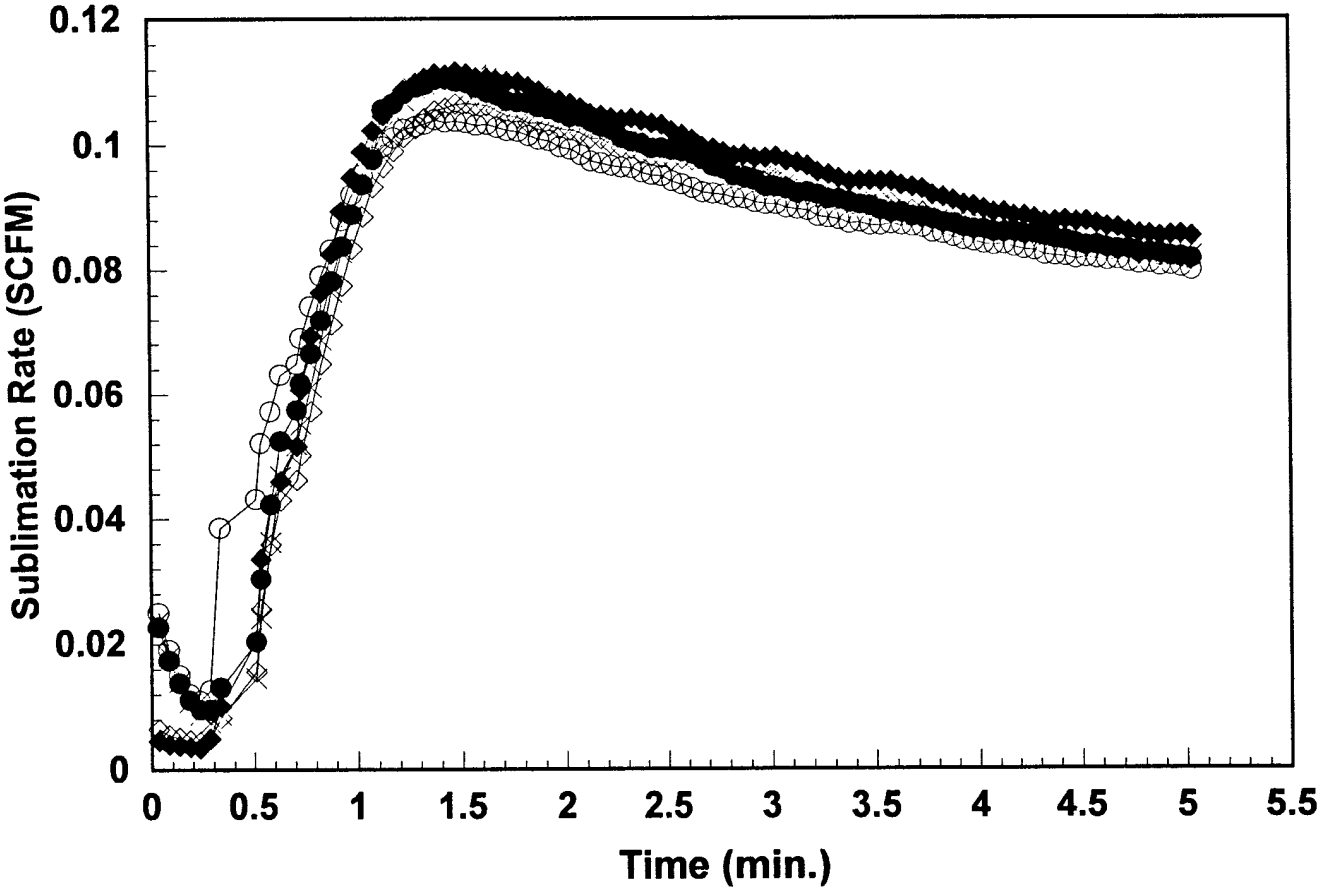

Figure 27. Series of tests demonstrating the repeatability of the start-up procedure

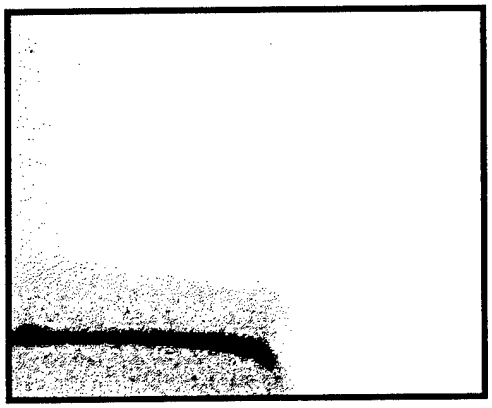

a) no oscillation, no mean flow

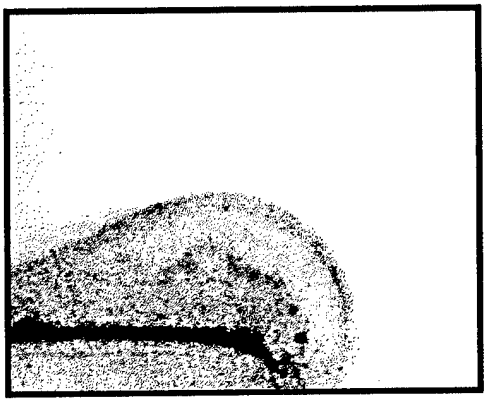

b) 150dB oscillation, no mean flow

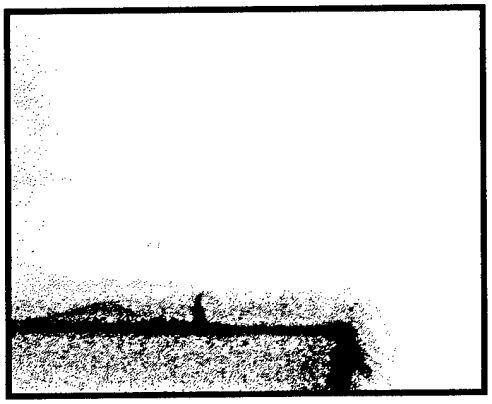

c) no oscillation, 0.5m/s mean flow

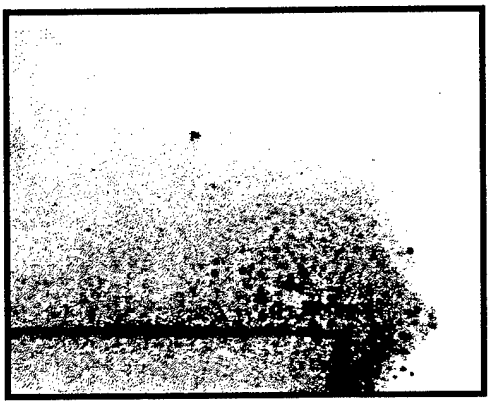

d) 150dB oscillation, 0.5m/s mean flow

Figure 28. Images of the fog layer at the downstream corner of the dry ice block under various conditions

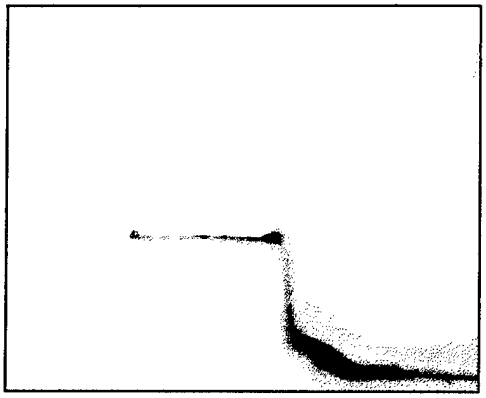

a) no oscillation, no mean flow

b) 150dB oscillation, no mean flow

c) no oscillation, 1.0/s mean flow

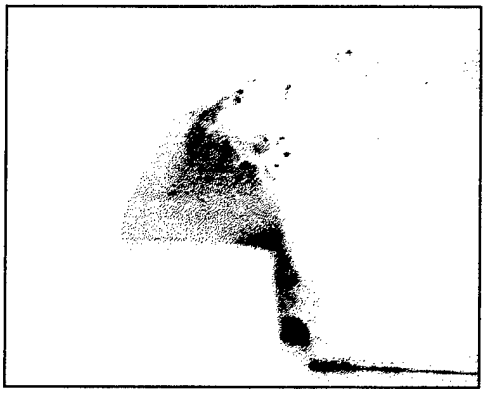

d) 150dB oscillation, 1.0m/s mean flow

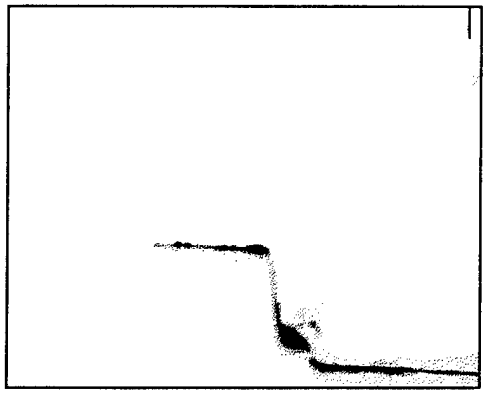

e) no oscillation, 1.8m/s mean flow

f) 150dB oscillation, 1.8m/s mean flow

Figure 29. Images of the fog layer at the downstream corner of the dry ice block under various conditions

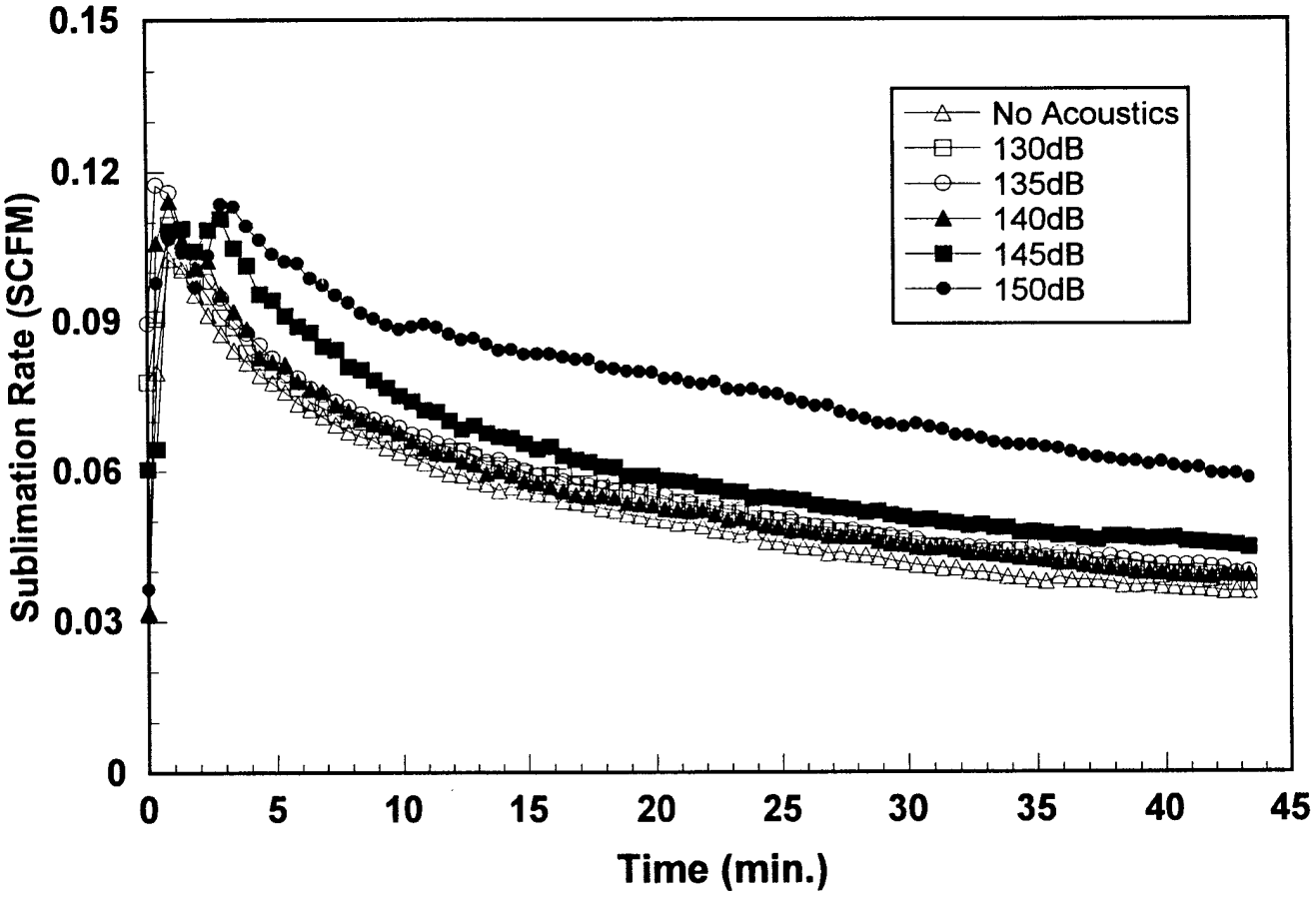

Figure 30. Measured sublimation rate at different acoustic amplitudes in the presence of a 1.25m/s mean flow velocity

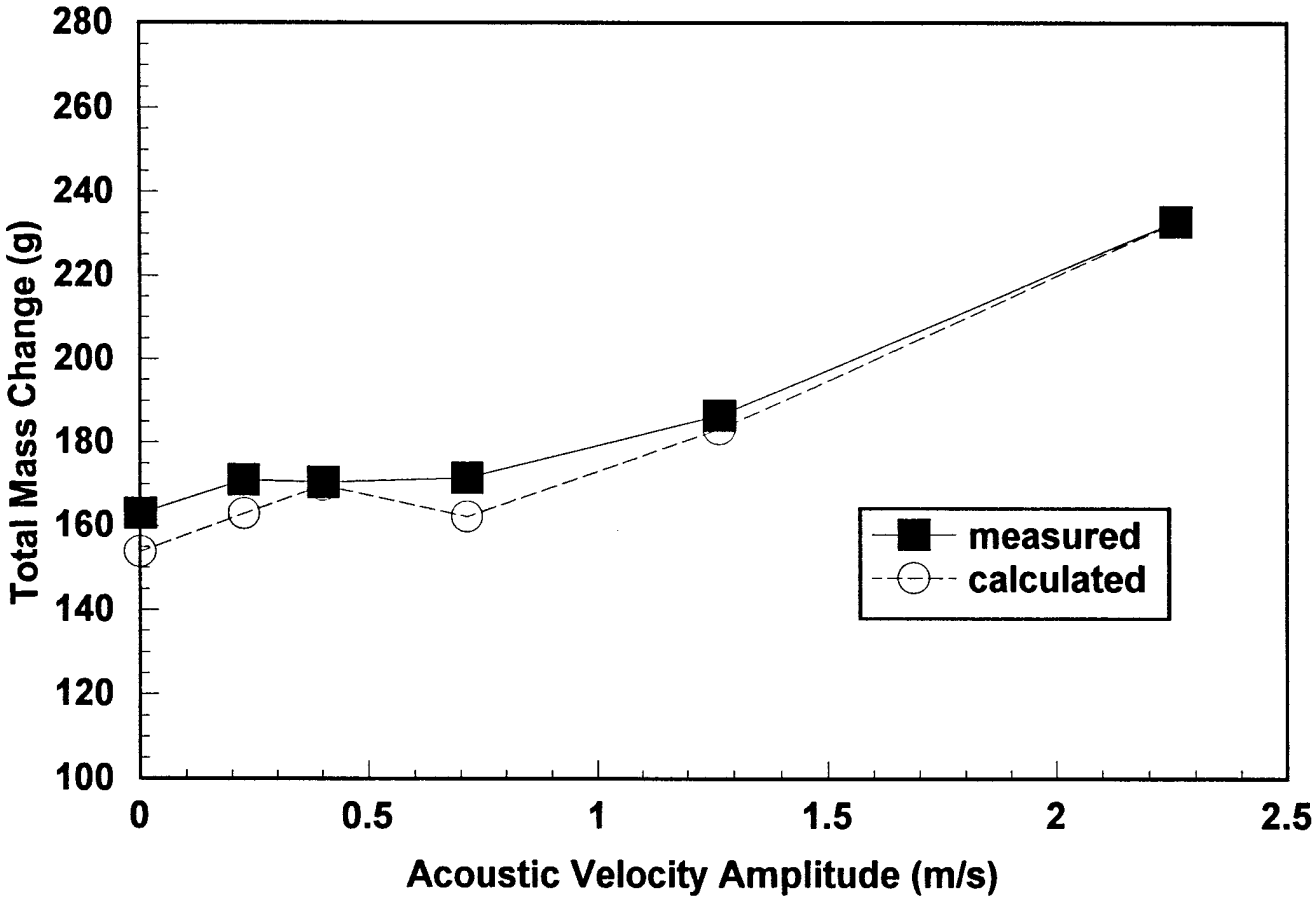

Figure 31. Comparison of the measured dry ice mass loss with that calculated from exhaust gas carbon dioxide sampling

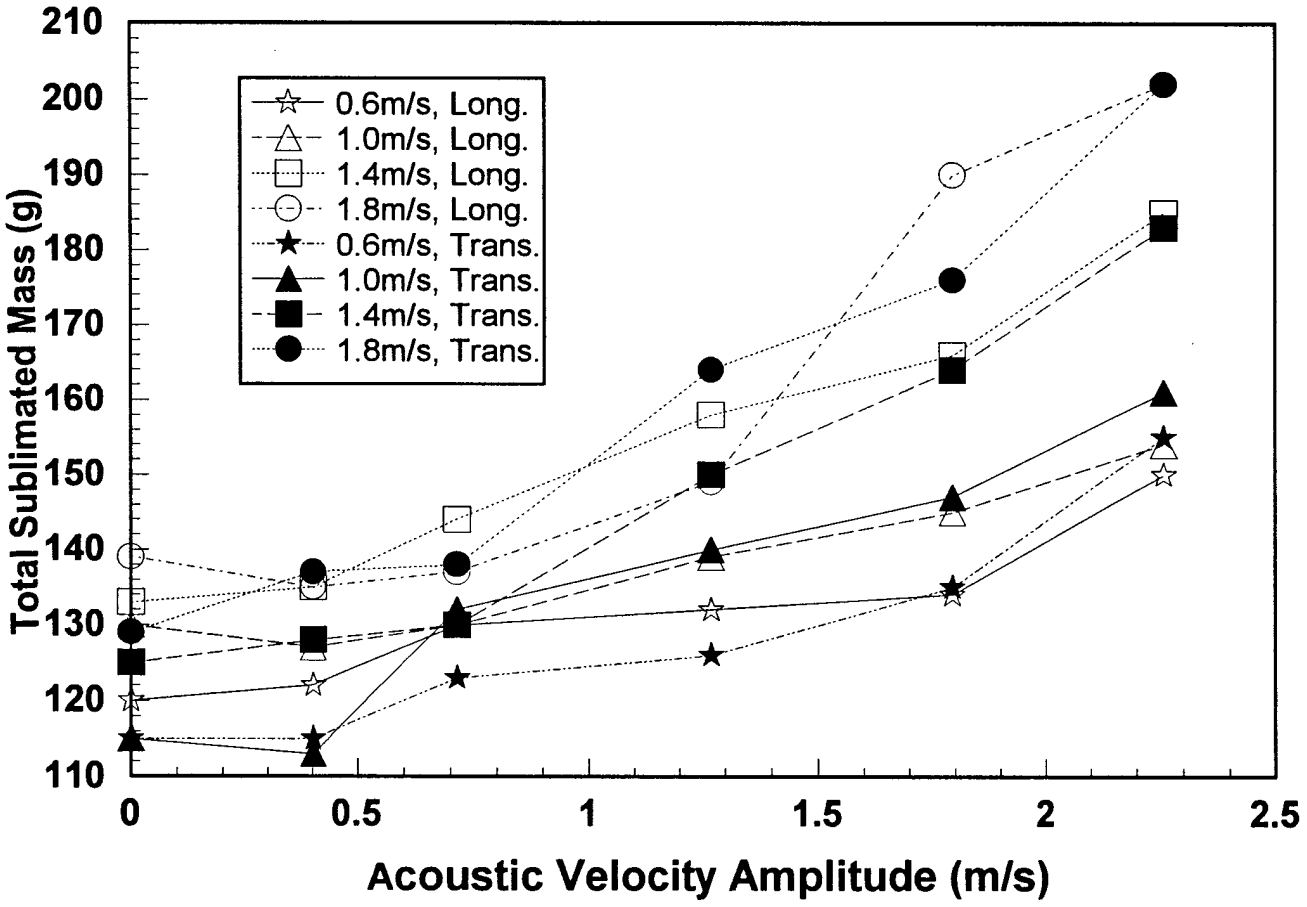

Figure 32. Dependence of the total dry ice mass loss on the excitation amplitude and mean flow velocity

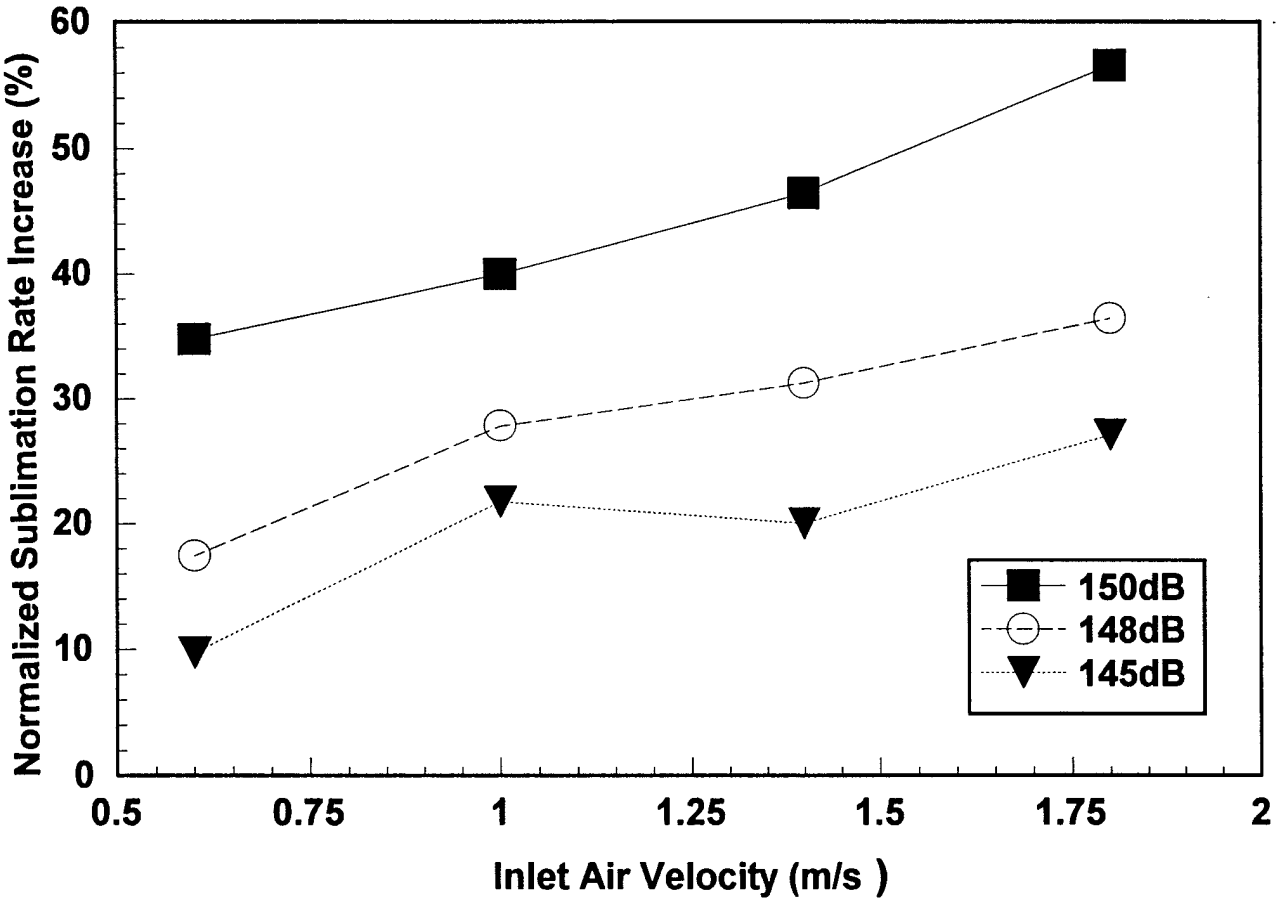

Figure 33. Effect of the air inlet velocity and oscillation amplitude on the acoustic enhancement of the dry ice sublimation rate

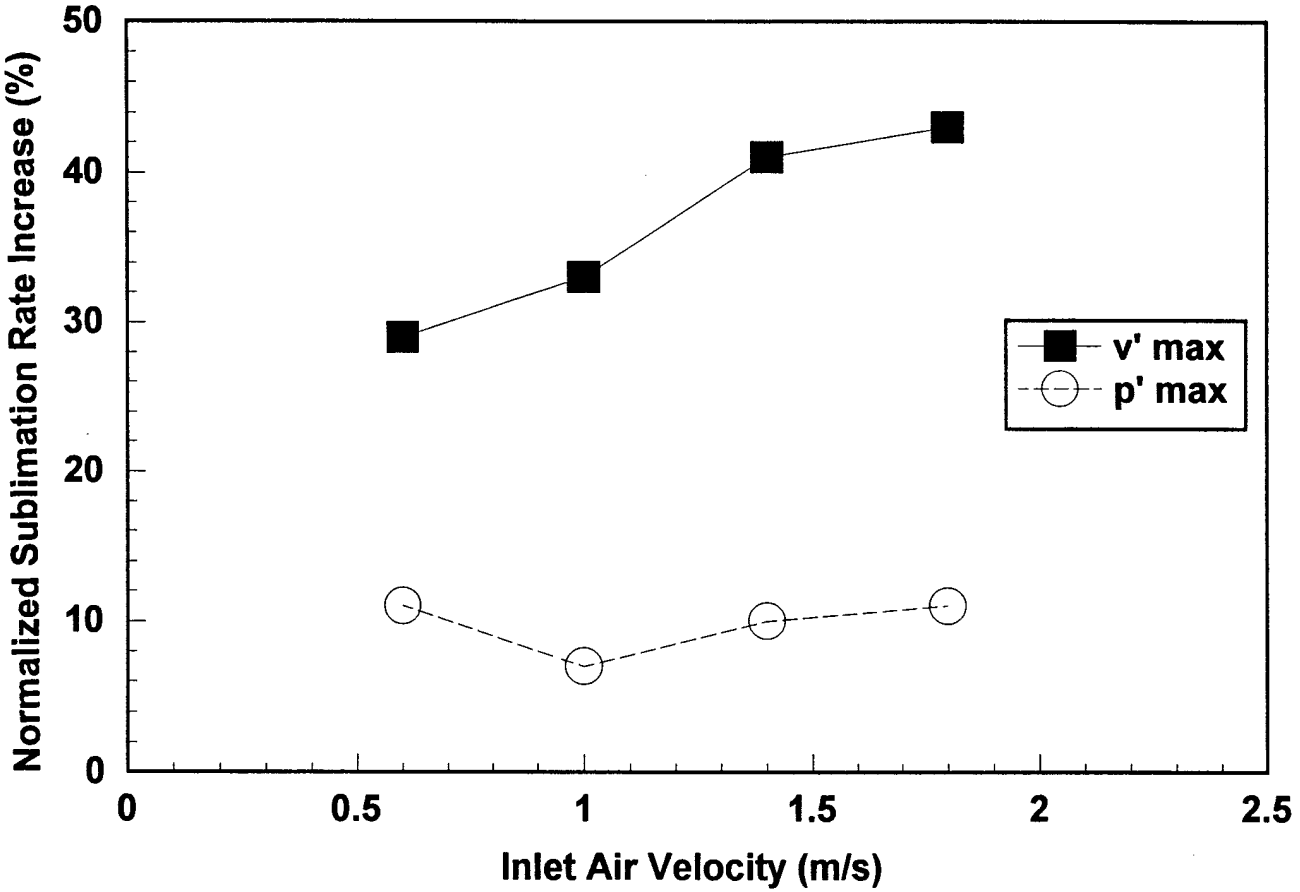

Figure 34. Effect of dry ice location relative to the standing acoustic oscillation on acoustic enhancement of the dry ice sublimation rate

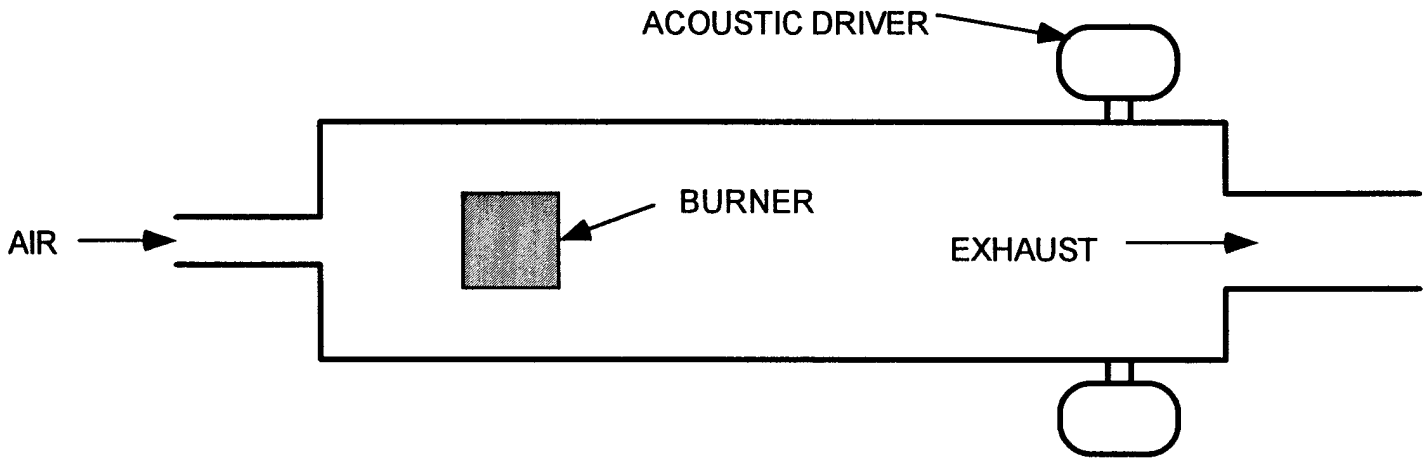

a) Top View

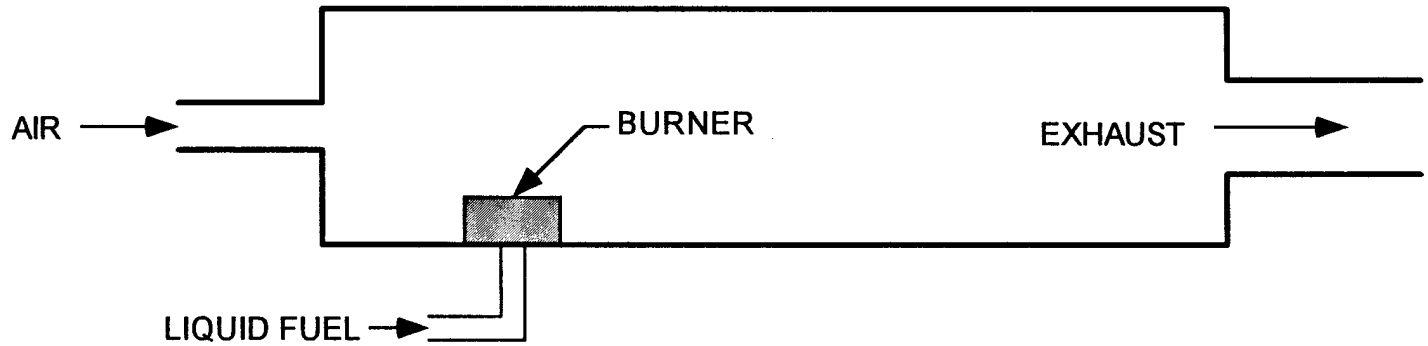

b) Side View

Figure 35. Schematic of the pulsed incineration facility confiured for liquid fuel combustion

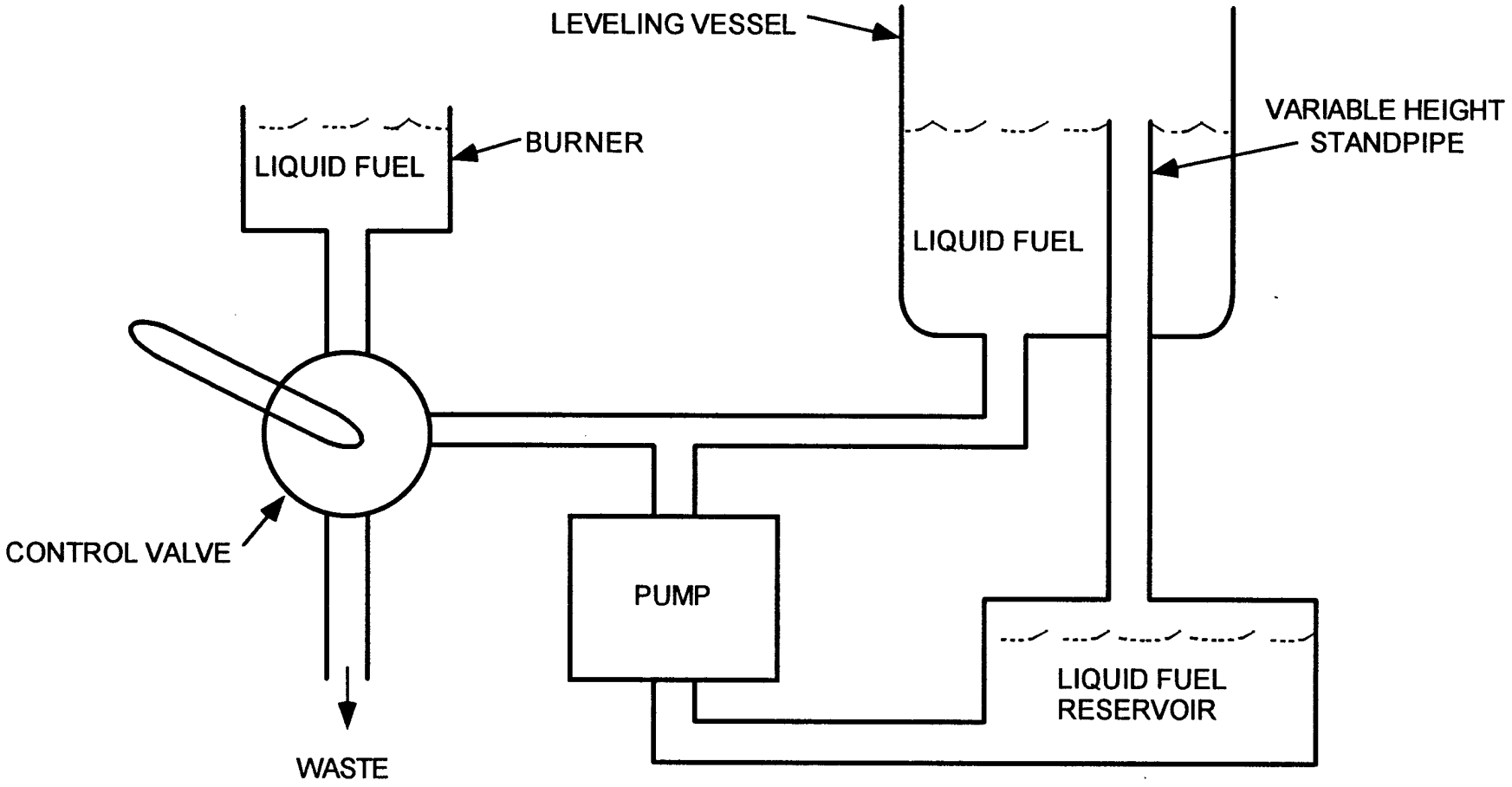

Figure 36. Schematic of the liquid fuel supply system

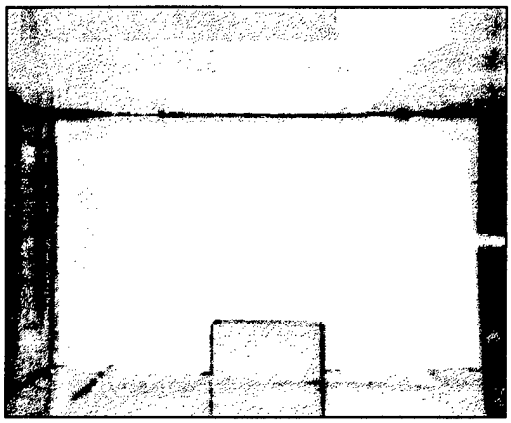

a) no oscillations present

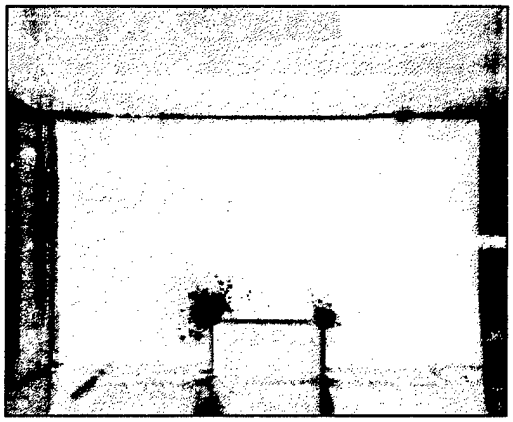

b) 158 dB, 850 Hz oscillation
0.05 seconds

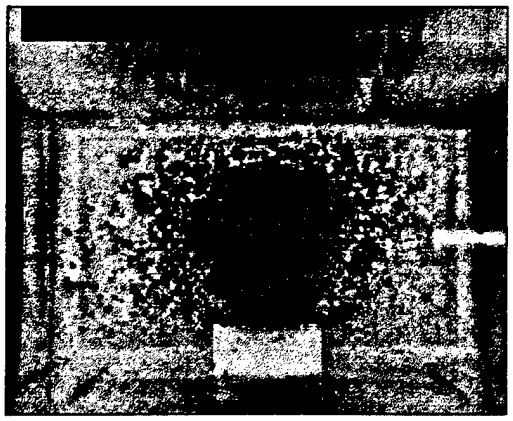

c) 158 dB, 850 Hz oscillation
0.40 seconds

Figure 37. Liquid methanol droplet spray generated with high-intensity acoustic driving

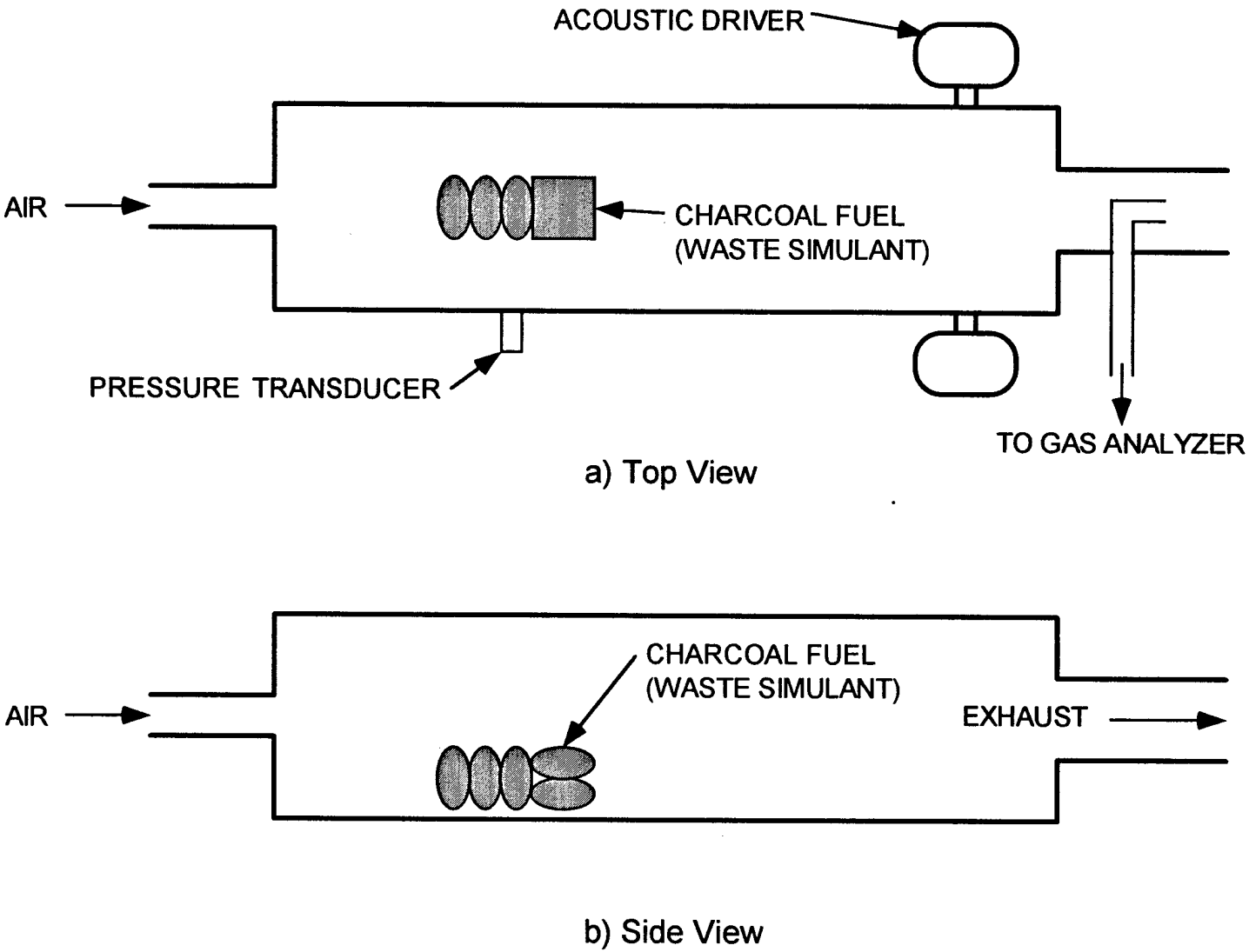

Figure 38. Schematic of the pulsed incineration facility configured for charcoal incineration

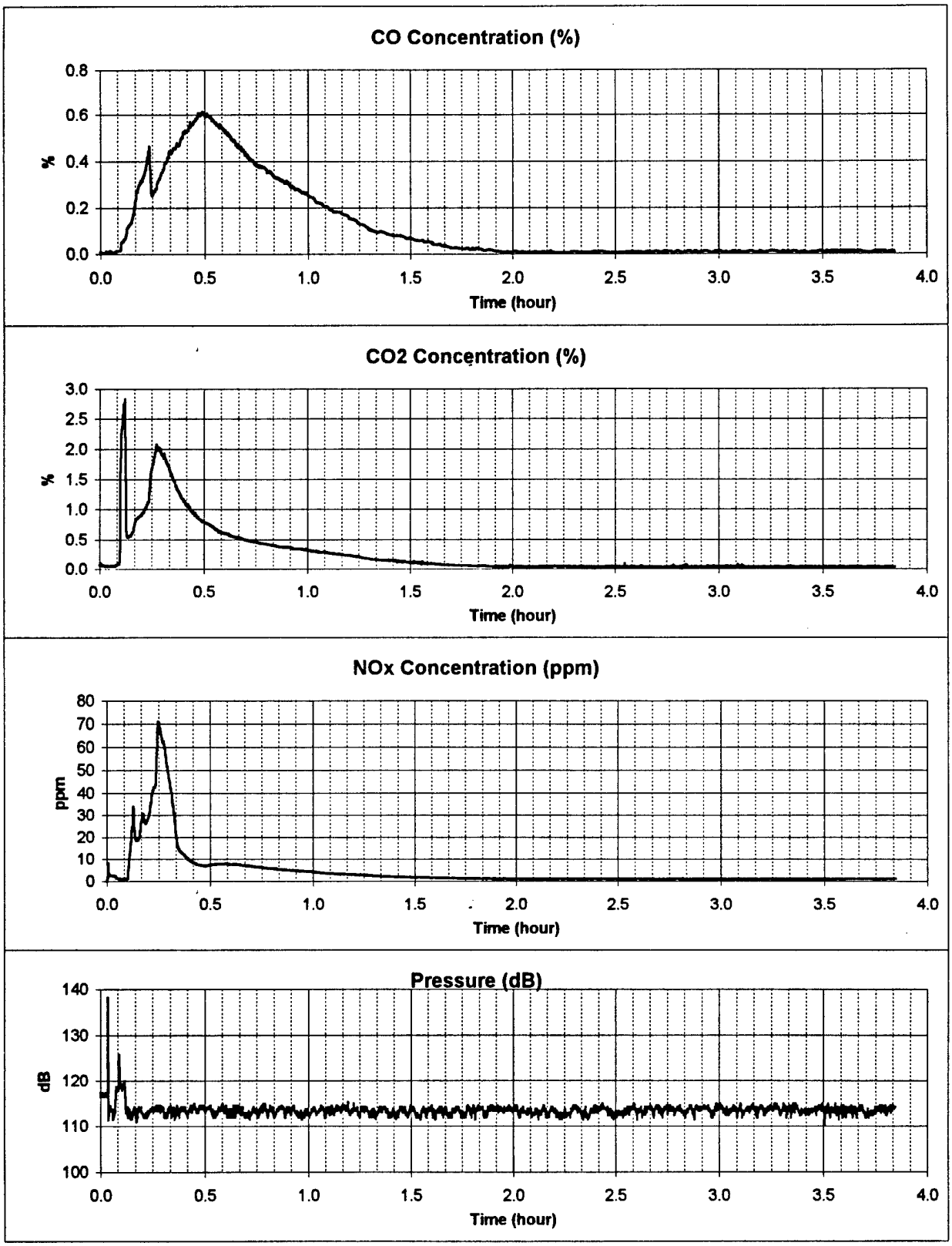

Figure 39. Exhaust gas analysis and pressure measurements from a typical charcoal incineration test with no oscillations present

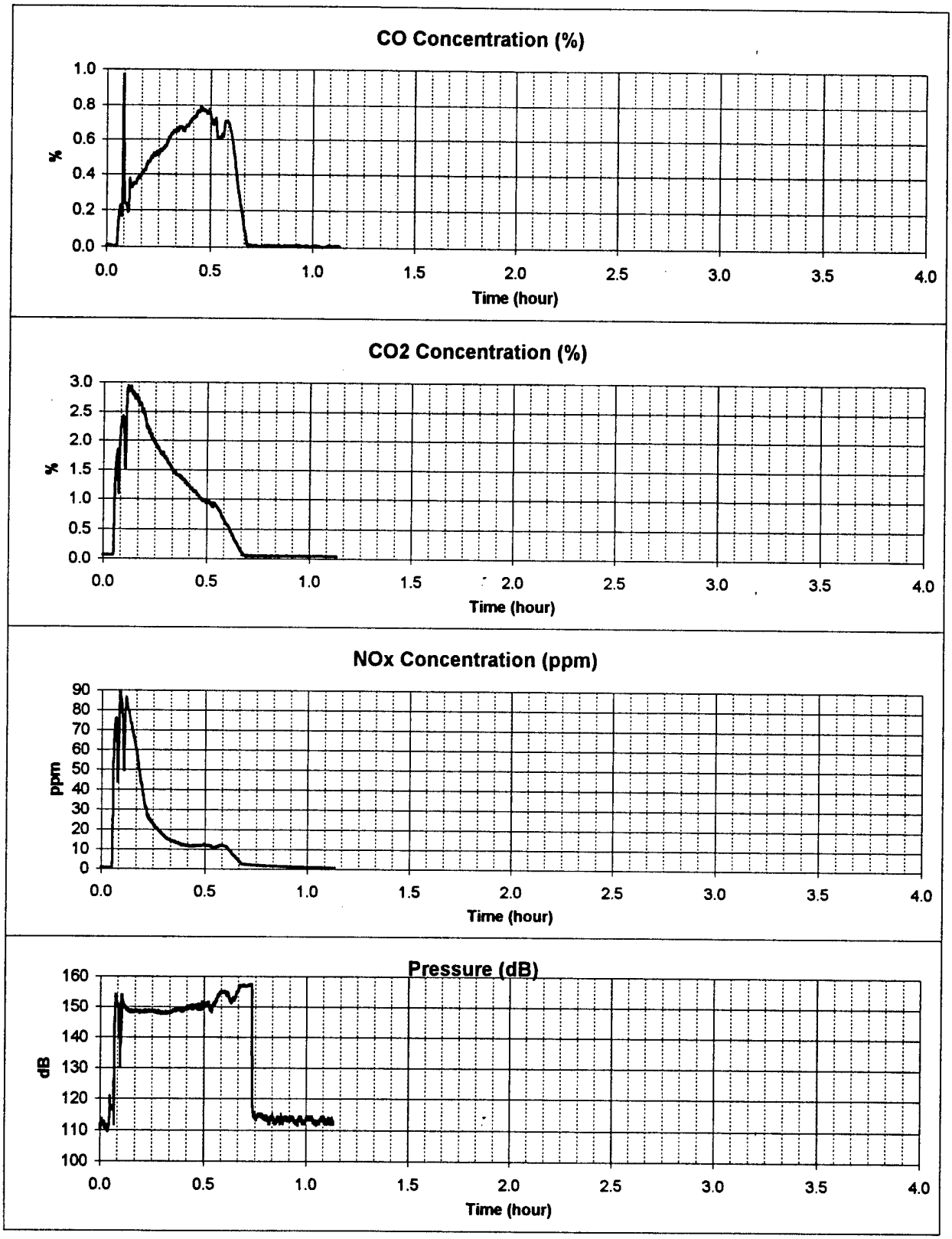

Figure 40. Exhaust gas analysis and pressure measurements from a typical charcoal incineration test with acoustic forcing

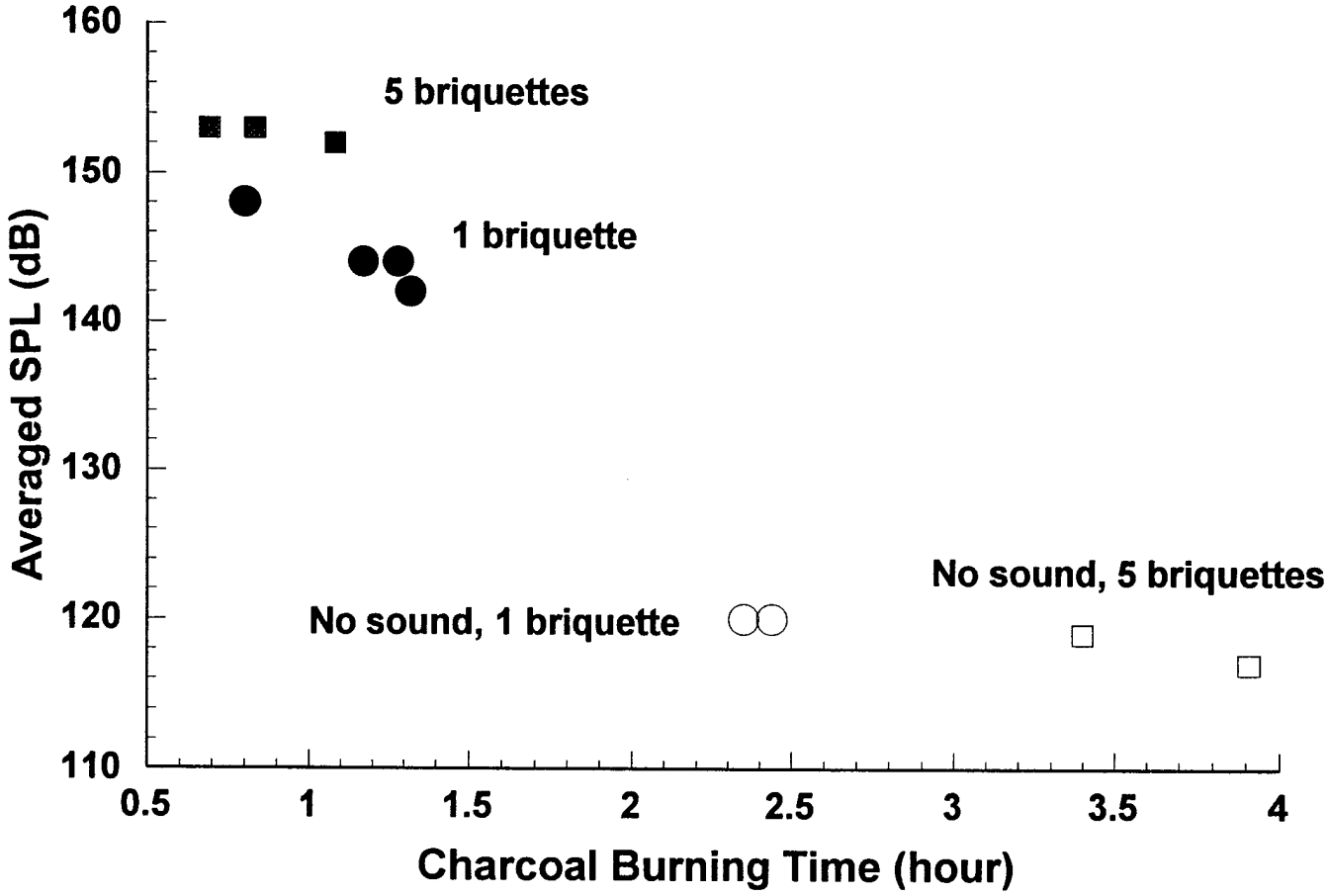

Figure 41. Relationship of Burning time to SPL

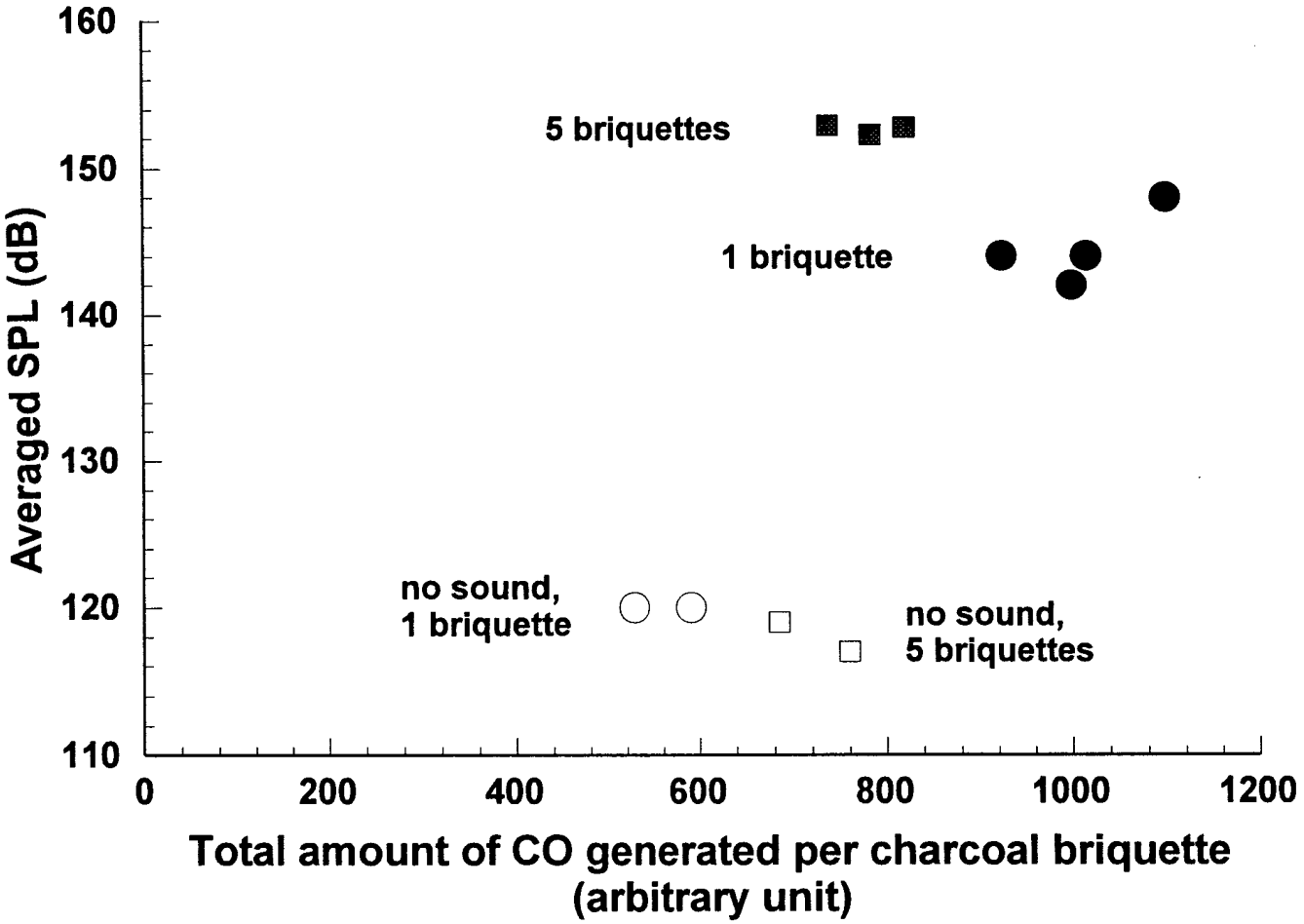

Figure 42. CO emission per charcoal briquette

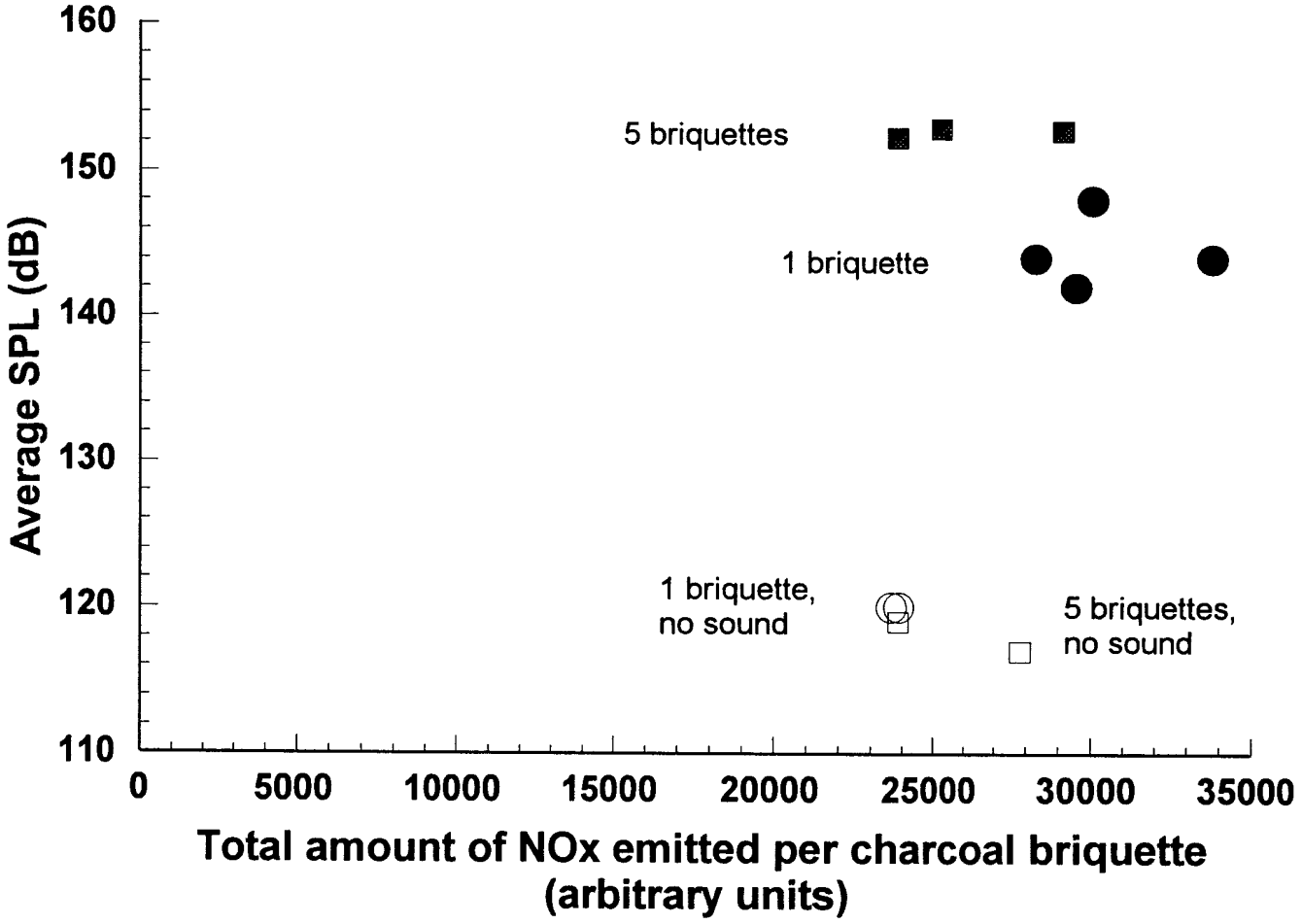

Figure 43. NOx emission per charcoal briquette

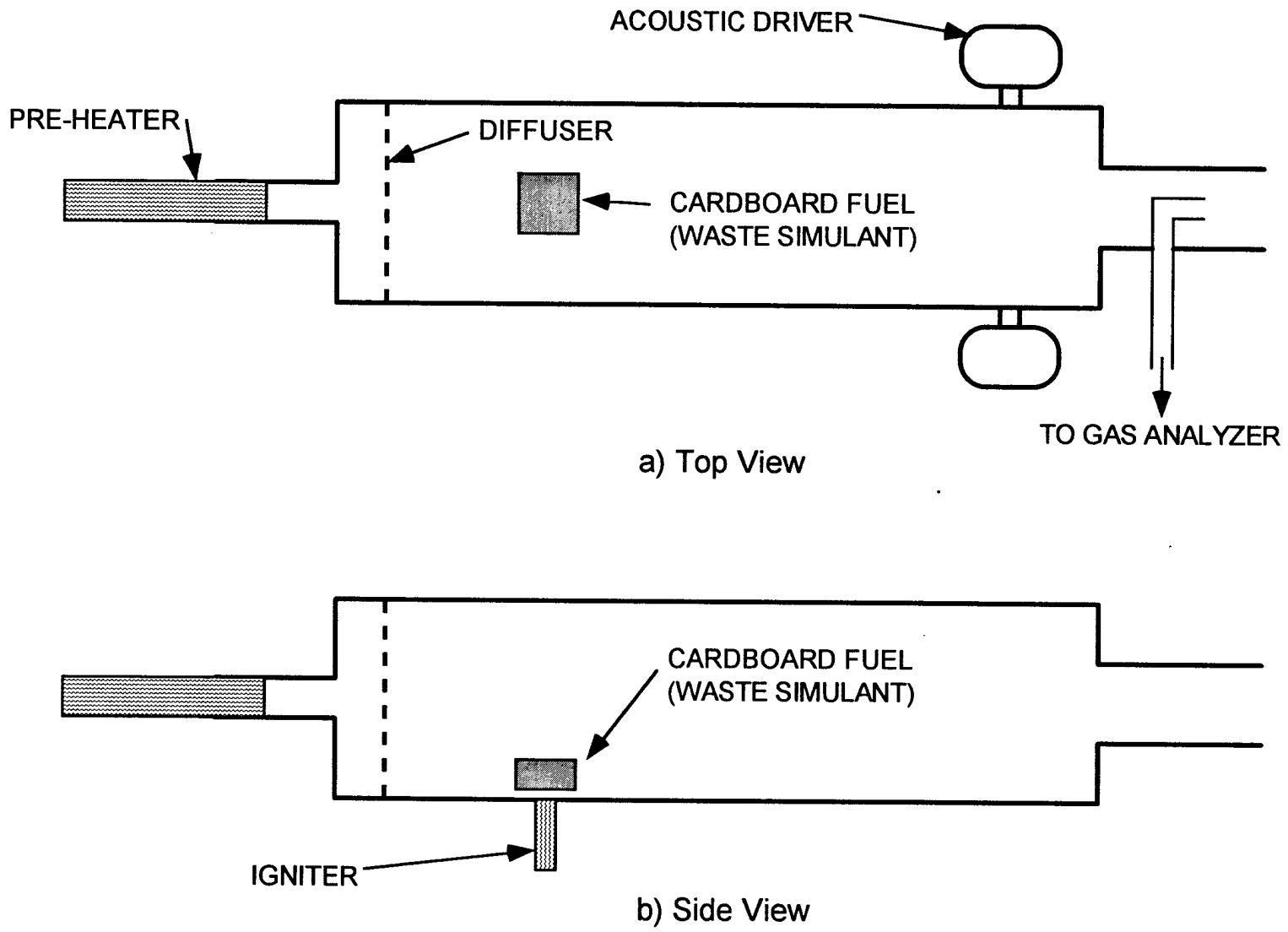

Figure 44. Schematic of the pulsed incineration facility configured for cardboard burning

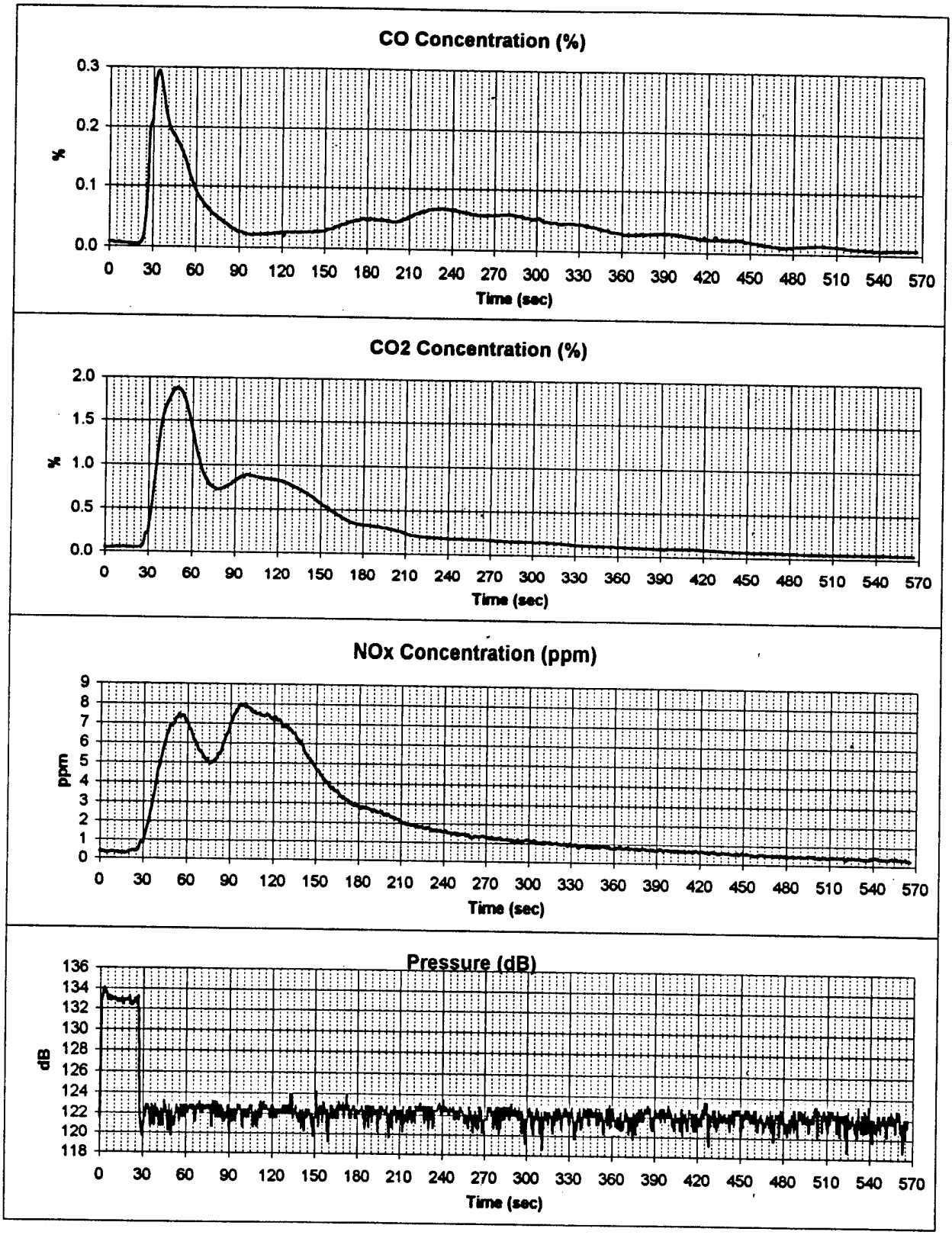

Figure 45. Exhaust gas analysis and pressure measurements from a typical cardboard incineration test with no oscillations present

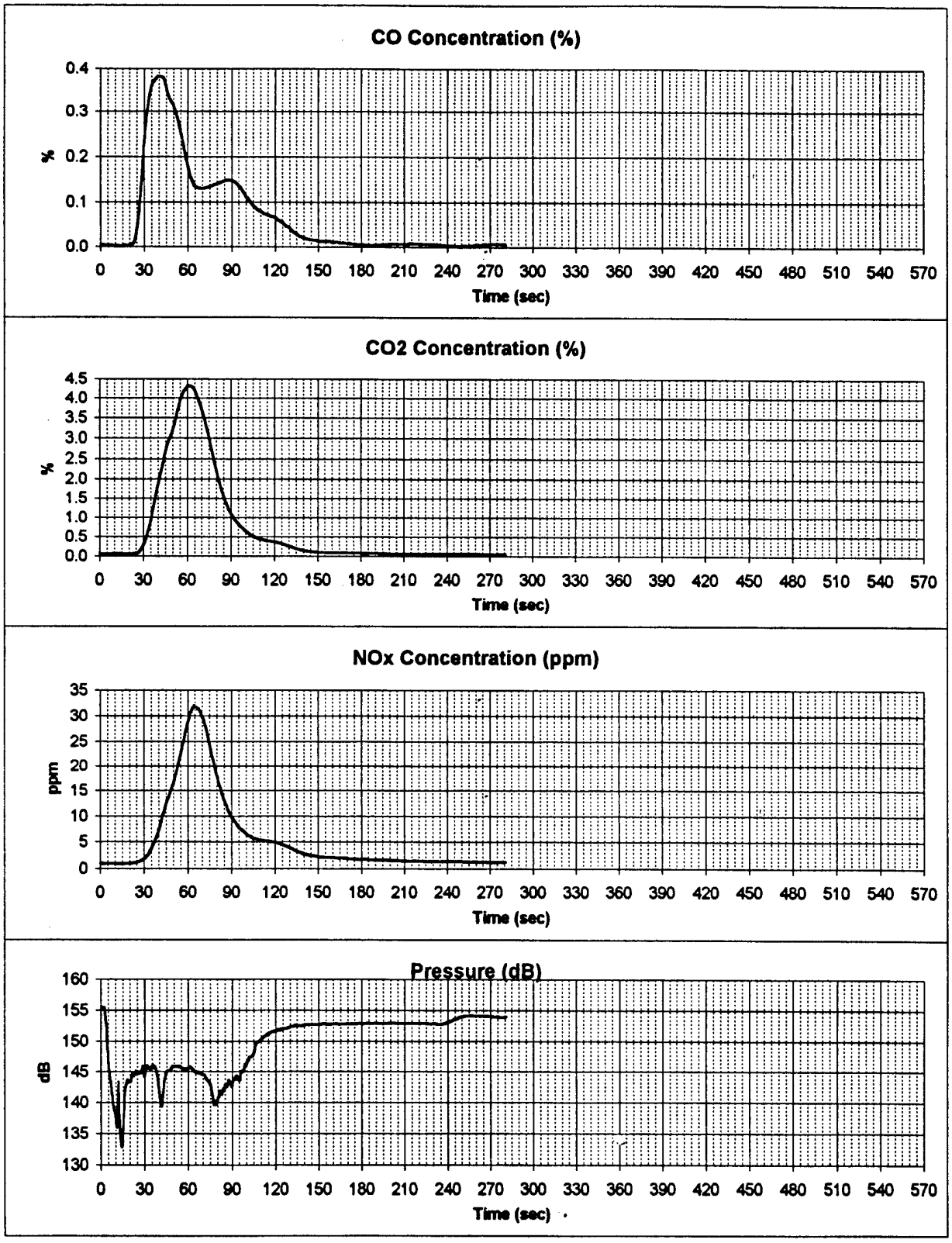

Figure 46. Exhaust gas analysis and pressure measurements from a typical cardboard incineration test with acoustic forcing

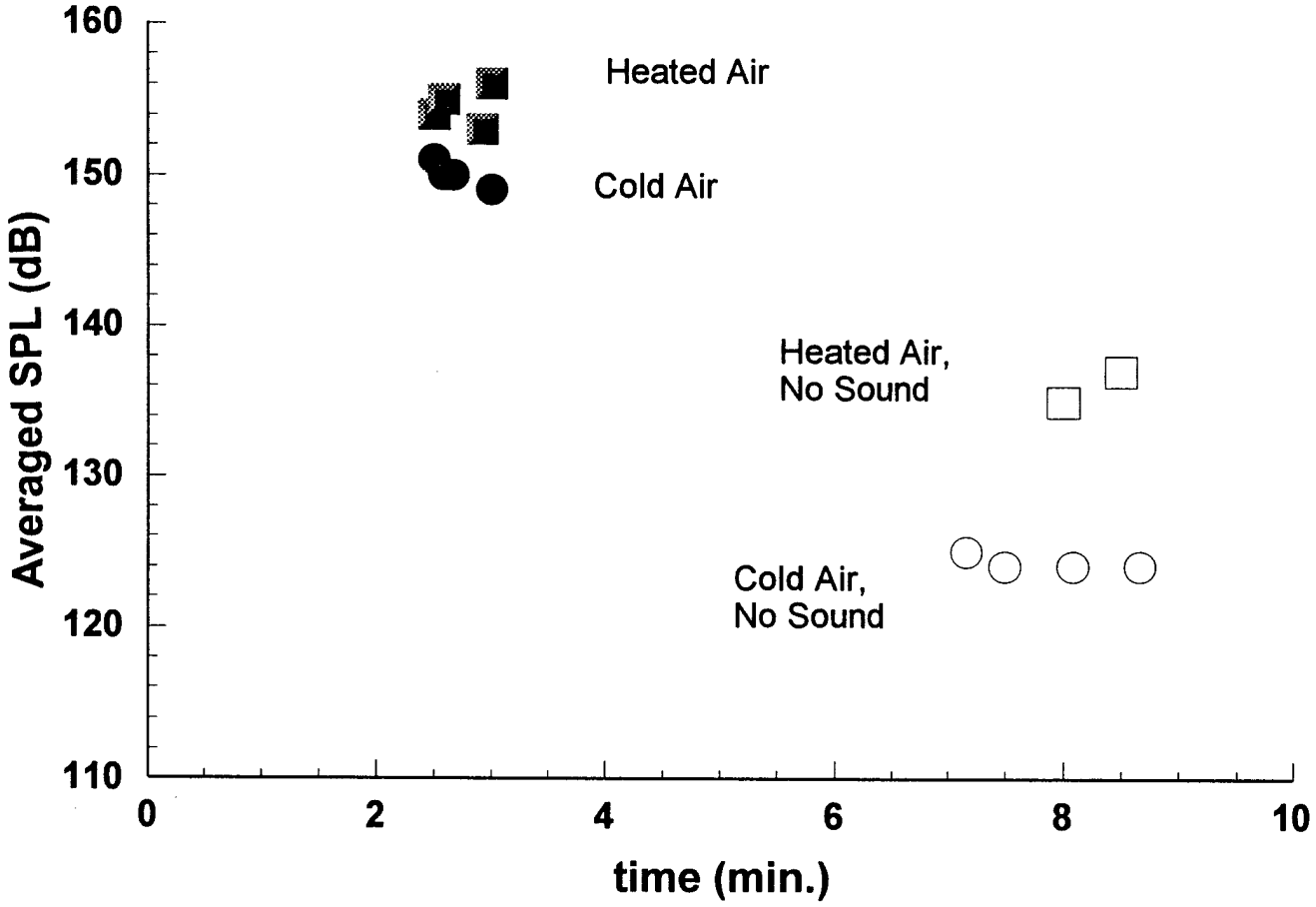

Figure 47. Relationship of Burning Time to SPL

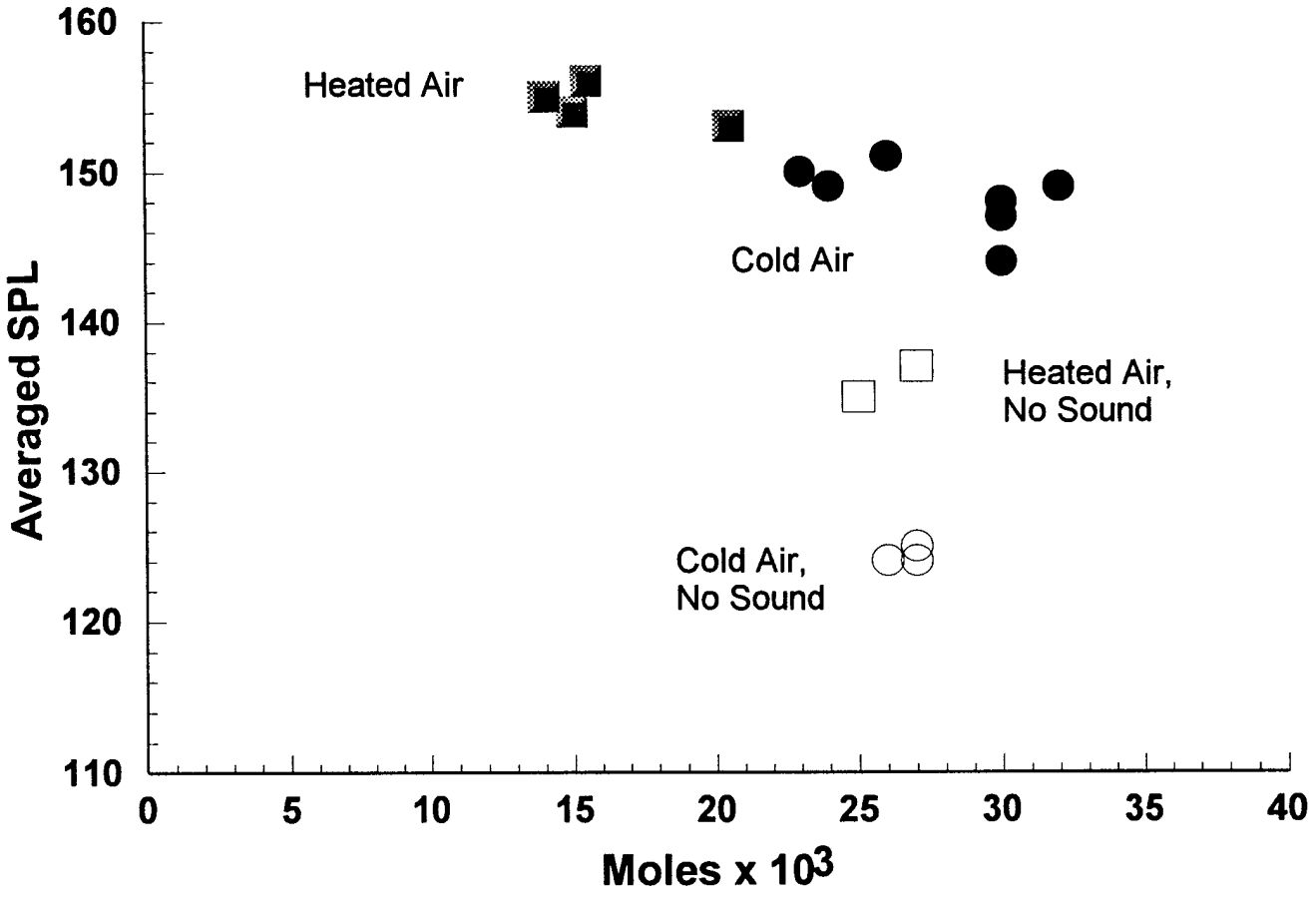

Figure 48. CO emissions from cardboard samples

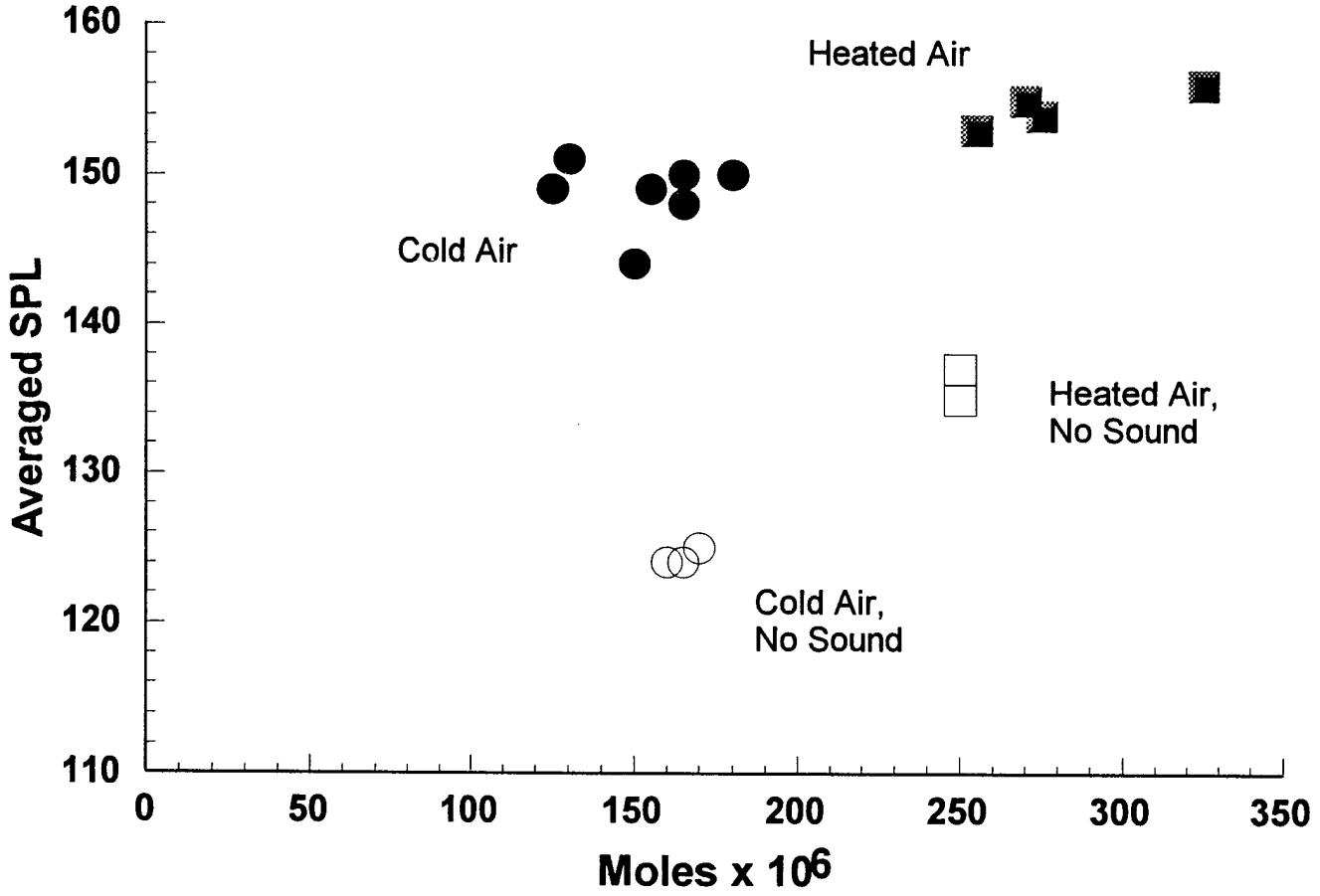

Figure 49. NOx emission from cardboard samples

SECURITY CLASSIFICATION OF THIS PAGE

REPORT DOCUMENTATION PAGE

Form Approved OMB No. 0704-0188

1a. REPORT SECURITY CLASSIFICATION: Unclassified	1b. RESTRICTIVE MARKINGS
2a. SECURITY CLASSIFICATION AUTHORITY	3. DISTRIBUTION/AVAILABILITY OF REPORT: approved for public release; distribution is unlimited
2b. DECLASSIFICATION/DOWNGRADING SCHEDULE	
4. PERFORMING ORGANIZATION REPORT NUMBER(S)	5. MONITORING ORGANIZATION REPORT NUMBER(S)
6a. NAME OF PERFORMING ORGANIZATION: Georgia Inst. of Technology School of Aerospace Eng. / 6b. OFFICE SYMBOL (If applicable)	7a. NAME OF MONITORING ORGANIZATION: Office of Naval Research
6c. ADDRESS (City, State, and ZIP Code)	7b. ADDRESS (City, State, and ZIP Code)
8a. NAME OF FUNDING/SPONSORING ORGANIZATION / 8b. OFFICE SYMBOL (If applicable)	9 PROCUREMENT INSTRUMENT IDENTIFICATION NUMBER: n00014-93-1-1349
8c. ADDRESS (City, State, and ZIP Code)	10. SOURCE OF FUNDING NUMBERS: PROGRAM ELEMENT NO. / PROJECT NO. / TASK NO. / WORK UNIT ACCESSION NO.

11. TITLE (Include Security Classification)
Controlling Mechanisms of Pulsating Incineration Processes

12. PERSONAL AUTHOR(S)
B. T. Zinn, J. I. Jagoda, L. M. Matta

13a. TYPE OF REPORT	13b. TIME COVERED	14. DATE OF REPORT (Year, Month, Day)	15. PAGE COUNT
Final Report	FROM 93/05/30 TO 96/09/29	96-09-29	89

16. SUPPLEMENTARY NOTATION

17. COSATI CODES			18. SUBJECT TERMS (Continue on reverse if necessary and identify by block number)
FIELD	GROUP	SUB-GROUP	Pulsed Combustion, Incineration, Jet Excitation, Sublimation, Bifurcating Jet

19. ABSTRACT (Continue on reverse if necessary and identify by block number)

SEE BACK

20. DISTRIBUTION/AVAILABILITY OF ABSTRACT: XX UNCLASSIFIED/UNLIMITED XX SAME AS RPT. ☐ DTIC USERS	21. ABSTRACT SECURITY CLASSIFICATION: Unclassified
22a. NAME OF RESPONSIBLE INDIVIDUAL	22b. TELEPHONE (Include Area Code) / 22c. OFFICE SYMBOL

DD Form 1473, JUN 86 *Previous editions are obsolete.* SECURITY CLASSIFICATION OF THIS PAGE

Unclassified

Abstract

The purpose of this research program is to study the fundamental processes that control the performance of acoustically excited incineration systems. The information learned will be used in the development of a compact, high-efficiency waste incinerator for shipboard use. Tests performed during the course of this program have demonstrated that mixing and heat transport processes, both crucial to the incineration process, can be enhanced by imposing acoustic oscillations. Because the combustion efficiency and pollutant emission characteristics of incinerators are directly affected by the mixing of in-flowing air with fuel, acoustic control of turbulent jets is of interest to the development of compact incinerators. Studies of jets subjected to transverse mode oscillations have shown that, under the proper conditions, the jet will shed large, alternating, vortical structures that can cause the jet to bifurcate. This process results in a greater spatial mixing rate. Transverse mode acoustic forcing had the greatest effect in the range of St = 0.2 - 0.3. The effect of acoustic oscillations upon solid fuel pyrolysis was investigated by studying the effect of acoustic oscillations upon dry ice sublimation. This study showed that the presence of pulsations enhanced the sublimation process, which strongly suggests that they would also enhance the processes involved in incinerating solid wastes. Finally, the effects of acoustic oscillations on the combustion of simulated solid wastes in an incinerator were studied. Measurements of the burning rates and the emissions of NOx, CO, and CO_2 were performed for different fuels and conditions. In all cases, it was shown that pulsations dramatically increased combustion rates. The results indicate that the effects of pulsations on NOx emissions are relatively insignificant with respect to other factors, such as combustor temperature. The effect of acoustic oscillations on the emission of CO differs with the fuel type used and the conditions present.